May 2015

Role of Non-Muscle Myosin II and Calcium in Zebrafish Midbrain-Hindbrain Boundary Morphogenesis

Srishti Upasana Sahu
University of Wisconsin-Milwaukee

ROLE OF NON-MUSCLE MYOSIN II AND CALCIUM IN ZEBRAFISH MIDBRAIN-HINDBRAIN BOUNDARY MORPHOGENESIS

by

Srishti Upasana Sahu

A Thesis Submitted in

Partial Fulfillment of the

Requirements for the Degree of

Master of Science

in Biological Sciences

at

The University of Wisconsin-Milwaukee

May 2015

ABSTRACT
ROLE OF NON-MUSCLE MYOSIN II AND CALCIUM IN ZEBRAFISH MIDBRAIN-HINDBRAIN BOUNDARY MORPHOGENESIS

by

Srishti Upasana Sahu

The University of Wisconsin-Milwaukee, 2015
Under the Supervision of Dr. Jennifer H. Gutzman, Ph.D.

Elucidating the molecular mechanisms that play a role in cellular morphogenesis is critical to our understanding of brain development and function. The midbrain-hindbrain boundary (MHB) is one of the first folds in the vertebrate embryonic brain and is highly conserved across species. We used the zebrafish MHB as a model for determining the molecular mechanisms that regulate these cell shape changes. Cellular morphogenesis is tightly regulated by signaling pathways that rearrange the cytoskeleton and produce mechanical forces that enable changes in cell and tissue morphology. The generation of force within a cell often depends on motor proteins, particularly non-muscle myosins (NMII). We found that non-muscle myosin IIA (NMIIA) regulates cell length at the MHBC, while NMIIB regulates cell width throughout the MHB region. The novel discovery of distinct roles for the NMII proteins leads to the question of what directs them to function differentially. We hypothesize that the two proteins are activated by differential upstream signaling pathways. We investigated the role of calcium signaling in zebrafish MHB morphogenesis. Inhibition of cytosolic calcium by the pharmacological drug, 2-APB showed that calcium regulates MHBC cell length, a phenotype similar to NMIIA

knockdown. We further show that the shorter MHBC cell length phenotype seen by overactivation of NMII is rescued by inhibition of cytosolic calcium. Thus, we hypothesize that calcium signals differentially to NMIIA, and not NMIIB. Further investigation of these pathways will help answer the question of how NMII proteins are regulated to carry out distinct functions. Identifying these mechanisms will advance the understanding of the molecular basis for morphogenetic processes during brain formation and are likely to be applicable to developmental events throughout the embryo.

ମୁଁ ମୋର ଏଇ କୃତି ମୋ ମା, ସ୍ତୁତି ସାହୁ କୁ ଉତ୍ସର୍ଗ କରୁଛି...

ଯାହା ସ୍ନେହ, ସହଯୋଗ ଓ ପ୍ରୋତ୍ସାହନ ରୁ

ମୁ ଆଜି ଏଇ ସଫଲତା ପ୍ରାପ୍ତ କରି ପାରିଛି

TABLE OF CONTENTS

LIST OF FIGURES

SUPPLEMENTAL FIGURES

LIST OF ABBREVIATIONS

2-APB	2-aminoethoxy phenyl borate
Co-IP	co-immunoprecipitation
DMSO	dimethyl sulfoxide
hpf	hours post fertilization
IP3	inositol 1,4,5- triphosphate
IP3R	inositol 1,4,5- triphosphate receptor
NMII	non-muscle myosin II
mGFP	membrane green fluorescent protein
MHB	midbrain-hindbrain boundary
MHBC	midbrain-hindbrain boundary constriction
MLC	myosin light chain
MLCK	myosin light chain kinase
MO	morpholino
MRLC	myosin regulatory light chain
mRNA	membrane RNA
pMLC	phospho myosin light chain
ss	somite stage

ACKNOWLEDGEMENTS

I find myself fortunate to have landed upon this project, which was a chance of effort, and last moment luck. The research that I was able to carry out in the process of this thesis was a topic I had ruminated about from the time I fell in love with biology. I am grateful to my advisor, Dr. Jennifer Gutzman, for her guidance and patience. Her passion ignited enthusiasm in me and helped me carry out this thesis work with persistence. I hope to have acquired, amongst others, some of her attention to detail abilities, including her ability to identify any discrepancies in font size in one glance.

I am extremely thankful to my committee members, Dr. Ava Udvadia and Dr. Kurt Svoboda, not just for their valuable inputs in my project, but for also taking special interest in guiding me through my career path. I could not have asked for better lab mates, who were always there to extend their help and support in research, and otherwise. I would also like to thank my little zebrafish embryos, without whom this thesis would definitely not have been possible. On days when things didn't go that well, just looking at the beauty of life under the microscope made me ponder over the biological and philosophical questions of life, reminding me of the reason why I was there.

I have been lucky to have made some wonderful friends upon moving to a new country. Without them, life in and outside of graduate school would not have been bearable. Lastly, without the continual support, love and understanding of my family, I could not have achieved all that I have today and for that, I am much grateful to them.

I dedicate this thesis to my mother, Stuti Sahu, who has always been a source of encouragement for me. Even if geographically located on opposite sides of the globe, her guidance through my life decisions is reflected in my success today.

CHAPTER 1

INTRODUCTION

A. BRAIN MORPHOGENESIS

Morphogenesis is a developmental process that gives shape to an organism and may occur at the level of a cell or tissue. Proper shape elicits proper function and this demonstrates the importance of morphogenesis in the context of structure-function abnormalities. Developmental disorders such as neural tube defects result from defects in morphogenesis and while birth defects are as frequent as one in every thirty three babies, 70 percent of birth defect causes are still unknown indicating the importance of determining the molecular mechanisms leading to these developmental disorders (Rynn, 2009).

During development, tissue morphogenesis plays an important role in giving rise to vital organs such as the brain, a highly complex and dynamic organ that controls the entire body. Brain morphogenesis begins early in development and involves the rearrangement of cells and folding of tissue sheets to give it a characteristic shape. Any structural abnormality in the formation of the brain, as seen in neural tube defects such as anencephaly and hydrocephaly can have adverse effects often resulting in fatal disruption of regular brain function. Brain morphogenesis begins with neurulation- the process of neural tube formation from the ectoderm (Colas and Schoenwolf, 2001) (Fig. 1A). Post neurulation, the neural tube, formed from a single layer of pseudo-stratified columnar epithelial cells, undergoes a

series of morphogenetic changes leading to tissue folding that divides the tube into the forebrain, midbrain and hindbrain (Lowery and Sive, 2009) (Fig. 1B). This process of fold formation occurs alongside the formation of the brain ventricular system within the neural tube. The ventricles of the brain constitute an interconnected system of cavities where cerebrospinal fluid is produced and circulated. The deepest point of constriction between the midbrain and hindbrain, the midbrain-hindbrain boundary constriction (MHBC), is one of the first folds formed during vertebrate brain morphogenesis (Gutzman et al., 2008). The midbrain eventually forms part of the tectum, responsible for auditory and visual reflexes in the adult brain; while the hindbrain forms the cerebellum, pons and medulla, parts of the adult brain with vital functions in motor control, cognitive functions, hearing and equilibrium (Louvi et al., 2003). Being a distinct and important first fold in the developing vertebrate brain, the midbrain-hindbrain boundary serves as a useful model to study brain formation and has allowed us to uncover novel mechanisms of tissue morphogenesis (Gutzman et al., 2015).

B. ZEBRAFISH MHB DEVELOPMENT AND MORPHOGENESIS MODEL

The midbrain-hindbrain boundary (MHB) is one of the earliest folds visible in the embryonic brain and is highly conserved across vertebrate species including human, mouse, chick and zebrafish (Lowery and Sive, 2009). The MHB tissue is the isthmic organizer, a neural signaling center that expresses transcription factors and signaling molecules that pattern the tissue to give it a mesencephalic

(midbrain) or metencephalic (hindbrain) fate (Louvi et al., 2003). Before morphogenesis, the neural tissue is patterned by the *Fgf* and *Wnt* genes to establish cell fates. Fgf8b activates the Ras-ERK pathway and induces cerebellar development (Sato et al., 2004). Wnt8 is involved in posteriorisation of the neural tube and is important for the onset of *otx2* and *gbx1* expression (Rhinn et al., 2005). *Otx2* expression establishes a midbrain fate while *gbx2* determines a hindbrain fate (Barkovich et al., 2009; Dworkin and Jane, 2013). The different stages of MHB tissue establishment are positioning, induction, and maintenance. The expression of patterning genes involved during each these steps have been relatively well studied (Martinez, 2001). Morphogenesis is now considered a fourth, distinct stage in MHB development and the molecular mechanisms that regulate MHB morphogenesis are the focus of more recent studies (Giraldez et al., 2005; Gutzman et al., 2008).

We use zebrafish as a model system to study the mechanisms involved in the formation of the midbrain-hindbrain boundary. Zebrafish is favorable due to various advantages. Zebrafish are easy to handle, breed, and have a faster embryonic developmental timeline when compared to other models (Kimmel et al., 1995). They produce large clutches of embryos which undergo synchronous development, allowing for a large sample size in experiments. Ex-utero development and transparency of embryos make it an excellent vertebrate model for early developmental studies because it allows for micromanipulation and high-resolution imaging to visualize cell shapes. Importantly, 70 percent of protein-

coding human genes have at least one ortholog in the zebrafish, which helps to correlate findings between the two organisms (Howe et al., 2013).

Zebrafish midbrain-hindbrain boundary morphogenesis occurs between 18 and 24 hours post fertilization (hpf) (Fig. 2). At 18 hpf, or 18 somite stage (ss), the hindbrain ventricle first starts opening, followed by the midbrain ventricle at around 20 hpf, or 22 ss. As these ventricles inflate due to secretion of embryonic cerebrospinal fluid, the neural tube gets segregated into three regions- the forebrain, midbrain and hindbrain. Boundaries between each of these regions begin appearing as a result of folding of the neuroepithelium. The junction between the midbrain and the hindbrain, the midbrain-hindbrain boundary is seen as a distinct fold in the tissue starting at 20 hpf (Gutzman et al., 2008). This progressive formation of the MHB to a distinct fold in the early neural tube structure can be observed through further time points from 22 hpf (24 ss) to 24 hpf (prim-6) (Fig. 2A-D). The cell shape changes occurring during this time have been previously characterized (Gutzman et al., 2008). At 17 hpf, the neuroepithelial cells of the MHB are of similar length. By 21-22 hpf, cells at the MHB shorten by about 25% in comparison to cells on the hindbrain side of the MHB and they further undergo apical expansion and basal constriction such that by 24 hpf, the midbrain-hindbrain boundary constriction (MHBC) is completely formed and the ventricles are open (Gutzman et al., 2008). We were interested in the early time point of 22 hpf or 24 ss, because this is when the tissue first folds between the midbrain and the hindbrain, forming the midbrain-hindbrain boundary. Understanding the

mechanisms that drive the formation of this initial fold will enable us to understand more complex morphogenetic processes that occur during development.

C. CELL SHAPE CHANGES LEAD TO TISSUE MORPHOGENESIS

During epithelial tissue morphogenesis, cells undergo changes in shape to enable the tissue to fold. Cellular morphogenesis can occur in various ways depending on the morphogenetic event required during that particular time of development. Some cell shape change mechanisms have been extensively studied in various models and will be the focus of this section.

An epithelial tissue has a distinct apical-basal polarity and cells of that tissue can change shape in multiple ways (Fig. 3). Cells can elongate to become columnar which happens when neural plate is formed, as the first step of neurulation (Schoenwolf and Franks, 1984) (Fig. 3A). Epithelial cells also undergo shortening along the apicobasal axis as seen in initial midbrain-hindbrain boundary formation, leading to tissue folding (Fig. 3B) (Gutzman et al., 2008). Additionally, shortening may occur along the lateral sides to cause flattening of tissue as seen during epiboly in zebrafish and frog embryos, and in drosophila wing imaginal disc formation (Fig. 3C) (Barkovich et al., 2009; Fristrom, 1988; Keller, 1980). In the zebrafish Kupffer's vesicle, a combination of regionalized cell shape changes occur where anterior cells elongate and posterior cells shorten, displaying apical expansion (Wang et al., 2012). Additionally, cells can undergo changes on either the apical side or the basal side. Apical constriction is a common cell shape change

that occurs during many developmental processes (Fig. 3D) (Sawyer et al., 2010). It occurs during ventral furrow formation in *Drosophila* (Kam et al., 1991; Leptin, 1999), gastrulation in *C.elegans* (Lee and Goldstein, 2003) and in vertebrates, involving bottle cells of the *Xenopus* dorsal marginal zone (Lee and Harland, 2007) and cells in the mouse embryo during neural tube closure (Bush et al., 1990). Although apical constriction has been well studied, examples of basal constriction in development are few (Fig. 3E). During brain morphogenesis, cells at the midbrain-hindbrain boundary undergo basal constriction to form the distinct constriction between the midbrain and hindbrain (Gutzman et al., 2008). Basal constriction has also been described in zebrafish during optic cup morphogenesis (Martinez-Morales et al., 2009).

Individual cell shape changes lead to tissue morphogenesis and the basic cell shape changes discussed above are usually a precursor step to more complicated tissue shape changes like folding, invagination and evagination. Invagination occurs when the epithelial tissue folds, often as a consequence of apical constriction (Llimargas and Casanova, 2010), while evagination leads to outpocketing of cells (Schock and Perrimon, 2002).

Cell shape changes are vital to morphogenesis and although there have been studies in various organisms during different stages of development, extensive studies of cellular morphogenesis in vertebrate systems is lacking. Here, we have studied the cell shape changes, and the molecular mechanisms by which those changes are regulated during midbrain-hindbrain boundary morphogenesis in a vertebrate model, the zebrafish.

D. FACTORS INFLUENCING CELL AND TISSUE MORPHOGENESIS

Morphogenetic processes are regulated by multiple factors involving tissue specific gene expression and protein regulation. Genes are transcribed and mRNA is translated to produce functional proteins. These proteins signal downstream to direct mechanical changes that ultimately cause cell and tissue morphogenesis (Fig. 4). Mechanical forces are ones that govern the architecture of the cell and establish the stability of the tissue. This stability of epithelia is dependent on two factors- the cytoskeleton and the extracellular matrix, which determines the strength and structure of the cell inside and outside (Fletcher and Mullins, 2010). Some of these factors that are critically important for morphogenesis will be discussed next.

Cytoskeleton

The cytoskeleton is a network of intracellular proteins that comprise of microfilaments, microtubules and intermediate filaments. Within the cell, the cytoskeleton gives it a backbone of support. Most cell shape changes discussed in the previous section require microfilaments or microtubules to carry out shape changes, and these will be discussed next (Mammoto and Ingber, 2010).

Actomyosins

Actin filaments are helical polymers of the protein, actin. This cytoskeletal component is highly enriched at the cell periphery, forming the cell cortex. Myosins

are specialized motor proteins that associate with actin and move along actin filaments to carry out force transduction (Fletcher and Mullins, 2010). They are a huge family of proteins, and non-muscle myosins II are a class of proteins found in all cells that are actively involved in cellular morphogenesis. Actomyosin complexes are known to play an important part in a variety of cellular functions involving cell motility, cell division, maintenance of tissue integrity, morphogenesis, and cell shape (Vicente-Manzanares et al., 2009). Apical constriction, one of the well-studied cell shape changes discussed above, is attributed to actomyosin activity. It is responsible for pulsed contractions that drive morphogenetic processes during gastrulation in *C. elegans*, *Drosophila* and *Xenopus* (Lee and Goldstein, 2003; Lee and Harland, 2007; Martin et al., 2009). Apical constriction is just one example depicting the role of actomyosins, as they play a role in almost all other cell shape changes (Fristrom, 1988; Schock and Perrimon, 2002).

Microtubules

The cytoskeleton is also comprised of microtubules, which are polymers of the protein tubulin and they arise from the centrosome. Microtubules are associated with the motor proteins, kinesin, that move away from the centrosome and dynein, that move towards the centrosome (Fletcher and Mullins, 2010). Microtubules are primarily responsible for cell division and cargo movement across the cell but they are also required for cell shape maintenance in events such as gastrulation in *Xenopus* and zebrafish (Lee and Harland, 2007; Sepich et al., 2011). Disruption of microtubule networks leads to increase in actin networks and adhesion dependent

signaling which hints toward microtubule involvement in regulation of cell shape (Elbaum et al., 1999; Rodionov et al., 1993).

Extracellular matrix

The physical properties of tissues are also determined by the extracellular matrix (ECM), which is composed of a variety of polysaccharides and proteins that form a meshwork outside the cell. The proteins produced here can be fibrous such as collagen and elastin, or adhesive, such as fibronectin and laminin. In epithelial cells, the boundary between the epithelium and the underlying connective tissue is called the basal lamina and laminin allows attachment of the tissue to the basal lamina (Parsons et al., 2010). Epithelial tissues have an apical-basal polarity with the lamina being on the basal side. During neural tube morphogenesis, constriction along the basal side allows formation of the zebrafish midbrain-hindbrain boundary, and this process has been shown to be laminin dependent (Gutzman et al., 2008).

Cell adhesion

Cell adhesion is the binding of cells within a tissue, to each other or to the extracellular matrix and is an important factor in morphogenesis, especially when cell movement is involved. The basal lamina is connected to the cell through cell-matrix adhesion molecules, integrins. Integrins are transmembrane receptors that are connected to the ECM through laminin and internally, to cytoskeletal actin stress filaments which allow the transmission of physical forces through the tissue, enabling morphogenesis (Barone and Heisenberg, 2012). Focal adhesion

molecules serve as a mechanical link to transduce force between the cell and the matrix. Integrin mediated focal adhesion kinase (FAK) signaling connects the basal lamina to intracellular actomyosins (Westhoff et al., 2004). FAK is localized at focal adhesions, interacts with paxillin, and is required for microtubule and spindle reorientation, making it essential for epithelial morphogenesis, determined by studies in *Xenopus* embryos and human cell lines. (Petridou and Skourides, 2014). Adherens junctions anchor the cytoskeleton, specifically actin filaments of a cell to that of another cell or the ECM. Neighboring cells within the epithelial tissue are connected through cell-cell adhesion molecules, cadherins. Cadherins are calcium dependent cell adhesion molecules and they play an important role in brain and nervous system development (Redies and Takeichi, 1996). Various cadherin isoforms are required during different stages of nervous system development such as neural tube and neuroepithelial layer formation, boundary formation and in the formation of brain nuclei and ganglia (Hirano and Takeichi, 2012).

Cell migration

Cell migration, or movement of cells, is critical to development as it allows cells to reach their destined location where they can differentiate and lead to development of organs (Aman and Piotrowski, 2010). Some of the most widely studied migratory events are gastrulation and neural crest cell migration. Cell migration in individual cells occurs through extension of actin filled lamellipodia, indicating the importance of the cytoskeleton in cellular morphogenesis (Giannone et al., 2007; Ponti et al., 2004). A decrease in cell adhesion causes an increase in cell motility, showing the interdependence of some of the factors discussed (Du et al., 2012).

Cell intercalation

Cell intercalation is the interspersing of individual cells between other cells and is also an important factor in some cellular morphogenetic events. The classic example of cell intercalation occurs during the process of convergence and extension. During this process mediolateral cells intercalate between cells along the anteroposterior axis of the embryo resulting in its narrowing and elongation along the anteroposterior body axis (Sepich et al., 2005). Cells also undergo rearrangement in the form of radial intercalation as seen during epiboly in *Xenopus* embryos where the inner layer of cells move out to the superficial layer and undergo convergence and extension. This process is also critically dependent upon cell-cell adhesion, again showing interconnection between factors (Marsden and DeSimone, 2001).

Cell division

Morphogenetic changes can occur due to the active growth of tissue which is regulated by region specific increases in cell proliferation, making cell proliferation another essential regulator of morphogenesis. In kidney development, the elongation of renal tubes requires extensive cell division (Jung et al., 2005). Wound healing is another example where cell division is required for replacement of lost or damaged tissue. In the drosophila wing imaginal disc, cells respond to tissue damage by changing their cell division orientation (Ruiz and Serras, 2014). In contrast to increased cell division, at times, cell division is stalled for the morphogenetic event to proceed, as seen in drosophila gastrulation to enable cell

shape changes (Seher and Leptin, 2000). In the zebrafish brain, greater cell proliferation is observed in the midbrain and hindbrain ventricle regions of the neural tube, indicating the role of cell proliferation in ventricle inflation (Lowery and Sive, 2005).

Cell death

Cell death is an integral process in development and has been described classically in *C. elegans* to occur by a tightly controlled genetic pathway involving genes *ced-3*, *ced-4* and *ced-9* that induce programmed cell death, apoptosis (Ellis et al., 1991). Cells in the interdigital spaces during animal limb formation undergo extensive apoptosis (Merino et al., 1999) and significant amounts of cell death occurs during *Drosophila* head involution and moth metamorphosis (Ellis et al., 1991; Grether et al., 1995).

Thus, morphogenesis can be controlled through a variety of complex processes. Elucidating the molecular mechanisms that regulate cell shape changes during brain morphogenesis has been challenging due to the complexities of the vertebrate system, the number of potential signaling pathways, and the likely interactions between factors and pathways. We are using the developing zebrafish midbrain-hindbrain boundary to understand the factors that regulate cell shape changes during morphogenesis.

E. NON-MUSCLE MYOSIN II

Non-muscle myosin II proteins are cytoskeletal molecular motors present in all cell types and, in association with actin filaments, carry out vital functions of cell

division, cell migration and cell shape maintenance (Sellers, 2000). Using the zebrafish midbrain-hindbrain boundary as a model, we studied the role of non-muscle myosin II (NMII) in regulating cell shape changes occurring during this process.

Classification and structure

The myosins are a superfamily of 35 classes of ATP-driven motor proteins that work in coordination with actin filaments (Odronitz and Kollmar, 2007). The class II myosin family includes NMII proteins which are present in all eukaryotic cells and are known to be involved in cell migration, cell adhesion, cytokinesis and cell shape (Sellers, 2000). Structurally, all class II myosins have a pair of heavy chains and two pairs of light chains- essential and regulatory light chains (Golomb et al., 2004) (Fig. 5). The heavy chains have a globular head domain and a long tail domain that forms a coiled rod-like helical tail and a terminal non-helical end. The two pairs of light chains are attached non-covalently to the heavy chain at the neck domain (Fig. 5). The head domain contains the ATP and actin binding units which allow for a change in conformation of the head domain enabling the molecule to convert ATP energy to mechanical energy and move along actin filaments (Pollard and Korn, 1973). The essential light chain is required for filament assembly and stability, while the regulatory light chain, apart from filament stability, plays a critical role in regulation of the active state of the molecule (Vicente-Manzanares et al., 2009). Overall, myosin II can exist in a compact folded conformation due to its C-terminal tail domain being linked to the neck region by a ‘proline-kink’ or in an elongated, filamentous form, where multiple myosin II molecules assemble in a

parallel or anti-parallel fashion to form thick filaments (Onishi and Wakabayashi, 1982; Trybus et al., 1982). In the filament form, actomyosin complexes can transduce force within the cell and between cells in a tissue (Onishi and Wakabayashi, 1982; Trybus et al., 1982).

Isoforms and functional differences

In mammals, there are three NMII isoforms, NMIIA, NMIIB and NMIIC, which differ from each other by the structure of their heavy chains. These are encoded by the genes *myh9*, *myh10* and *myh14*, respectively (Fig. 6) (Golomb et al., 2004). Zebrafish also have three isoforms with the exception that there are two ohnologs for the human *MYH9* gene- *myh9* and *myh9a* (Flicek et al., 2014). Although the three isoforms have a high degree of heavy chain sequence similarity with differences mainly in the terminal tail portion, they have different binding affinities to actin, which results in a difference in their kinetic properties (Heissler and Manstein, 2011; Kovacs et al., 2003; Wang et al., 2011).

All three gene isoforms have a vast, yet distinct tissue expression. This suggests that in spite of the high degree of sequence similarities between them, their activation state and kinetic properties enable them to have potentially distinct functions. NMIIA is predominantly expressed in platelets and spleen, NMIIB is expressed largely in neuronal tissues (Calaminus et al., 2007). Most human fetal tissues express significantly less amounts of NMIIC, in comparison to NMIIA and NMIIB (Golomb et al., 2004). NMIIC also has low expression in adult mouse tissues, with significant amounts detected only in lung tissue and in cell cultures (Ma et al., 2010).

Distinct functions for each of the isoforms have been identified which suggests that each may be differentially regulated. NMIIA is important for cell migration and knockout mice fail to develop a visceral endoderm layer (Sandquist et al., 2006). NMIIB functions in cell motility and tissue organization and these knockout mice display severe cardiovascular and brain defects including hydrocephaly (Getty et al., 2011; Tullio et al., 1997; Tullio et al., 2001). Being a recently identified homolog, compared to NMIIA and NMIIB, not much is known about the functional role and kinetics of NMIIC (Golomb et al., 2004; Heissler and Manstein, 2013). It has a lower homology of 62% between human and fish, compared to around 75% for NMIIA and 90% for NMIIB, and is more closely related to muscle myosin than to other NMII proteins (Flicek et al., 2014). Further, the NMIIC knockout mice survive to adulthood with no obvious phenotypes, while their IIA and IIB counterparts do not (Ma et al., 2010). As also mentioned earlier, NMIIC has low expression in fetal tissues (Golomb et al., 2004). Due to these reasons, we have focused our current study on the role of NMIIA and NMIIB in regulating brain morphogenesis.

Regulation of non-muscle myosin II activity

Activation by light chain phosphorylation

In the zebrafish, there are multiple isoforms of the myosin regulatory light chain; however, only one isoform has been identified to be specific for non-muscle myosin II (*myl12.1*) (Flicek et al., 2014). Activation of NMII molecules is primarily carried out by the phosphorylation of the regulatory light chain at two sites- serine-19 and threonine-18 (Somlyo and Somlyo, 2003). Phosphorylation at either ser-19 alone, or both ser-19 and thr-18 increases the Mg^{2+}-ATPase activity of myosin and its

association with actin, causing activation of the entire molecule (Somlyo and Somlyo, 2003; Vicente-Manzanares et al., 2009). The myosin specific enzyme, myosin light chain kinase (MLCK), phosphorylates and activates the regulatory myosin light chain (MLC) (Nishikawa et al., 1984). There are three MLCK isoforms- a long non-muscle isoform, a short smooth muscle isoform, and a telokin with no enzymatic activity (Guo et al., 2013). The non-muscle MLCK has been shown to be involved in cell migration (Reynoso et al., 2007) and cell adhesion (Xu et al., 2008). It is also known to be regulated in a calcium-calmodulin dependent manner in smooth muscle (Martinsen et al., 2013; Mizuno et al., 2008). A variety of other enzymes also phosphorylate the MLC and they include Rho, Rho associated coiled-coil kinase (ROCK), myotonic dystrophy kinase-related cdc42-binding kinase (MRCK), protein kinase A (PKA) and mitogen activated protein kinase (MAPK), among others (Fig. 7) (Betapudi, 2014; Matsumura, 2005; Vicente-Manzanares et al., 2009). Myosin phosphatase dephosphorylates the MLC, inactivating NMII. Rho also inhibits *mypt1*, a subunit of the myosin phosphatase, and in this way it can indirectly activate NMII (Chu et al., 2012).

Activation by heavy chain phosphorylation

NMII proteins can also be regulated by multiple serine and threonine phosphorylation sites on the tail domain of the heavy chain, some of which are specific to individual homologs. The NMIIA heavy chain has a thr-1800, ser-1803 and ser-1808 site in the coiled-coil portion of the tail and a ser-1943 site in the non-helical tail domain, which is phosphorylated by casein kinase II (Clark et al., 2008). Absence of this phosphorylation prevents the binding of NMIIA to s100A4, member

of the s100 family of calcium binding proteins. This results in inhibition of filament assembly, disrupting its regular function (Dulyaninova and Bresnick, 2013).The NMIIB heavy chain also has a ser-1937 site phosphorylated by protein kinase C (PKC), which is responsible for filament assembly (Vicente-Manzanares et al., 2009). These distinct sites in the two homologs phosphorylated by different enzymes, but carrying out the same function could indicate a differential regulation of the NMII proteins at the level of the two heavy chains (Dulyaninova and Bresnick, 2013).

Inactivation of non-muscle myosin II

Phosphorylation on other sites of the MLC, including ser-1, ser-2 and thr-9 and dephosphorylation on ser-19 or thr-18 are known to deactivate NMII (Betapudi, 2014; Vicente-Manzanares et al., 2009). A myosin specific enzyme that directly dephosphorylates the MLC is the myosin phosphatase, which results in inactivation of the myosin molecule (Ito et al., 2004). Myosin phosphatase has three subunits- PP1c, MYPT1 and M20. PP1c and M20 interact with the N and C terminal domains of MYPT1 and affect its function. The PP1 subunit of myosin phosphatase dephosphorylates the MLC, inactivating the entire myosin molecule (Fig 7). *Mypt1* zebrafish mutants show an abnormal neuroepithelial cell shape phenotype in the hindbrain, indicating the importance of NMII in brain development (Gutzman and Sive, 2010). *Mypt1* has also been implicated in key developmental processes involving convergence extension, gastrulation, and dorsal closure which involve NMII functions (Conti and Adelstein, 2008; Franke et al., 2005; Heissler and Manstein, 2013).

Upstream signaling pathways regulating NMII phosphorylation state

Based on the vast literature of the structure and function of NMII isoforms, it is surprising that it is still not well understood if they function differentially and how they are differentially activated. Many studies in the last few decades have tried to tease out the mechanism in which NMII is regulated to carry out its function. The multiple kinases and phosphatases discussed in the previous section only depict the regulation of NMII at one level. Upstream of each of these enzymes are multiple signaling molecules that carry out molecular cross-talk within the cell and extracellularly. NMII is activated by ROCK mediated phosphorylation of the MLC (Nakajima and Tanoue, 2010). Shroom3 is a recently identified protein required for apical constriction in chick and mouse neural tube closure (Nishimura and Takeichi, 2008). It recruits ROCK to apical cell junctions. *Shroom3* mutants and morphants show reduced accumulation of F-actin and phosphorylated MLC, indicating its role in regulating NMII (Hildebrand and Soriano, 1999; Nishimura and Takeichi, 2008). In the same context, the Rho-ROCK signaling axis has been widely studied for its role in morphogenetic processes that especially involve cytoskeletal remodeling and cell shape changes (Suzuki et al., 2012). Inhibition of Rho causes a decrease in phosphorylation of the MLC and leads to defects in neural tube closure (Kinoshita et al., 2008). Further, the Rho-ROCK axis is known to be regulated by Wnt and the planar cell polarity (PCP) pathway in vertebrate cardiac development (Phillips et al., 2005). Calcium mediated regulation of myosin II has been studied intensely in muscle contraction, and more recently, in non-muscle cells as well (Szent-Gyorgyi, 1975). Calcium regulates myosin II

phosphorylation through MLCK in smooth muscle and endothelium (Martinsen et al., 2013). The JNK pathway also controls NMII localization in fly wound healing (Kwon et al., 2010). Thus, there are multiple signaling pathways regulating NMII and we are interested in understanding this regulation during zebrafish midbrain-hindbrain boundary morphogenesis. We are specifically interested in the role of calcium signaling, which will be covered in the next section.

F. CALCIUM SIGNALING PATHWAY

Calcium signaling in development and regulation of cell shape

Calcium has been implicated in early development during various events (Slusarski and Pelegri, 2007). Waves of calcium are observed in dorsal explants of *Xenopus* embryos and inhibition of calcium causes convergence and extension defects (Wallingford et al., 2001). In zebrafish embryos, intercellular calcium waves are observed at the margin of gastrulating embryos (Gilland et al., 1999). Calcium signaling is also important in maintenance of left-right body axis during development. In zebrafish, cilia in the Kupffer's vesicle collectively beat in a coordinated left-sided rotation to produce a calcium gradient that regulates left-right symmetry of visceral organs (McGrath et al., 2003; Sarmah et al., 2005). Similarly, in chick embryos, left-right axis determination requires extracellular calcium waves (Raya et al., 2004). Calcium channel blockade causes defects in organ formation, as seen in heart morphogenesis (Porter et al., 2003). Thus, calcium is required in many vital developmental processes and could potentially be important in midbrain-hindbrain boundary morphogenesis.

Calcium also plays a role in cell shape changes. Regulation of platelet shape has been widely studied and is regulated by calcium induced phosphorylation of the MLC (Porter et al., 2003). Calcium entry into the cell through store operated calcium channels (SOC) causes cell shape changes in pulmonary endothelial cells by rearrangement of microfilaments (Moore et al., 1998). During wound healing in the *Xenopus* ectoderm, cell shape changes at the edge of the wound are disrupted when calcium levels are pharmacologically altered (Stanisstreet, 1982). Thus, we hypothesize that calcium may have a critical role in regulation of cell shape changes that mediate brain morphogenesis.

Overview of the calcium signaling pathway

Calcium signaling pathways are highly versatile and signal to affect various processes within the cell. Since calcium is not metabolized by the cell, it is stored inside cells and released when required (Berridge, 1997). A delicate balance of cytosolic calcium ion concentration is maintained by various channels on the plasma membrane or membranes of the storage organelles (Duchen, 2000). The basic mechanism of this pathway is calcium induced calcium release, where an initial amount of calcium induces the release of greater amounts of calcium from its intracellular stores, triggering regenerative calcium waves (Berridge et al., 2000). Apart from calcium entry into cells from the external environment through channels in the plasma membrane, calcium within the cell can be released from membrane bound organelles that store calcium which include the endoplasmic reticulum (ER) and mitochondria (Fig. 8) (Duchen, 2000). A major source of stored intracellular calcium in non-neural cells is the endoplasmic reticulum, the release

of Ca^{2+} ions depends on the opening of specific membrane channels- the ryanodine (Ryr) receptor channels, SERCA channels or the inositol triphosphate receptor (IP3R) channels (Putney, 1986). The Ryr receptor channels are predominantly present in cardiac and skeletal muscles and are regulated by cytosolic calcium through calcium-induced calcium release (Fill and Copello, 2002). The SERCA channels or the sarco/endoplasmic reticulum Ca^{2+}-ATPase channels are exclusive to muscle cells and transport calcium ions from the cytosol into the sarcoplasmic reticulum (Gomez-Viquez et al., 2003). The opening of the IP3R channels is stimulated by inositol 1,4,5- triphosphate (IP3) which is a product of a signaling pathway initiated at the cell membrane through extracellular ligands. Hormones or growth factors can bind to extracellular receptors such as the receptor tyrosine kinases (RTK) or G protein coupled receptors (GPCR), activating phospholipase C (PLC), that converts membrane bound phosphatidylinositol 4, 5 bisphosphate (PIP_2) to IP_3 and diacylglycerol (DAG) (Slusarski and Pelegri, 2007). The release of IP3 then allows release of calcium from the ER by stimulation of the IP3R (Fig. 8). Once released, calcium can act as a secondary messenger and signal to downstream molecules like troponin C, calmodulin and cyclic AMP (cAMP) which are calcium dependent proteins that can, in turn signal to various downstream effectors (Slusarski and Pelegri, 2007).

Unlike other signaling molecules, which are synthesized in the body and are ultimately products of cellular transcription and translation, calcium, in order to be able to transmit signals across the cellular system, needs to bind to certain proteins or kinases that can transmit and induce downstream effects (Yanez et al., 2012).

Several calcium binding molecules exist such as calmodulin and calcineurin (Kawasaki et al., 1998). Calcineurin, or protein phosphatase IIB, is activated by calcium-calmodulin and is a serine/threonine protein phosphatase that links calcium to phosphorylation states of proteins. Calmodulin is one of the extensively studied calcium-binding proteins. It is directly affected by the concentration of intracellular calcium. Interestingly, MLCK is affected by calmodulin levels, indicating that actomyosins could be potential downstream effectors of calcium (Van Lierop et al., 2002).

Calcium signaling and regulation of non-muscle myosin II

The role of calcium in regulating myosin has been classically studied in skeletal muscles with respect to its function in muscle contraction (Szent-Gyorgyi, 1975). In comparison, the regulation of actomyosins by calcium signaling in non-muscle models is less studied (Somlyo and Somlyo, 2003). Calcium has been shown to regulate NMII through MLCK in smooth muscle and endothelium (Martinsen et al., 2013; Watanabe et al., 2001). However, its regulation of NMII in development and morphogenetic processes are yet to be determined.

We know that actin filaments in association with their molecular motors, myosins, drive cell shape changes during developmental processes such as germ band elongation, mesoderm invagination, dorsal closure and egg chamber elongation (He et al., 2010; Martin et al., 2009; Rauzi et al., 2010; Solon et al., 2009). Interestingly, most of these processes are also regulated by calcium signaling. For example, in the zebrafish embryo, at 75% epiboly, an actomyosin ring is formed along the margin and an increased amount of calcium is observed at the margin

during the epiboly stages (Popgeorgiev et al., 2011). We also know that NMII phosphorylation is carried out by MLCK, and it has been shown that the activation of MLCK is required for epiboly to progress (Popgeorgiev et al., 2011). Additionally, in the zebrafish embryo, misexpression of cAMP response element binding protein (CREB) causes defects in MHB morphogenesis (Dworkin et al., 2007). cAMP, being a common second messenger in the calcium signaling pathway, suggests possible calcium regulation of NMII in MHB formation (Dworkin et al., 2007; Dworkin and Jane, 2013).

In the current research, we have studied the role of NMII and its regulation by calcium signaling during MHB morphogenesis in zebrafish. We discover that NMIIA regulates cell length while NMIIB regulates cell width during MHB formation in zebrafish. We further find that calcium is required in this process, and that it specifically regulates MHBC cell length. These and future findings will be important in expanding our knowledge of the mechanisms of other similar developmental processes as well.

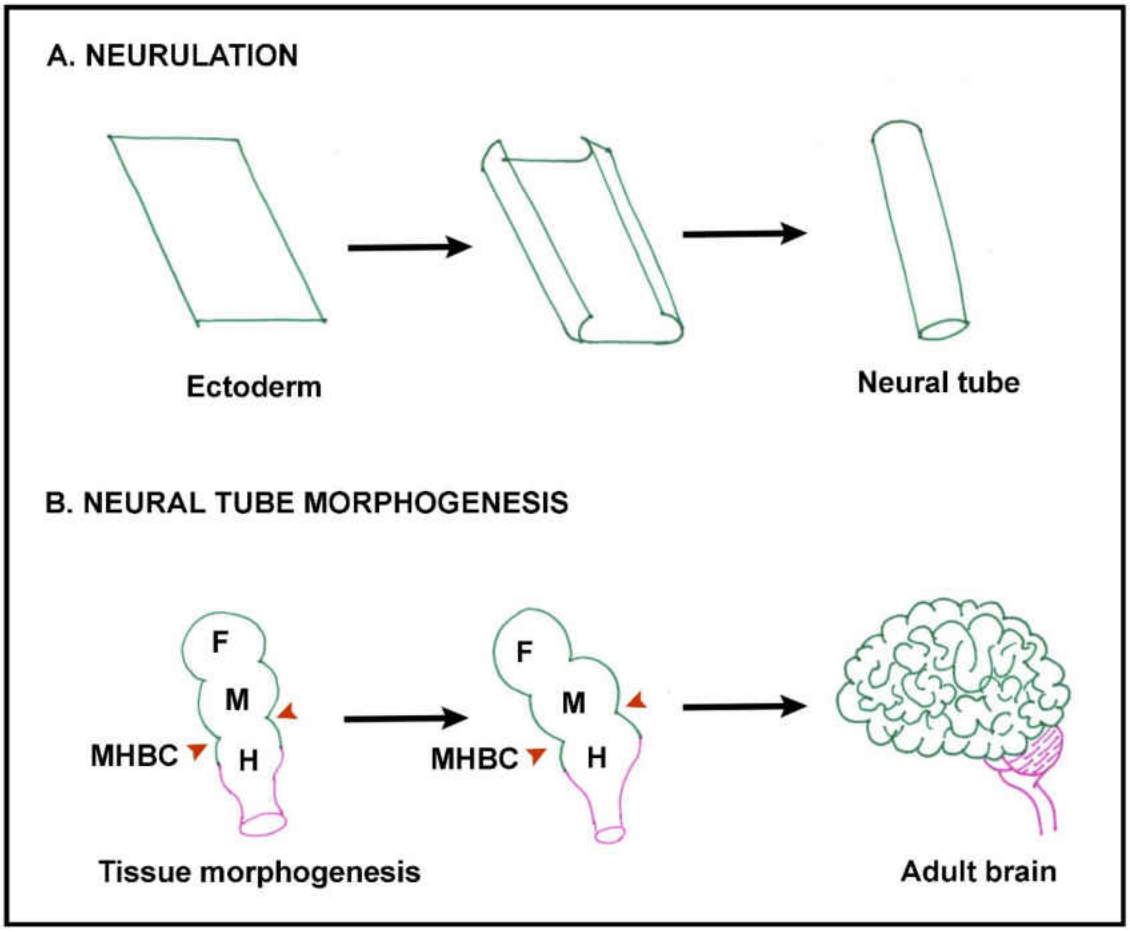

Figure 1. Schematic showing early brain development and morphogenesis. (A) Brain is derived from the ectoderm which folds to form the neural tube by the process of neurulation. (B) The neural tube undergoes morphogenesis to form the future forebrain, midbrain and hindbrain. The midbrain-hindbrain boundary constriction (MHBC) is a distinct visible fold (red arrowheads). The neural tube develops and differentiates to eventually form the complex adult brain. F, Forebrain; M, Midbrain; and H, Hindbrain.

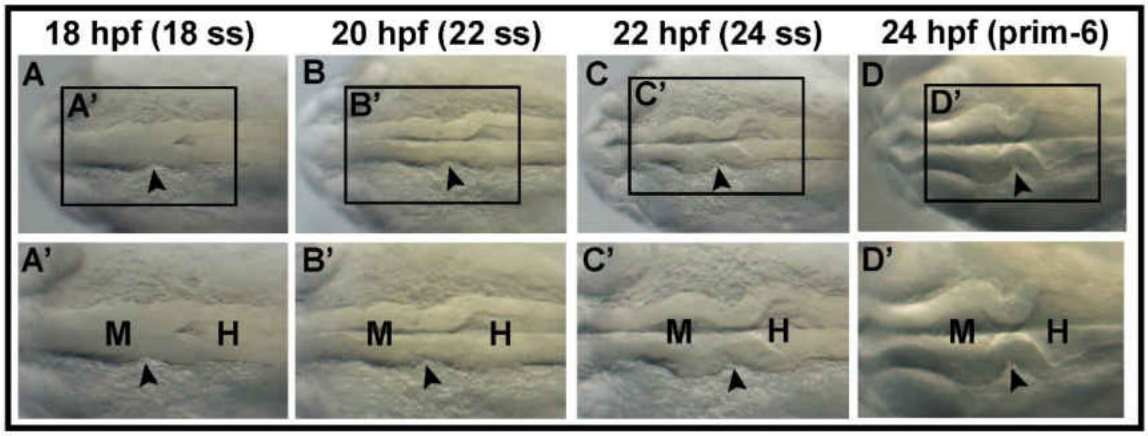

Figure 2. Midbrain-hindbrain boundary formation in zebrafish. (A-D) Brightfield dorsal images of zebrafish embryos showing midbrain-hindbrain boundary formation at (A) 18 hpf or 18 ss, (B) 20 hpf or 22 ss, (C) 22 hpf or 24 ss and (D) 24 hpf or prim-6. (A'-D') Enlarged images of boxed regions in A-D. Embryos are oriented anterior to the left and posterior to the right. Hpf, hours post fertilization; ss: somite stage; M, midbrain; H, hindbrain.

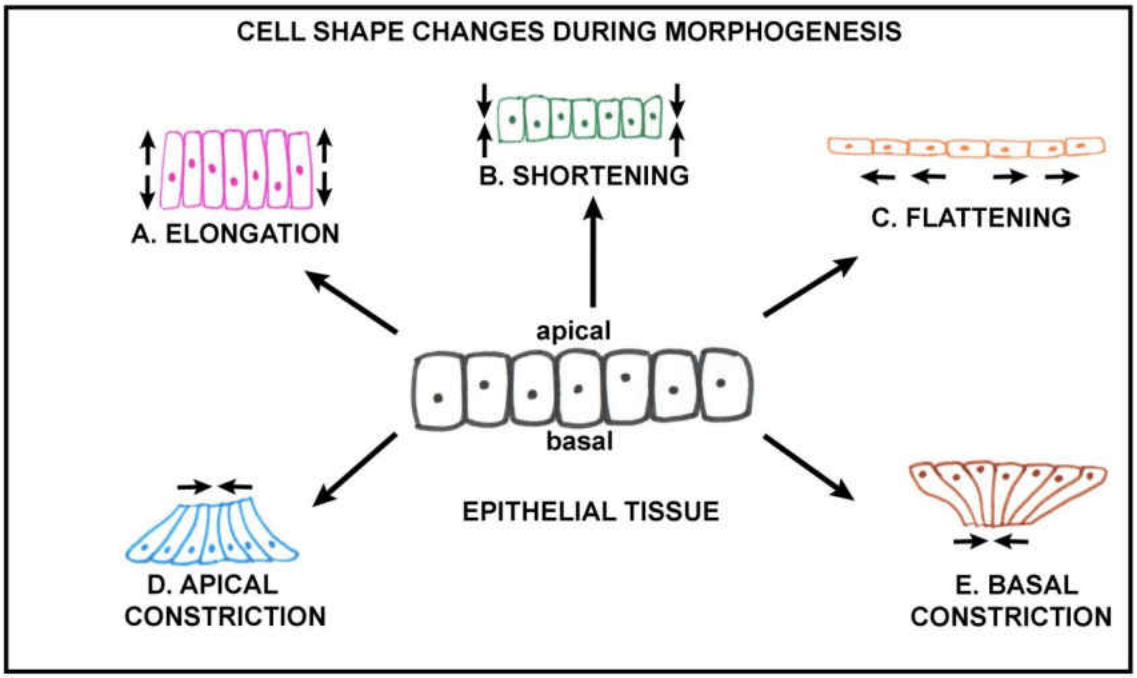

Figure 3. Schematic showing various cell shape changes that can occur in an epithelial tissue during morphogenesis. (A) cell elongation, (B) cell shortening, (C) flattening, (D) apical constriction, and (E) basal constriction.

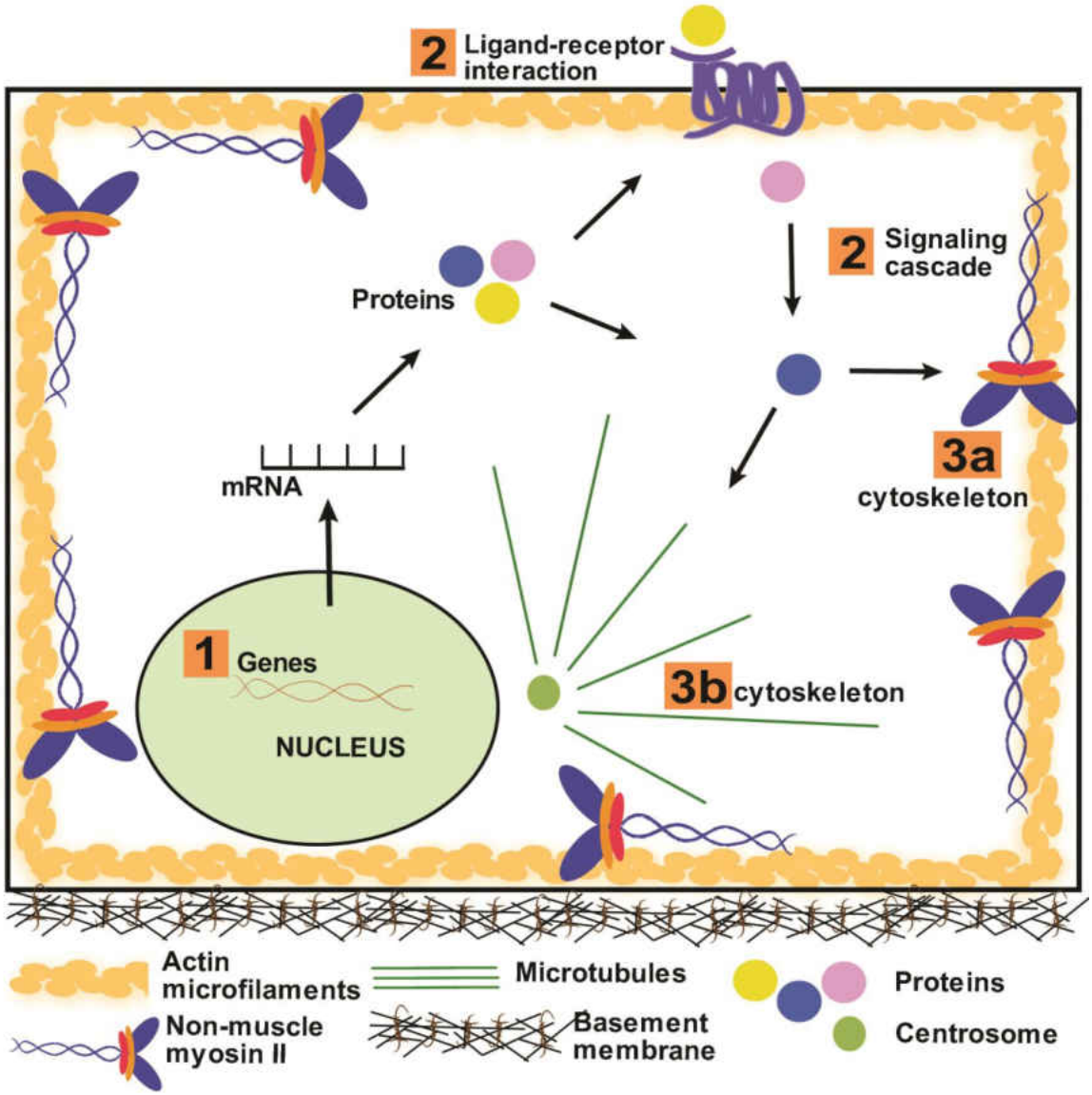

Figure 4. Schematic showing various cellular factors that can affect morphogenesis. 1. Specific gene expression is initiated in the nucleus and mRNA is transcribed and then translated to produce functional proteins. 2. Intracellular proteins and extracellular ligands signal to intermediate molecules. 3. Mechanical forces generated by cytoskeletal elements- (3a) microfilaments and (3b) microtubules ultimately carry out specific cell shape changes resulting in morphogenesis.

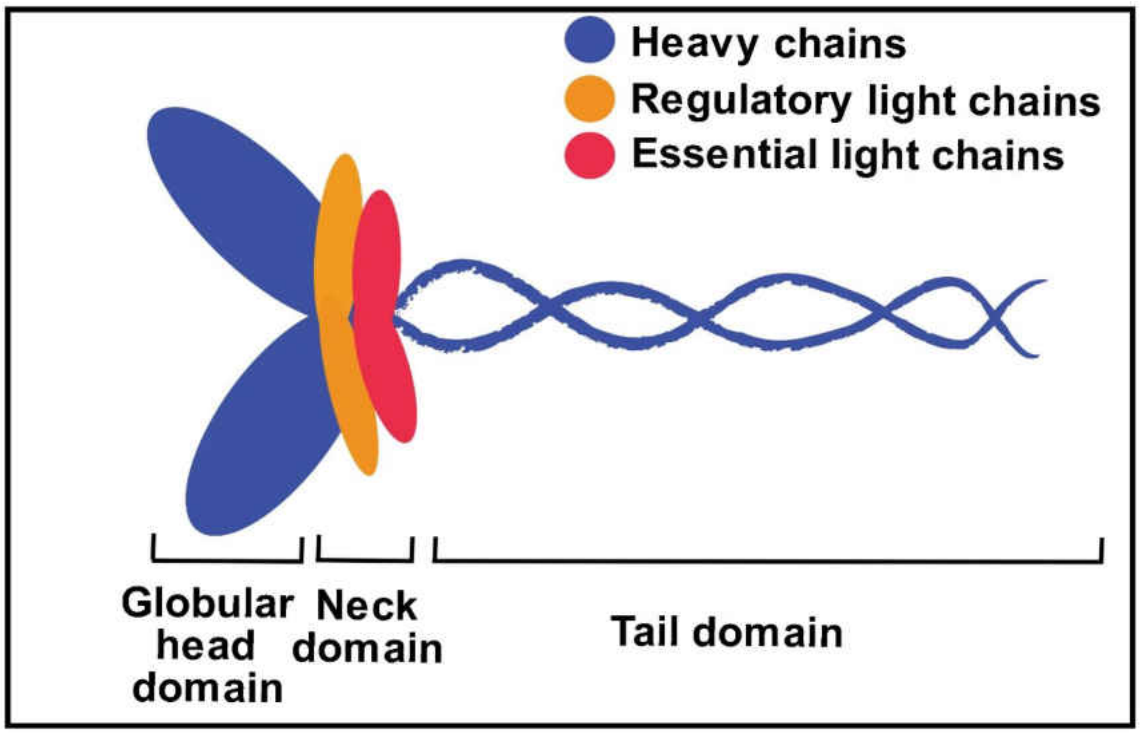

Figure 5. Non-muscle myosin II structure. Diagram of the basic structure of non-muscle myosin II proteins showing the heavy and light chains along with the head, neck and tail domains.

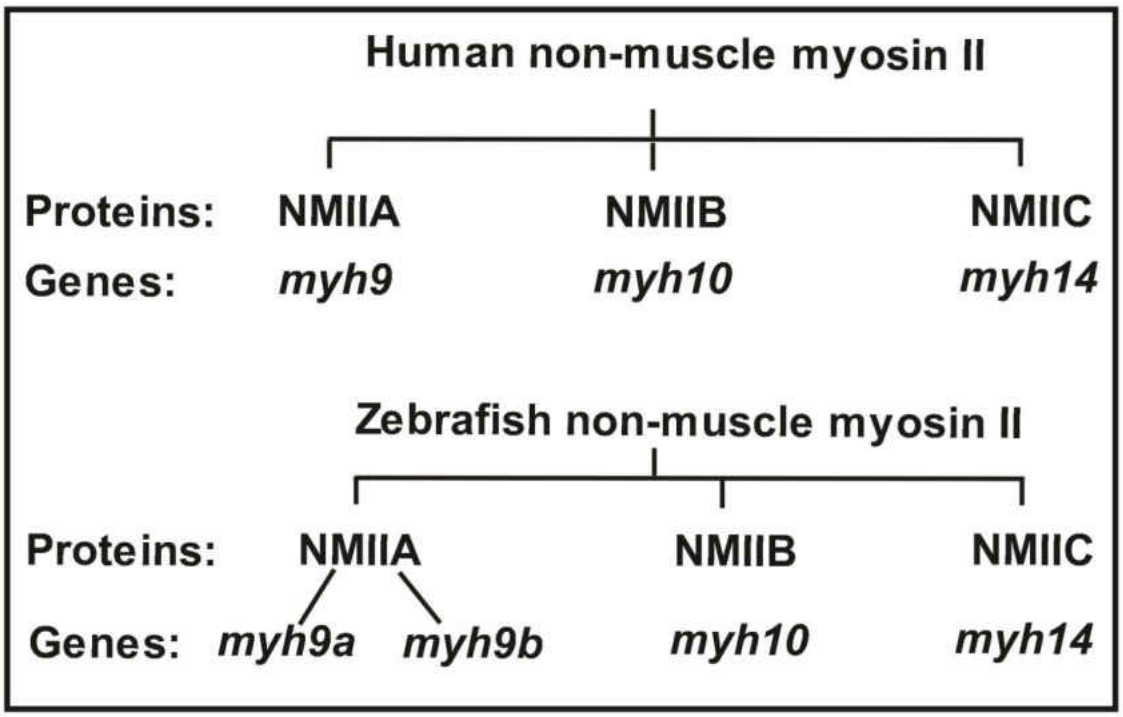

Figure 6. Non-muscle myosin II genes. Schematic showing the different non-muscle myosin II (NMII) homologs- NMIIA, NMIIB and NMIIC, encoded by their respective genes- *MYH9*, *MYH10* and *MYH14*. Corresponding analogous genes in the zebrafish are also shown.

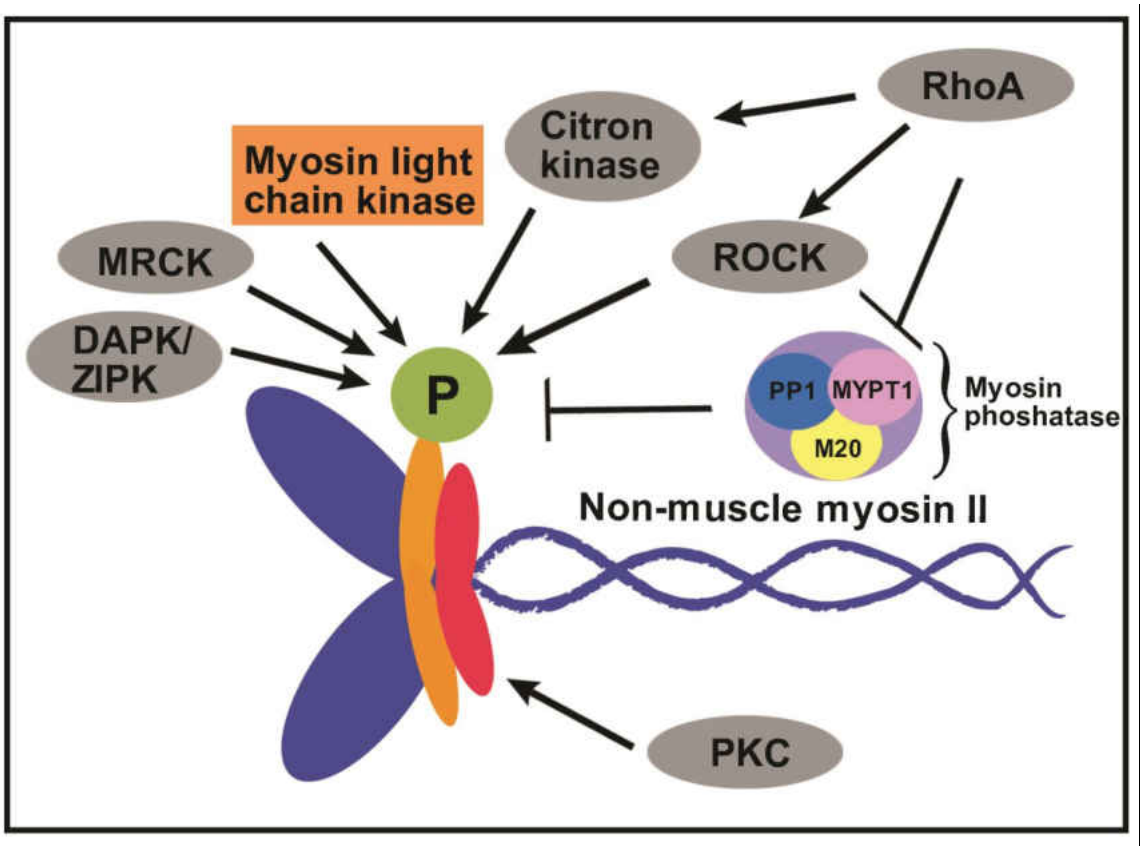

Figure 7. Regulation of the phosphorylation state of non-muscle myosin II. Schematic showing activation of non-muscle myosin II by phosphorylation of the regulatory light chain by myosin light chain kinase and dephosphorylation by myosin phosphatase. Shown in grey are various other kinases that also regulate the phosphorylation state of non-muscle myosin II molecules. DAPK, Death Associated Protein Kinase; ZIPK, Leucine Zipper interacting kinase; MRCK, Myotonic Dystrophy kinase related CDC42-binding Kinase; ROCK, Rho-associated coiled-coiled kinase; PKC, Protein Kinase C; P, phosphate molecule.

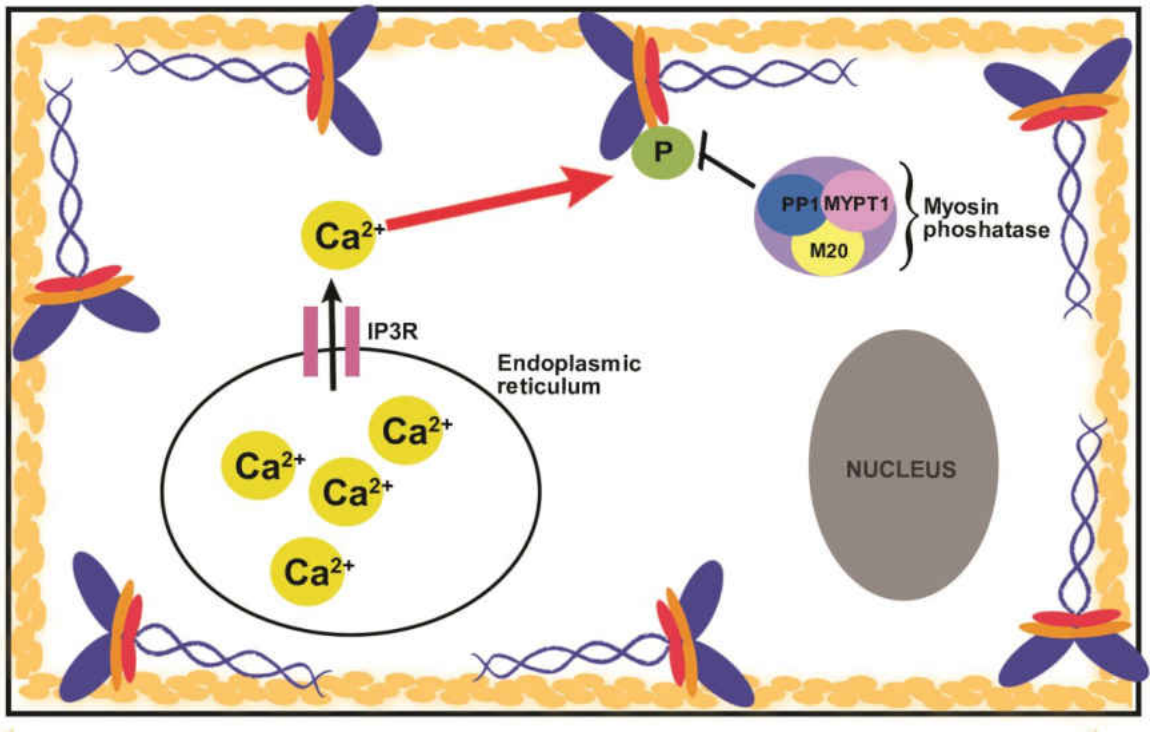

Figure 8. Schematic representing the proposed hypothesis. Diagram representing the hypothesis that calcium signals to regulate non-muscle myosin II by phosphorylation of the myosin light chain. A major source of intracellular calcium is the endoplasmic reticulum (ER). Calcium is released by the opening of the IP3R channels on the ER membrane. Red arrow indicates hypothesized interaction.

REFERENCES

Aman, A., and T. Piotrowski. 2010. Cell migration during morphogenesis. *Developmental biology*. 341:20-33.

Barkovich, A.J., K.J. Millen, and W.B. Dobyns. 2009. A developmental and genetic classification for midbrain-hindbrain malformations. *Brain : a journal of neurology*. 132:3199-3230.

Barone, V., and C.P. Heisenberg. 2012. Cell adhesion in embryo morphogenesis. *Current opinion in cell biology*. 24:148-153.

Berridge, M.J. 1997. Elementary and global aspects of calcium signalling. *The Journal of physiology*. 499 (Pt 2):291-306.

Berridge, M.J., P. Lipp, and M.D. Bootman. 2000. The versatility and universality of calcium signalling. *Nature reviews. Molecular cell biology*. 1:11-21.

Betapudi, V. 2014. Life without double-headed non-muscle myosin II motor proteins. *Frontiers in chemistry*. 2:45.

Bush, K.T., F.J. Lynch, A.S. DeNittis, A.B. Steinberg, H.Y. Lee, and R.G. Nagele. 1990. Neural tube formation in the mouse: a morphometric and computerized three-dimensional reconstruction study of the relationship between apical constriction of neuroepithelial cells and the shape of the neuroepithelium. *Anatomy and embryology*. 181:49-58.

Calaminus, S.D., J.M. Auger, O.J. McCarty, M.J. Wakelam, L.M. Machesky, and S.P. Watson. 2007. MyosinIIa contractility is required for maintenance of platelet structure during spreading on collagen and contributes to thrombus stability. *Journal of thrombosis and haemostasis : JTH*. 5:2136-2145.

Chu, J., C.T. Miller, K. Kislitsyna, G.A. Laine, R.H. Stewart, C.S. Cox, and K.S. Uray. 2012. Decreased myosin phosphatase target subunit 1(MYPT1) phosphorylation via attenuated rho kinase and zipper-interacting kinase activities in edematous intestinal smooth muscle. *Neurogastroenterology and motility : the official journal of the European Gastrointestinal Motility Society*. 24:257-266, e109.

Clark, K., J. Middelbeek, E. Lasonder, N.G. Dulyaninova, N.A. Morrice, A.G. Ryazanov, A.R. Bresnick, C.G. Figdor, and F.N. van Leeuwen. 2008. TRPM7 regulates myosin IIA filament stability and protein localization by heavy chain phosphorylation. *Journal of molecular biology*. 378:790-803.

Colas, J.F., and G.C. Schoenwolf. 2001. Towards a cellular and molecular understanding of neurulation. *Developmental dynamics : an official publication of the American Association of Anatomists*. 221:117-145.

Conti, M.A., and R.S. Adelstein. 2008. Nonmuscle myosin II moves in new directions. *Journal of cell science*. 121:11-18.

Du, M., G. Wang, T.M. Ismail, S. Gross, D.G. Fernig, R. Barraclough, and P.S. Rudland. 2012. S100P dissociates myosin IIA filaments and focal adhesion sites to reduce cell adhesion and enhance cell migration. *The Journal of biological chemistry*. 287:15330-15344.

Duchen, M.R. 2000. Mitochondria and calcium: from cell signalling to cell death. *The Journal of physiology*. 529 Pt 1:57-68.

Dulyaninova, N.G., and A.R. Bresnick. 2013. The heavy chain has its day: regulation of myosin-II assembly. *Bioarchitecture*. 3:77-85.

Dworkin, S., J.K. Heath, T.A. deJong-Curtain, B.M. Hogan, G.J. Lieschke, J. Malaterre, R.G. Ramsay, and T. Mantamadiotis. 2007. CREB activity modulates neural cell proliferation, midbrain-hindbrain organization and patterning in zebrafish. *Developmental biology*. 307:127-141.

Dworkin, S., and S.M. Jane. 2013. Novel mechanisms that pattern and shape the midbrain-hindbrain boundary. *Cellular and molecular life sciences : CMLS*. 70:3365-3374.

Elbaum, M., A. Chausovsky, E.T. Levy, M. Shtutman, and A.D. Bershadsky. 1999. Microtubule involvement in regulating cell contractility and adhesion-dependent signalling: a possible mechanism for polarization of cell motility. *Biochemical Society symposium*. 65:147-172.

Ellis, R.E., J.Y. Yuan, and H.R. Horvitz. 1991. Mechanisms and functions of cell death. *Annual review of cell biology*. 7:663-698.

Fill, M., and J.A. Copello. 2002. Ryanodine receptor calcium release channels. *Physiological reviews*. 82:893-922.

Fletcher, D.A., and R.D. Mullins. 2010. Cell mechanics and the cytoskeleton. *Nature*. 463:485-492.

Flicek, P., M.R. Amode, D. Barrell, K. Beal, K. Billis, S. Brent, D. Carvalho-Silva, P. Clapham, G. Coates, S. Fitzgerald, L. Gil, C.G. Giron, L. Gordon, T. Hourlier, S. Hunt, N. Johnson, T. Juettemann, A.K. Kahari, S. Keenan, E. Kulesha, F.J. Martin, T. Maurel, W.M. McLaren, D.N. Murphy, R. Nag, B. Overduin, M. Pignatelli, B. Pritchard, E. Pritchard, H.S. Riat, M. Ruffier, D. Sheppard, K. Taylor, A. Thormann, S.J. Trevanion, A. Vullo, S.P. Wilder, M. Wilson, A. Zadissa, B.L. Aken, E. Birney, F. Cunningham, J. Harrow, J. Herrero, T.J. Hubbard, R. Kinsella, M. Muffato, A. Parker, G. Spudich, A. Yates, D.R. Zerbino, and S.M. Searle. 2014. Ensembl 2014. *Nucleic acids research*. 42:D749-755.

Franke, J.D., R.A. Montague, and D.P. Kiehart. 2005. Nonmuscle myosin II generates forces that transmit tension and drive contraction in multiple tissues during dorsal closure. *Current biology : CB*. 15:2208-2221.

Fristrom, D. 1988. The cellular basis of epithelial morphogenesis. A review. *Tissue & cell*. 20:645-690.

Getty, A.L., J.W. Benedict, and D.A. Pearce. 2011. A novel interaction of CLN3 with nonmuscle myosin-IIB and defects in cell motility of Cln3(-/-) cells. *Experimental cell research*. 317:51-69.

Giannone, G., B.J. Dubin-Thaler, O. Rossier, Y. Cai, O. Chaga, G. Jiang, W. Beaver, H.G. Dobereiner, Y. Freund, G. Borisy, and M.P. Sheetz. 2007. Lamellipodial actin mechanically links myosin activity with adhesion-site formation. *Cell*. 128:561-575.

Gilland, E., A.L. Miller, E. Karplus, R. Baker, and S.E. Webb. 1999. Imaging of multicellular large-scale rhythmic calcium waves during zebrafish gastrulation. *Proceedings of the National Academy of Sciences of the United States of America*. 96:157-161.

Giraldez, A.J., R.M. Cinalli, M.E. Glasner, A.J. Enright, J.M. Thomson, S. Baskerville, S.M. Hammond, D.P. Bartel, and A.F. Schier. 2005. MicroRNAs regulate brain morphogenesis in zebrafish. *Science*. 308:833-838.

Golomb, E., X. Ma, S.S. Jana, Y.A. Preston, S. Kawamoto, N.G. Shoham, E. Goldin, M.A. Conti, J.R. Sellers, and R.S. Adelstein. 2004. Identification and characterization of nonmuscle myosin II-C, a new member of the myosin II family. *The Journal of biological chemistry*. 279:2800-2808.

Gomez-Viquez, L., G. Guerrero-Serna, U. Garcia, and A. Guerrero-Hernandez. 2003. SERCA pump optimizes Ca2+ release by a mechanism independent of store filling in smooth muscle cells. *Biophysical journal*. 85:370-380.

Grether, M.E., J.M. Abrams, J. Agapite, K. White, and H. Steller. 1995. The head involution defective gene of Drosophila melanogaster functions in programmed cell death. *Genes & development*. 9:1694-1708.

Guo, W.L., Q. Zhang, J. Wang, and M.F. Jin. 2013. Higher expression of phosphorylated myosin regulatory light chain in the common bile duct in pancreaticobiliary maljunction accompanied by bile duct dilatation in children: a post-mortem observational study. *Pediatric surgery international*. 29:293-298.

Gutzman, J.H., E.G. Graeden, L.A. Lowery, H.S. Holley, and H. Sive. 2008. Formation of the zebrafish midbrain-hindbrain boundary constriction requires laminin-dependent basal constriction. *Mechanisms of development*. 125:974-983.

Gutzman, J.H., S.U. Sahu, and C. Kwas. 2015. Non-muscle myosin IIA and IIB differentially regulate cell shape changes during zebrafish brain morphogenesis. *Developmental biology*. 397:103-115.

Gutzman, J.H., and H. Sive. 2010. Epithelial relaxation mediated by the myosin phosphatase regulator Mypt1 is required for brain ventricle lumen expansion and hindbrain morphogenesis. *Development*. 137:795-804.

He, L., X. Wang, H.L. Tang, and D.J. Montell. 2010. Tissue elongation requires oscillating contractions of a basal actomyosin network. *Nature cell biology*. 12:1133-1142.

Heissler, S.M., and D.J. Manstein. 2011. Comparative kinetic and functional characterization of the motor domains of human nonmuscle myosin-2C isoforms. *The Journal of biological chemistry*. 286:21191-21202.

Heissler, S.M., and D.J. Manstein. 2013. Nonmuscle myosin-2: mix and match. *Cellular and molecular life sciences : CMLS*. 70:1-21.

Hildebrand, J.D., and P. Soriano. 1999. Shroom, a PDZ domain-containing actin-binding protein, is required for neural tube morphogenesis in mice. *Cell*. 99:485-497.

Hirano, S., and M. Takeichi. 2012. Cadherins in brain morphogenesis and wiring. *Physiological reviews*. 92:597-634.

Howe, K., M.D. Clark, C.F. Torroja, J. Torrance, C. Berthelot, M. Muffato, J.E. Collins, S. Humphray, K. McLaren, L. Matthews, S. McLaren, I. Sealy, M. Caccamo, C. Churcher, C. Scott, J.C. Barrett, R. Koch, G.J. Rauch, S. White, W. Chow, B. Kilian, L.T. Quintais, J.A. Guerra-Assuncao, Y. Zhou, Y. Gu, J. Yen, J.H. Vogel, T. Eyre, S. Redmond, R. Banerjee, J. Chi, B. Fu,

E. Langley, S.F. Maguire, G.K. Laird, D. Lloyd, E. Kenyon, S. Donaldson, H. Sehra, J. Almeida-King, J. Loveland, S. Trevanion, M. Jones, M. Quail, D. Willey, A. Hunt, J. Burton, S. Sims, K. McLay, B. Plumb, J. Davis, C. Clee, K. Oliver, R. Clark, C. Riddle, D. Elliot, G. Threadgold, G. Harden, D. Ware, B. Mortimore, G. Kerry, P. Heath, B. Phillimore, A. Tracey, N. Corby, M. Dunn, C. Johnson, J. Wood, S. Clark, S. Pelan, G. Griffiths, M. Smith, R. Glithero, P. Howden, N. Barker, C. Stevens, J. Harley, K. Holt, G. Panagiotidis, J. Lovell, H. Beasley, C. Henderson, D. Gordon, K. Auger, D. Wright, J. Collins, C. Raisen, L. Dyer, K. Leung, L. Robertson, K. Ambridge, D. Leongamornlert, S. McGuire, R. Gilderthorp, C. Griffiths, D. Manthravadi, S. Nichol, G. Barker, S. Whitehead, M. Kay, et al. 2013. The zebrafish reference genome sequence and its relationship to the human genome. *Nature*. 496:498-503.

Ito, M., T. Nakano, F. Erdodi, and D.J. Hartshorne. 2004. Myosin phosphatase: structure, regulation and function. *Molecular and cellular biochemistry*. 259:197-209.

Jung, A.C., B. Denholm, H. Skaer, and M. Affolter. 2005. Renal tubule development in Drosophila: a closer look at the cellular level. *Journal of the American Society of Nephrology : JASN*. 16:322-328.

Kam, Z., J.S. Minden, D.A. Agard, J.W. Sedat, and M. Leptin. 1991. Drosophila gastrulation: analysis of cell shape changes in living embryos by three-dimensional fluorescence microscopy. *Development*. 112:365-370.

Kawasaki, H., S. Nakayama, and R.H. Kretsinger. 1998. Classification and evolution of EF-hand proteins. *Biometals : an international journal on the role of metal ions in biology, biochemistry, and medicine*. 11:277-295.

Keller, R.E. 1980. The cellular basis of epiboly: an SEM study of deep-cell rearrangement during gastrulation in Xenopus laevis. *Journal of embryology and experimental morphology*. 60:201-234.

Kimmel, C.B., W.W. Ballard, S.R. Kimmel, B. Ullmann, and T.F. Schilling. 1995. Stages of embryonic development of the zebrafish. *Developmental dynamics : an official publication of the American Association of Anatomists*. 203:253-310.

Kinoshita, N., N. Sasai, K. Misaki, and S. Yonemura. 2008. Apical accumulation of Rho in the neural plate is important for neural plate cell shape change and neural tube formation. *Molecular biology of the cell*. 19:2289-2299.

Kovacs, M., F. Wang, A. Hu, Y. Zhang, and J.R. Sellers. 2003. Functional divergence of human cytoplasmic myosin II: kinetic characterization of the non-muscle IIA isoform. *The Journal of biological chemistry*. 278:38132-38140.

Kwon, Y.C., S.H. Baek, H. Lee, and K.M. Choe. 2010. Nonmuscle myosin II localization is regulated by JNK during Drosophila larval wound healing. *Biochemical and biophysical research communications*. 393:656-661.

Lee, J.Y., and B. Goldstein. 2003. Mechanisms of cell positioning during C. elegans gastrulation. *Development*. 130:307-320.

Lee, J.Y., and R.M. Harland. 2007. Actomyosin contractility and microtubules drive apical constriction in Xenopus bottle cells. *Developmental biology*. 311:40-52.

Leptin, M. 1999. Gastrulation in Drosophila: the logic and the cellular mechanisms. *The EMBO journal*. 18:3187-3192.

Llimargas, M., and J. Casanova. 2010. Apical constriction and invagination: a very self-reliant couple. *Developmental biology*. 344:4-6.

Louvi, A., P. Alexandre, C. Metin, W. Wurst, and M. Wassef. 2003. The isthmic neuroepithelium is essential for cerebellar midline fusion. *Development*. 130:5319-5330.

Lowery, L.A., and H. Sive. 2005. Initial formation of zebrafish brain ventricles occurs independently of circulation and requires the nagie oko and snakehead/atp1a1a.1 gene products. *Development*. 132:2057-2067.

Lowery, L.A., and H. Sive. 2009. Totally tubular: the mystery behind function and origin of the brain ventricular system. *BioEssays : news and reviews in molecular, cellular and developmental biology*. 31:446-458.

Ma, X., S.S. Jana, M.A. Conti, S. Kawamoto, W.C. Claycomb, and R.S. Adelstein. 2010. Ablation of nonmuscle myosin II-B and II-C reveals a role for nonmuscle myosin II in cardiac myocyte karyokinesis. *Molecular biology of the cell*. 21:3952-3962.

Mammoto, T., and D.E. Ingber. 2010. Mechanical control of tissue and organ development. *Development*. 137:1407-1420.

Marsden, M., and D.W. DeSimone. 2001. Regulation of cell polarity, radial intercalation and epiboly in Xenopus: novel roles for integrin and fibronectin. *Development*. 128:3635-3647.

Martin, A.C., M. Kaschube, and E.F. Wieschaus. 2009. Pulsed contractions of an actin-myosin network drive apical constriction. *Nature*. 457:495-499.

Martinez-Morales, J.R., M. Rembold, K. Greger, J.C. Simpson, K.E. Brown, R. Quiring, R. Pepperkok, M.D. Martin-Bermudo, H. Himmelbauer, and J. Wittbrodt. 2009. ojoplano-mediated basal constriction is essential for optic cup morphogenesis. *Development*. 136:2165-2175.

Martinez, S. 2001. The isthmic organizer and brain regionalization. *The International journal of developmental biology*. 45:367-371.

Martinsen, A., O. Schakman, X. Yerna, C. Dessy, and N. Morel. 2013. Myosin light chain kinase controls voltage-dependent calcium channels in vascular smooth muscle. *Pflugers Archiv : European journal of physiology*.

Matsumura, F. 2005. Regulation of myosin II during cytokinesis in higher eukaryotes. *Trends in cell biology*. 15:371-377.

McGrath, J., S. Somlo, S. Makova, X. Tian, and M. Brueckner. 2003. Two populations of node monocilia initiate left-right asymmetry in the mouse. *Cell*. 114:61-73.

Merino, R., Y. Ganan, D. Macias, J. Rodriguez-Leon, and J.M. Hurle. 1999. Bone morphogenetic proteins regulate interdigital cell death in the avian embryo. *Annals of the New York Academy of Sciences*. 887:120-132.

Mizuno, Y., E. Isotani, J. Huang, H. Ding, J.T. Stull, and K.E. Kamm. 2008. Myosin light chain kinase activation and calcium sensitization in smooth muscle in vivo. *American journal of physiology. Cell physiology*. 295:C358-364.

Moore, T.M., G.H. Brough, P. Babal, J.J. Kelly, M. Li, and T. Stevens. 1998. Store-operated calcium entry promotes shape change in pulmonary endothelial cells expressing Trp1. *The American journal of physiology*. 275:L574-582.

Nakajima, H., and T. Tanoue. 2010. Epithelial cell shape is regulated by Lulu proteins via myosin-II. *Journal of cell science*. 123:555-566.

Nishikawa, M., J.R. Sellers, R.S. Adelstein, and H. Hidaka. 1984. Protein kinase C modulates in vitro phosphorylation of the smooth muscle heavy meromyosin by myosin light chain kinase. *The Journal of biological chemistry*. 259:8808-8814.

Nishimura, T., and M. Takeichi. 2008. Shroom3-mediated recruitment of Rho kinases to the apical cell junctions regulates epithelial and neuroepithelial planar remodeling. *Development*. 135:1493-1502.

Odronitz, F., and M. Kollmar. 2007. Drawing the tree of eukaryotic life based on the analysis of 2,269 manually annotated myosins from 328 species. *Genome biology*. 8:R196.

Onishi, H., and T. Wakabayashi. 1982. Electron microscopic studies of myosin molecules from chicken gizzard muscle I: the formation of the intramolecular loop in the myosin tail. *Journal of biochemistry*. 92:871-879.

Parsons, J.T., A.R. Horwitz, and M.A. Schwartz. 2010. Cell adhesion: integrating cytoskeletal dynamics and cellular tension. *Nature reviews. Molecular cell biology*. 11:633-643.

Petridou, N.I., and P.A. Skourides. 2014. FAK transduces extracellular forces that orient the mitotic spindle and control tissue morphogenesis. *Nature communications*. 5:5240.

Phillips, H.M., J.N. Murdoch, B. Chaudhry, A.J. Copp, and D.J. Henderson. 2005. Vangl2 acts via RhoA signaling to regulate polarized cell movements during development of the proximal outflow tract. *Circulation research*. 96:292-299.

Pollard, T.D., and E.D. Korn. 1973. Acanthamoeba myosin. II. Interaction with actin and with a new cofactor protein required for actin activation of Mg 2+ adenosine triphosphatase activity. *The Journal of biological chemistry*. 248:4691-4697.

Ponti, A., M. Machacek, S.L. Gupton, C.M. Waterman-Storer, and G. Danuser. 2004. Two distinct actin networks drive the protrusion of migrating cells. *Science*. 305:1782-1786.

Popgeorgiev, N., B. Bonneau, K.F. Ferri, J. Prudent, J. Thibaut, and G. Gillet. 2011. The apoptotic regulator Nrz controls cytoskeletal dynamics via the regulation of Ca2+ trafficking in the zebrafish blastula. *Developmental cell*. 20:663-676.

Porter, G.A., Jr., R.F. Makuck, and S.A. Rivkees. 2003. Intracellular calcium plays an essential role in cardiac development. *Developmental dynamics : an official publication of the American Association of Anatomists*. 227:280-290.

Putney, J.W., Jr. 1986. A model for receptor-regulated calcium entry. *Cell calcium*. 7:1-12.

Rauzi, M., P.F. Lenne, and T. Lecuit. 2010. Planar polarized actomyosin contractile flows control epithelial junction remodelling. *Nature*. 468:1110-1114.

Raya, A., Y. Kawakami, C. Rodriguez-Esteban, M. Ibanes, D. Rasskin-Gutman, J. Rodriguez-Leon, D. Buscher, J.A. Feijo, and J.C. Izpisua Belmonte. 2004. Notch activity acts as a sensor for extracellular calcium during vertebrate left-right determination. *Nature*. 427:121-128.

Redies, C., and M. Takeichi. 1996. Cadherins in the developing central nervous system: an adhesive code for segmental and functional subdivisions. *Developmental biology*. 180:413-423.

Reynoso, R., R.M. Perrin, J.W. Breslin, D.A. Daines, K.D. Watson, D.M. Watterson, M.H. Wu, and S. Yuan. 2007. A role for long chain myosin light chain kinase (MLCK-210) in microvascular hyperpermeability during severe burns. *Shock*. 28:589-595.

Rhinn, M., K. Lun, M. Luz, M. Werner, and M. Brand. 2005. Positioning of the midbrain-hindbrain boundary organizer through global posteriorization of the neuroectoderm mediated by Wnt8 signaling. *Development*. 132:1261-1272.

Rodionov, V.I., F.K. Gyoeva, E. Tanaka, A.D. Bershadsky, J.M. Vasiliev, and V.I. Gelfand. 1993. Microtubule-dependent control of cell shape and pseudopodial activity is inhibited by the antibody to kinesin motor domain. *The Journal of cell biology*. 123:1811-1820.

Ruiz, P.S., and F. Serras. 2014. Mind the gap: cells respond to tissue damage by changing orientation of cell divisions. *Fly*. 8:33-35.

Rynn, L., Cragan, J., Correa, A. 2009. Update on Overall Prevalence of Major Birth Defects.

Sandquist, J.C., K.I. Swenson, K.A. Demali, K. Burridge, and A.R. Means. 2006. Rho kinase differentially regulates phosphorylation of nonmuscle myosin II isoforms A and B during cell rounding and migration. *The Journal of biological chemistry*. 281:35873-35883.

Sarmah, B., A.J. Latimer, B. Appel, and S.R. Wente. 2005. Inositol polyphosphates regulate zebrafish left-right asymmetry. *Developmental cell*. 9:133-145.

Sato, T., A.L. Joyner, and H. Nakamura. 2004. How does Fgf signaling from the isthmic organizer induce midbrain and cerebellum development? *Development, growth & differentiation*. 46:487-494.

Sawyer, J.M., J.R. Harrell, G. Shemer, J. Sullivan-Brown, M. Roh-Johnson, and B. Goldstein. 2010. Apical constriction: a cell shape change that can drive morphogenesis. *Developmental biology*. 341:5-19.

Schock, F., and N. Perrimon. 2002. Molecular mechanisms of epithelial morphogenesis. *Annual review of cell and developmental biology*. 18:463-493.

Schoenwolf, G.C., and M.V. Franks. 1984. Quantitative analyses of changes in cell shapes during bending of the avian neural plate. *Developmental biology*. 105:257-272.

Seher, T.C., and M. Leptin. 2000. Tribbles, a cell-cycle brake that coordinates proliferation and morphogenesis during Drosophila gastrulation. *Current biology : CB*. 10:623-629.

Sellers, J.R. 2000. Myosins: a diverse superfamily. *Biochimica et biophysica acta*. 1496:3-22.

Sepich, D.S., C. Calmelet, M. Kiskowski, and L. Solnica-Krezel. 2005. Initiation of convergence and extension movements of lateral mesoderm during zebrafish gastrulation. *Developmental dynamics : an official publication of the American Association of Anatomists*. 234:279-292.

Sepich, D.S., M. Usmani, S. Pawlicki, and L. Solnica-Krezel. 2011. Wnt/PCP signaling controls intracellular position of MTOCs during gastrulation convergence and extension movements. *Development*. 138:543-552.

Slusarski, D.C., and F. Pelegri. 2007. Calcium signaling in vertebrate embryonic patterning and morphogenesis. *Developmental biology*. 307:1-13.

Solon, J., A. Kaya-Copur, J. Colombelli, and D. Brunner. 2009. Pulsed forces timed by a ratchet-like mechanism drive directed tissue movement during dorsal closure. *Cell*. 137:1331-1342.

Somlyo, A.P., and A.V. Somlyo. 2003. Ca2+ sensitivity of smooth muscle and nonmuscle myosin II: modulated by G proteins, kinases, and myosin phosphatase. *Physiological reviews*. 83:1325-1358.

Stanisstreet, M. 1982. Calcium and wound healing in Xenopus early embryos. *Journal of embryology and experimental morphology*. 67:195-205.

Suzuki, M., H. Morita, and N. Ueno. 2012. Molecular mechanisms of cell shape changes that contribute to vertebrate neural tube closure. *Development, growth & differentiation*. 54:266-276.

Szent-Gyorgyi, A.G. 1975. Calcium regulation of muscle contraction. *Biophysical journal*. 15:707-723.

Trybus, K.M., T.W. Huiatt, and S. Lowey. 1982. A bent monomeric conformation of myosin from smooth muscle. *Proceedings of the National Academy of Sciences of the United States of America*. 79:6151-6155.

Tullio, A.N., D. Accili, V.J. Ferrans, Z.X. Yu, K. Takeda, A. Grinberg, H. Westphal, Y.A. Preston, and R.S. Adelstein. 1997. Nonmuscle myosin II-B is required for normal development of the mouse heart. *Proceedings of the National Academy of Sciences of the United States of America*. 94:12407-12412.

Tullio, A.N., P.C. Bridgman, N.J. Tresser, C.C. Chan, M.A. Conti, R.S. Adelstein, and Y. Hara. 2001. Structural abnormalities develop in the brain after ablation of the gene encoding nonmuscle myosin II-B heavy chain. *The Journal of comparative neurology*. 433:62-74.

Van Lierop, J.E., D.P. Wilson, J.P. Davis, S. Tikunova, C. Sutherland, M.P. Walsh, and J.D. Johnson. 2002. Activation of smooth muscle myosin light chain kinase by calmodulin. Role of LYS(30) and GLY(40). *The Journal of biological chemistry*. 277:6550-6558.

Vicente-Manzanares, M., X. Ma, R.S. Adelstein, and A.R. Horwitz. 2009. Non-muscle myosin II takes centre stage in cell adhesion and migration. *Nature reviews. Molecular cell biology*. 10:778-790.

Wallingford, J.B., A.J. Ewald, R.M. Harland, and S.E. Fraser. 2001. Calcium signaling during convergent extension in Xenopus. *Current biology : CB*. 11:652-661.

Wang, A., X. Ma, M.A. Conti, and R.S. Adelstein. 2011. Distinct and redundant roles of the non-muscle myosin II isoforms and functional domains. *Biochemical Society transactions*. 39:1131-1135.

Wang, G., M.L. Manning, and J.D. Amack. 2012. Regional cell shape changes control form and function of Kupffer's vesicle in the zebrafish embryo. *Developmental biology*. 370:52-62.

Watanabe, H., Q.K. Tran, K. Takeuchi, M. Fukao, M.Y. Liu, M. Kanno, T. Hayashi, A. Iguchi, M. Seto, and K. Ohashi. 2001. Myosin light-chain kinase regulates endothelial calcium entry and endothelium-dependent vasodilation. *FASEB journal : official publication of the Federation of American Societies for Experimental Biology*. 15:282-284.

Westhoff, M.A., B. Serrels, V.J. Fincham, M.C. Frame, and N.O. Carragher. 2004. SRC-mediated phosphorylation of focal adhesion kinase couples actin and adhesion dynamics to survival signaling. *Molecular and cellular biology*. 24:8113-8133.

Xu, J., X.P. Gao, R. Ramchandran, Y.Y. Zhao, S.M. Vogel, and A.B. Malik. 2008. Nonmuscle myosin light-chain kinase mediates neutrophil transmigration in sepsis-induced lung inflammation by activating beta2 integrins. *Nature immunology*. 9:880-886.

Yanez, M., J. Gil-Longo, and M. Campos-Toimil. 2012. Calcium binding proteins. *Advances in experimental medicine and biology*. 740:461-482.

CHAPTER 2

NON-MUSCLE MYOSIN IIA AND IIB DIFFERENTIALLY REGULATE CELL SHAPE CHANGES DURING ZEBRAFISH BRAIN MORPHOGENESIS

*THIS CHAPTER HAS BEEN ADAPTED FROM:

Jennifer H. Gutzman, **Srishti U. Sahu**, Constance Kwas
Developmental Biology, Volume 397, Issue 1, 1 January 2015, Pages 103–115

Contributions: Work performed by Srishti Sahu includes partial contribution to Figures 9-13, S1, S3 and sole contribution to Figure S4.

A. INTRODUCTION

Morphogenesis is a key developmental process that shapes all organs and is required for proper organ function. Regulation of individual cell shape changes are at the core of morphogenetic events which together give rise to whole tissue shape (Heisenberg and Bellaiche, 2013; Lecuit and Lenne, 2007). During vertebrate brain development, neuroepithelial cells of the neural tube fold in specific regions giving rise to the characteristic embryonic vertebrate brain shape. The fold at the midbrain-hindbrain boundary (MHB) functions as a crucial organizing center for the developing embryo and is one of the earliest and most highly conserved folds in the vertebrate brain (Brand et al., 1996; Rhinn and Brand, 2001). Given the high degree of conservation of the MHB across vertebrate species in terms of function and form, understanding the molecular mechanisms underlying its development is critical to our understanding of brain morphogenesis.

Our previous work characterized the basic morphogenetic events that occur to form this highly conserved fold in the zebrafish. We demonstrated that cell shortening and basal constriction occur in cells at the point of deepest constriction of the MHB, the midbrain-hindbrain boundary constriction (MHBC) (Gutzman et al., 2008). While we previously determined that basal constriction is dependent on laminin, the mechanisms that regulate cell shortening at the MHBC are unknown.

Neuroepithelial cell shape and brain morphogenesis are also dependent upon the contractile state of the neuroepithelium (Gutzman and Sive, 2010). This contractile state is tightly regulated by non-muscle myosin II (NMII) activity. We demonstrated that *mypt1*, the myosin phosphatase regulatory subunit, is required for cell shape regulation during hindbrain morphogenesis and important for regulating the activity of NMII (Gutzman and Sive, 2010). Myosin phosphatase dephosphorylates the myosin regulatory light chain (MRLC) where MRLC, in the phosphorylated state, activates the contraction of NMII. NMII proteins are critical regulators of cell motility, cytokinesis, polarity, and adhesion. In addition, it has been established in multiple systems, that cell shape is critically dependent upon NMII function (Vicente-Manzanares et al., 2009).

Depending on the tissue and cell type, NMIIA and NMIIB may have either overlapping or distinct roles during embryonic development (Wang et al., 2011). For example, NMIIA and NMIIB knockout mice have different phenotypes. NMIIA knockouts are embryonic lethal and die before gastrulation due to defects in cell-cell adhesion (Conti et al., 2004). In contrast, NMIIB knockout mice display heart defects, hydrocephalus, and abnormal neuronal migration (Ma et al., 2007; Ma et

al., 2004). In migrating cells, NMIIA and NMIIB have different localization and function, which depends on the rigidity of the specific migratory substrate (Raab et al., 2012).

Given that non-muscle myosins have important roles in regulating cell and tissue shape, we hypothesized that NMIIA and NMIIB regulate cell shape changes that occur to form the MHBC. Here we used the zebrafish MHB as a model for determining the molecular mechanisms regulating the initial cell shape changes that occur during brain morphogenesis. We discovered distinct roles for NMIIA and NMIIB in MHB morphogenesis using live imaging to quantify changes in cell shape. We determined that NMIIA controls the length of the cells specifically at the MHBC, while NMIIB regulates the width of cells throughout the MHB tissue. Thus NMIIA and NMIIB perform non-redundant functions in regulating the morphogenesis of the MHB.

B. MATERIALS AND METHODS

Zebrafish maintenance and husbandry

Standard procedures were used for zebrafish maintenance and husbandry (Kimmel et al., 1995; Westerfield, 2000). Wild-type AB zebrafish embryos were used for all experiments. Embryos were staged according to Kimmel et al., 1995. For all experiments somite number was counted to allow for consistent staging comparisons and to eliminate the possibility of phenotypes resulting from developmental delay. The following equivalent staging points were used; 18 somite stage (ss) is equal to 18 hours post fertilization (hpf); 22 ss is equal to 20 hpf; and 24 ss is equal to 22 hpf.

Embryonic gene expression analysis

For all of our studies we used the following sequence information from Zebrafish Ensembl (Flicek et al., 2013). *myh9a* located on the reverse strand of chromosome 6, ENSDART00000149823. *myh9b* located on the reverse strand of chromosome 3, ENSDART00000137105. *myh10* homolog was found to be located on the forward strand of a different region of chromosome 6, ENSDART00000151114. RT-PCR was conducted on RNA isolated from wild-type embryos over time. Primers used include:

myh9a forward primer (5'-AAATTCAGCAAGGTGGAGGA-3');
myh9a reverse primer (5'-TTGGTGTTTTCGGTTTTTCC-3');
myh9b forward primer: (5'-CCTGCCCATCTACTCAGAGG-3');
myh9b reverse primer (5'-TGTGGAAGGTTCGCTCTTCT-3');
myh10 forward primer (5'-CTTCTGAACGGCATGGATTT-3');
myh10 reverse primer (5'-TTGGCATTTCCAAAGGATTC-3');
Ef1α forward primer (5'-GATGCACCACGAGTCTCTGA-3');
Ef1α reverse primer (5'-TGATGACCTGAGCGTTGAAG-3').

Antisense morpholino oligonucleotide injections

Splice site-blocking morpholino antisense oligonucleotides (morpholino: MO) were used for all knockdown experiments. MO details for each gene are as follows: *myh9a* MO (5'-AGCAAGAGAGACTTACAAATCGAGA-3'; Gene Tools) that targets intron1-EXON2. *myh9b* MO (5'-ATGTCTGAAACAGTCGTTTACAA GC-3'; Gene Tools) that targets EXON6-intron6. *myh10* MO (5'-CTTCACAAAT GTGGTCTTACCTTGA-3'; Gene Tools) that targets EXON2-intron2. *mypt1* MO (5′-ATTTTTTGTGACTTACTCAGCGATG-3′; Gene Tools) that targets exon 2-intron 2 (Gutzman and Sive, 2010). Standard control MO (5′-

CCTCTTACCTCAGTTACAATTTATA-3′) was used were indicated (Gene Tools). Zebrafish *p53* MO (5'-GCGCCATTGCTTTTGCAAGAATTG-3'; Gene Tools) was only used in conjunction with the *myh9b* MO (Robu et al., 2007). For all MO knockdown experiments, the following concentrations were used and injected into one cell stage embryos either alone or in conjunction with membrane targeting GFP (mGFP). 4ng *myh9a* MO, 3 ng *myh9b* MO with 3ng *p53* MO, 3ng *myh10* MO, 5ng *mypt1* MO. The concentration of control MO was equal to the highest concentration of any experimental MO used in that experiment. Up to 6ng of *myh9a* MO was used with no obvious brain phenotype. All confocal evaluation for *myh9a* MO was conducted at 4ng.

In situ hybridization

In situ hybridization was conducted according to standard procedures. RNA probes were designed to unique UTR sequences due to the high sequence similarities in the coding regions of these genes (probe regions are shown in Fig. 9). The *myh9a* probe was cloned from the 3'end into the 3' UTR of *myh9a* from 24 hpf wild type embryos using the following primers. *myh9a* primer 3'end forward (5'-TGGAGGAGACTGAGGAGGAA-3'), *myh9a* primer 3'UTR reverse (5'-GAACAGGCCGAATGAAACAT-3') resulting in a 502 bp probe. The *myh9b in situ* probe was cloned from the 5'UTR into the 5'end of *myh9b* from 24 hpf wild type embryos using the following primers. *myh9b* primer 5'UTR forward (5'-GTGGAAGAGGGAGGGAAGAG-3'), *myh9b* primer 5'end reverse (5'-AAGGCACCCACACTAGCTTC-3') resulting in a 290 bp probe. The PCR fragments above were subcloned into pGEM using the pGEM T-Easy Vector

System Kit (Promega) for probe synthesis. The *myh10 in situ* probe was made from Image clone 8801976 from Open Biosystems and is located in the 3'UTR of the gene and results in an 810 bp probe. Sense and antisense probes were made and used for each *in situ* experiment to test for specificity.

Actin staining

Embryos were fixed in 4% paraformaldehyde for 2 h at room temperature or overnight at 4 °C and washed in PBT. Embryos were incubated at 4 °C overnight in Alexa Fluor 488 phalloidin (Invitrogen A12379) 1:40 in PBT, washed 3X in PBT, mounted in glycerol, and imaged using a Nikon CS2 laser-scanning confocal microscope. Images were analyzed with Nikon Elements software and Photoshop (Adobe).

Non-muscle myosin IIA and IIB immunostaining

Embryos were fixed in Dents for 2 h at room temperature, deyolked, blocked overnight at 4 °C, and then washed in PBT. Embryos were incubated in primary antibody (anti-myosin IIA antibody raised in rabbit, Sigma-Aldrich , M8064, 1:500; and anti-myosin IIB antibody raised in mouse, Santa Cruz Biotechnology, sc-376942, 1:100) overnight at 4 °C, washed in PBT, then incubated in secondary antibody (Alexa Fluor 488 goat anti-rabbit, Life Technologies, 1:500 and/or Alexa Fluor 555 goat anti-mouse, Life Technologies, 1:500). Embryos were flat mounted in glycerol, imaged using a Nikon CS2 laser-scanning confocal microscope, and images were analyzed with Nikon elements and Photoshop (Adobe) software.

Imaging

All live confocal imaging was conducted as previously described (Graeden and Sive, 2009) using a Nikon CS2 scanning confocal and Nikon Elements software. Briefly, embryos were co-injected at the one-cell stage with membrane GFP (mGFP) mRNA (GFP-CAXX) and the morpholinos indicated. Live embryos were then mounted in agarose wells on a slide and oriented for imaging. A z-series of images was taken for each embryo. Live confocal images presented in each figure are single slices taken from a z-series of images approximately 15-20 microns into the tissue from the dorsal surface. Brightfield and *in situ* hybridization imaging was conducted using an Olympus SZX12 stereomicroscope with an Olympus DP72 camera. All images were processed using Nikon Elements software or Photoshop (Adobe).

Cell Shape Analysis

For all cell measurements, single cells were selected based on the ability to see one single cell spanning the entire width of the neuroepithelium from apical to basal in a single z-plane in the region of interest. Cell length was determined using the Nikon Imaging Systems (NIS) Elements software measurement tool by measuring from apical to basal of a single cell spanning the neuroepithelium. The cell width measurement was obtained from the NIS-Elements software as an average width of a cell. Single cells were manually outlined in a single z-series image to create an object. Then the NIS-Elements software determined the average width of the object (cell) by first calculating the area and the perimeter of the object (cell). The

software then calculated the length of the object using the formula: Length = (Perimeter + Sqrt (Perimeter^2 – 16*Area))/4. The width of the object was in turn calculated using the formula: Width = Area/Length.

Statistical Analysis

Statistical analysis for comparisons between all treatment groups was carried out by ANOVA. For significant results by ANOVA, further t-tests were performed to determine significance between control treatment and experimental treatment groups. p-values for t-test comparisons are presented in each figure legend. All analysis was computed using R-3.0.1.

C. RESULTS

Expression of non-muscle myosin IIA and IIB during embryonic development

Non-muscle myosins are known to be key regulators of cell shape during embryonic morphogenesis (Lecuit and Lenne, 2007; Vicente-Manzanares et al., 2009). We hypothesized that these proteins also play an integral role in shaping the cells that contribute to the MHB tissue fold. In order to test this hypothesis we first determined the zebrafish homologs of human non-muscle myosin II proteins. Zebrafish have two homologs of human *MYH9* (*myh9a* and *myh9b*) encoding for NMIIA, one homolog for *MYH10* (*myh10*) which encodes for NMIIB, and one homolog for *MYH14* (*myh14*), which encodes for NMIIC. According to the current zebrafish genome assembly, the sequence homology for *myh9a* and *myh9b* is 77% and 79% respectively, compared to the human *MYH9* (Flicek et al., 2013). Zebrafish *myh10* is 90% similar to the human homolog, while *myh14* is only 62%

similar to the human homolog. It has been demonstrated in the mouse that all three isoforms are expressed broadly throughout the embryo; however, there are tissues that express relatively higher levels of one isoform compared to others (Golomb et al., 2004). *myh14* appears to have the lowest expression level in the developing mouse brain (Golomb et al., 2004), and has the lowest sequence homology from human to zebrafish; therefore, we did not investigate the role of NMIIC in cell shape changes during MHB morphogenesis in the zebrafish.

Diagrams of the three zebrafish genes investigated in this study are shown (Fig. 9A). Using RT-PCR we confirmed that all three genes were expressed embryonically during the time of MHB development (Fig. 9B). We further analyzed gene expression using *in situ* hybridization to determine the localization of expression within the developing embryo (Fig. 9C). We found low levels of expression for *myh9a* maternally (4 hpf) and at early stages (12 hpf). There was some localized expression of *myh9a* within the forebrain, eyes, and tail between 18 and 24 hpf. Non-specific staining for *myh9a* was detected within the brain ventricle space and in the yolk in both antisense and sense controls. *myh9a* did not have obvious expression in the neuroepithelium of the MHB region during morphogenesis. *myh9b* was found to be expressed maternally (4hpf) and expression was detected throughout the whole embryo and brain at each time point analyzed. *myh10* had a low level of maternal expression at 4 hpf; however, by 12 hpf *myh10* was also found to be expressed throughout the whole embryo and brain. Together these data indicate that the zebrafish non-muscle myosin II genes *myh9b* and *myh10* are expressed during the time of MHB morphogenesis

and are found throughout the embryo and brain. While *myh9a* is also expressed, it does not appear to be as highly localized to the brain or MHB region as *myh9b* or *myh10* at these times. These data are consistent with the reported expression patterns for *myh9* and *myh10* during mouse embryonic development (Golomb et al., 2004). Next, we investigated the role for *myh9a, myh9b,* and *myh10* in regulating the cell shape changes that are required for the formation of the MHB fold.

Characterization of early MHB morphogenesis and cell shape changes

In order to better characterize the initial tissue and cell shape changes that lead to the MHB tissue fold, we performed detailed analysis of wild type MHB development during early stages of MHB formation when cells are shortening (Gutzman et al., 2008). We injected wild type embryos with membrane GFP (mGFP) mRNA and imaged the developing MHB in live embryos using scanning confocal microscopy at the somite stages indicated (Fig. 10). We quantified changes in the tissue over this time frame by analyzing tissue angle, cell length, and cell width. We found that the angle of the fold changes from 140 degrees to less than 100 degrees between 18 and 24 somite stage (ss) (Fig. 10A-D). We found that cells at the MHBC shorten from 50 microns to less than 40 microns during this time frame (Fig. 10E). We also found that cells outside the MHBC get slightly shorter during this time; however, there is still a large difference in cell length at the MHBC compared to cells outside (Fig. 10F). By 24 ss cells at the MHBC are approximately 75% of the length of the outside cells (Fig. 10G) which is consistent with our previous findings (Gutzman et al., 2008). Importantly, we also discovered that the width of the cells changes

between 22 and 24 ss (Fig. 10H) and cells in the MHB region get narrower as the morphology of the MHB is changing and the MHBC is forming.

myh9b and *myh10* are required for MHB development

In order to define the role for NMIIA and NMIIB in embryonic MHB morphogenesis, we conducted knockdown experiments using splice-site targeting, antisense oligonucleotide morpholino (MO) knockdown of *myh9a*, *myh9b*, and *myh10*. Splice targeting morpholinos were chosen due to the essential requirement for non-muscle myosins during early development and cell division (Conti et al., 2004; Ma et al., 2007; Maciver, 1996; Urven et al., 2006). We were able to carefully titrate the concentration of each splice targeting morpholino to prevent abnormal levels of cell death while maintaining normal levels of cells division, which allowed us to determine the role for these proteins in regulating cell shape during morphogenesis. Splice blocking morpholinos were confirmed at the concentrations used for all of the experiments presented here using RT-PCR or Western blot analysis (Fig. S1).

Embryos were injected with morpholinos at the one-cell stage and analyzed for gross embryonic phenotypes and for overall brain morphology at 24 ss using brightfield microscopy. Although we focused specifically on brain morphogenesis defects and cell shape changes at the MHB for this study, we did observe other gross phenotypes in morpholino injected embryos (Fig. S2). *myh9b* morphants demonstrated somite defects, abnormal tail curvature, pigmentation defects, heart abnormalities, slight edema, and abnormal eye and ear formation. *myh10*

morphants had abnormal body axis curvature, heart abnormalities, and abnormal eye development. *myh9a* morphants injected with our splice site targeting MO did not appear to have any observable gross morphology defects with the concentrations of morpholino tested (Fig. S2). This is in contrast to the studies by Muller et al. where they demonstrated that knockdown of *myh9a* (previously called *zmyh9* and *myh9-like2*) using a MO targeting the 5'-untranslated region and translational start site, leads to abnormal development of the glomerulus and causes gross embryonic edema at 5 days post fertilization (Muller et al., 2011). In those studies Muller et al. did not investigate the role of the other zebrafish *myh9* gene, *myh9b* (previously called *myhz9* and *myh9-like1*). This difference in overall gross phenotype for *myh9a* knockdown between our studies and Muller et al. is likely due to the timing of phenotypic analysis, the nature of the morpholinos utilized, and their respective target sequences.

Analysis of overall MHB morphology in control MO injected embryos at 24 ss showed normal formation of the MHB, visible with a clear and distinct fold in the tissue at the point of deepest constriction (MHBC) and normal openings in the midbrain and hindbrain ventricles (Fig. 11A). These results are consistent with our previous reports (Gutzman et al., 2008). A morpholino designed specifically to target only *myh9a* did not result in any visible abnormal MHB or brain phenotype when imaged with brightfield microscopy (Fig. 11B). In contrast, embryos injected with the *myh9b* MO or the *myh10* MO had abnormal MHB development. *myh9b* morphants did not have a sharp fold in the tissue at the point of deepest constriction, instead the fold was a curved shape (Fig. 11C). *myh10* morphants,

similar to *myh9b* morphants, failed to form a sharp tissue bend at the MHB (Fig. 11D). *myh10* morphants also had decreased midbrain ventricle opening (Fig. 11D). We have previously shown that abnormal brain ventricle inflation, due to lack of cerebrospinal fluid as found in the *snakehead* mutant, did not affect cell shape at the MHB (Gutzman et al., 2008). Therefore, the *myh10* morphant ventricle defect is likely due to abnormal dorsolateral hinge-point formation which is also dependent on non-muscle myosin II (Nyholm et al., 2009). Knockdown of both *myh9a* and *myh9b* together, or *myh9a* and *myh10* together, at the same concentration of morpholino used for single knockdown, did not worsen or change the MHB phenotype observed (data not shown). However, the double knockdown of *myh9a* and *myh9b* did appear to worsen the gross whole embryo tail and eye phenotypes at 24 ss, which is consistent with the localization of *myh9a* gene expression at this time point (data not shown).

We rescued the 24 ss brain phenotypes in *myh9b* and *myh10* morphants by co-injection of human *MYH9* or *MYH10* mRNA (Fig. S3). Quantification and representative images are shown for normal, mild, and severe *myh9b* and *myh10* morphant phenotypes (Fig. S3). For all of the experiments presented here investigating MHB defects and cell shape analysis, only mild phenotypes were analyzed. This is consistent with the level of protein knockdown we detect using the *myh10* morpholino, where our knockdown results in approximately 40% loss of the NMIIB protein (Fig. S1D). Together these data demonstrate that knockdown of both *myh9b* and *myh10*, but not *myh9a* knockdown, results in abnormal formation of the MHB indicating a role for *myh9b* and *myh10* in brain

morphogenesis. More detailed and quantitative comparisons of the knockdown MHB phenotypes are described in the following sections.

MHB tissue angle is dependent upon non-muscle myosin IIA and IIB

After determining that knockdown for both *myh9b* and *myh10* led to defects in MHB formation by brightfield microscopy, we wanted to determine the specific role for these non-muscle myosin proteins in regulating cell and tissue shape during morphogenesis. We performed detailed analyses on our non-muscle myosin II morphant brains and compared them to control morpholino injected embryos. We first examined the MHB tissue angle. Single-cell embryos were injected with MO and mGFP, and then imaged live using confocal microscopy. The angle at the MHBC was measured and compared (Fig. 11E-J). The average angle at 24 ss in control MO injected embryos was approximately 100 degrees. *myh9a* morphants had a normal tissue angle; however, *myh9b* MO injected embryos had a broader tissue angle of 125 degrees, and *myh10* MO injected embryos had an abnormal MHB tissue angle of 140 degrees (Fig. 11E-J). These results indicate that both *myh9b* and *myh10* contribute to the formation of the tissue angle at the MHB. We also analyzed the tissue angle in *mypt1* morphants. *mypt1* is the regulatory subunit of myosin phosphatase and *mypt1* knockdown results in non-functional myosin phosphatase and overactive non-muscle myosin II activity (Hartshorne et al., 2004). In addition, our previous report demonstrated that *mypt1* knockdown leads to abnormal tissue and cell shape in the hindbrain (Gutzman and Sive, 2010). With *mypt1* knockdown, and therefore overactive NMIIA and NMIIB, we found that the *mypt1* morphants also had an abnormal tissue angle with an average of 130

degrees at 24 ss (Fig. 11I-J). This result further supports the observation that regulation of non-muscle myosin activity is important for this morphogenetic process.

Since non-muscle myosin II is known to be required for normal cell proliferation, we confirmed that the brain phenotypes observed were not a result of increased or decreased cell proliferation or cell death. We analyzed cell proliferation with PH3 staining and cell death with TUNEL staining. We found that cell proliferation and cell death were normal in *myh9b* and *myh10* morphants at the concentrations of MO used for these experiments (Fig. S4). Together, these results indicate that *myh9b* and *myh10* have critical roles in determining the proper angle of tissue folding at the MHB, and that *myh9a* does not appear to be involved in this process. The *mypt1* knockdown phenotype also confirms the importance of specific regulation of the contractile state of the NMII proteins during MHB morphogenesis.

myh9b **is required for cell shortening at the MHBC**

During MHB morphogenesis, the first cell shape change occurs between 17 and 22 hours post fertilization (equivalent to 16 to 24 ss) where cells at the MHBC shorten to 75% of the length of cells outside of the MHBC (Fig. 10 and (Gutzman et al., 2008). The mechanisms that regulate cell shortening at the MHBC are unknown. We hypothesized that NMII proteins regulate this cell shape change which is required for the formation of the normal MHB tissue angle. We tested this hypothesis using knockdown experiments and then quantifying the length of the cells at the MHBC and outside of the MHBC (Fig. 12). Embryos were injected with

mGFP and specific morpholinos targeting *myh9a*, *myh9b*, *myh10*, or *mypt1*, and then live imaged at 24 ss using confocal microscopy. Cell length was quantified at the MHBC. At this stage of development neuroepithelial cells span the entire epithelium from apical to basal; therefore, we used the width of the single layer of pseudostratified epithelium as a measure of cell length. We measured cell length on one side of the neural tube at the MHBC (X) (Fig. 12A). Then we measured the length of cells 40 microns posterior to the MHBC (approximately 15 cells) outside of the MHBC region (Y) (Fig. 12B). We found that *myh9b* morphants had significantly longer cells at the MHBC compared to controls, while the length of the MHBC cells in *myh9a* and *myh10* morphant cells were unchanged (Fig. 12C-G). In the surrounding region posterior to the MHBC we found that cell length in *myh9b* morphants was the same as control, but *myh10* cells were slightly, but significantly, shorter (Fig. 12H). However, this small change in cell length outside of the MHBC from *myh10* morphants would still not account for the dramatic angle change observed at the MHBC.

At the MHBC, and outside of the MHBC, *mypt1* morphant cells were shorter than control cells (Fig. 12F, H). This observation continues to support the role for *mypt1* in regulating myosin contraction. *mypt1* morphants have overactive myosin, which causes increasing actomyosin contraction within the cells and leads to a shortening of the cells, consistent with the cell shape phenotype previously observed in the hindbrain (Gutzman and Sive, 2010).

Together these data indicate that cell shortening at the MHBC is dependent upon the function of *myh9b,* and not *myh10*, suggesting a different role for these two

non-muscle myosin proteins in regulating cell shape changes during MHB morphogenesis.

myh10 is required for regulating cell width in the MHB

In our detailed analysis of wild type embryos we discovered that cells throughout the MHB region become narrower during the formation of the fold (Fig. 10). While conducting our knockdown experiments and confocal imaging, we noticed that cells of the MHB in some morpholino-injected embryos looked wider than in control-injected embryos. Therefore, we conducted additional quantification of cell shapes by determining cell width and area in the MHB neuroepithelium in knockdown embryos. Embryos were injected with mGFP and morpholinos, and then live imaged at 24 ss using confocal microscopy. We quantified cell width and cell area in cells at the MHBC and in the posterior part of the MHB (Fig. 13). We found that cells in the *myh9a* and *myh9b* morphants had normal cell width and area (Fig. 13A-C, F, G); however, cells from embryos injected with *myh10* morpholino had significantly increased cell width and area (Fig. 13D, F, G). *mypt1* morphants also had significant differences in cell area and width (Fig. 13E-G) as would be predicted by over activation of non-muscle myosin and as previously observed in the hindbrain (Gutzman and Sive, 2010).

These data indicate that *myh10*, and not *myh9b*, is critical for the regulation and maintenance of cell width in the MHB region of the neuroepithelium. This further supports the differential role for *myh9b* and *myh10* in regulating cell shape at the MHB.

Abnormal distribution of actin at the MHB with NMIIA and NMIIB knockdown

The discovery that NMIIA and NMIIB have different roles in regulating cell shape changes at the MHB led us to ask, what are the mechanisms for this differential regulation? We have previously demonstrated that later in MHB formation (24 hpf) actin is enriched at the MHBC (Gutzman et al., 2008), and since we know that non-muscle myosin proteins are actin motors, we asked whether or not the distribution of actin in our knockdown embryos was also differentially disrupted with NMIIA or NMIIB knockdown.

Embryos were injected with the morpholino indicated, stained with phalloidin, and imaged using confocal microscopy to show actin localization in the MHB region (Fig. 14). We quantified the relative distribution of actin within the MHB in three regions. We determined the amount of actin within the neuroepithelium at the MHBC compared to the neuroepithelium outside the MHBC (Fig. 14A). We compared the amount of actin located apically at the midline of the neural tube compared to the amount of actin within the neuroepithelium at the apical edge of the MHBC cells (Fig. 14B), and we compared the amount of actin located on the basal side of the neural tube compared to the amount of actin within the neuroepithelium at the basal edge of the MHBC cells (Fig. 14C). These different regions of the neuroepithelium were used for comparison in B and C to more carefully address changes at the extreme apical or basal edges of the cells compared to just inside the adjacent neuroepithelium. We used the ratio of mean fluorescence intensity of actin staining in two regions within each embryo for comparison, shown by box 1 and box 2 (Fig. 14A-C). The actin mean intensity ratio

for box 1 was divided by box 2 in that given region. A ratio of 1 would indicate equal distribution of actin in box 1 and box 2. In control embryos there is approximately 1.5 times more actin within the neuroepithelium at the MHBC compared to more posterior neuroepithelium. This reflects the actin distribution previously described (Gutzman et al., 2008). There is 2 times more actin localized to the apical region of cells compared to the adjacent apical side of the neuroepithelial cells, and there is 1.5 times more actin on the basal side of the epithelium compared to the adjacent basal side of the neuroepithelium in the region of the MHBC (Fig. 14A-C, G). When we investigated actin distribution with *myh9b* knockdown we found a decrease in actin localization within the MHBC neuroepithelium and apically, while basal actin was unchanged (Fig. 14D, G). With *myh10* knockdown there was a significant decrease in actin localized to the MHBC neuroepithelium, apically, and basally indicating that actin in all areas of the MHBC cells was disrupted (Fig. 14E, G). *mypt1* knockdown did not affect apical actin distribution, as previously reported in the hindbrain (Gutzman and Sive, 2010); however, actin within the MHBC neuroepithelium was disrupted, as was basal actin distribution (Fig. 14F-G). Together, the differences in actin distribution with *myh9b* knockdown compared to *myh10* knockdown are consistent with *myh9b* and *myh10* having differential effects on regulating the actin cytoskeleton and neuroepithelial cell shape changes at the MHBC. *myh9b* affected actin only in the neuroepithelium and apically at the midline, while *myh10* affected actin within the neuroepithelium, apically, and basally.

Non-muscle myosin IIA and IIB protein localization

We also hypothesized that NMIIA and NMIIB would be differentially localized within the cells which could in turn explain their ability to differentially regulate cell shape. In order to test this hypothesis we used antibody staining specific for either NMIIA or NMIIB to see their localization pattern within the MHB region (Fig. 15). We did not detect any obvious differences between NMIIA and NMIIB localization in control embryos (Fig. 15A-C). The localization pattern was consistent with what has been demonstrated in the mouse neural tube (Ma et al., 2007). We did, however, see changes in both NMIIA and NMIIB localization with *mypt1* knockdown where non-muscle myosin II proteins accumulated apically and basally in the neuroepithelium as seen previously for NMIIA (Fig. 15D and (Gutzman and Sive, 2010)). Interestingly, when we stained for NMIIA with knockdown of *myh10* we found a change in NMIIA localization from generally cytoplasmic and apical to more diffuse and basally localized (Fig. 15E). We also found a change in NMIIB localization with *myh9b* knockdown, again from mostly cytoplasmic to more diffuse with increased basal localization (Fig. 15F). No primary controls are shown to indicate the specificity of the staining (Fig. 15G-H).

These data indicate that normally, the localization of NMIIA and NMIIB is overlapping within the neuroepithelium of the MHB region at this time, suggesting that the mechanism by which NMIIA and NMIIB are differentially regulating cell shape changes during brain morphogenesis is not due to differential localization, but likely due to differential regulation of activity. Furthermore, our analysis of

localization of one NMII protein with knockdown of other indicates that NMIIA and NMIIB depend on each other for proper localization.

D. DISCUSSION

myh9b and *myh10* differentially regulate cell shape during MHB morphogenesis

In wild type embryos, the basal angle of the MHB changes over time from 140 degrees at 18 ss to a more acute angle of 95 degrees by 24 ss (Fig. 10). During this time, cells at the MHBC are changing shape to allow this angle to form. Cells at the MHBC shorten by approximately 25%, while cells outside the MHBC also shorten slightly over this time window (Fig. 10). Concurrently, cells throughout the MHB region become narrower between 22 ss and 24 ss (Fig. 10). Together these morphogenetic changes lead to the formation of the highly conserved MHB fold (Fig. 16A).

Here, we demonstrate for the first time that non-muscle myosin IIA and IIB have distinct roles in regulating cell shape changes during brain morphogenesis. We discovered that NMIIA is required for the shortening of the cells specifically at the MHBC, while NMIIB is required for the narrowing of the cells throughout the MHB region (Fig. 16B and C). In contrast to our knockdown studies, we investigated non-muscle myosin II gain of function using *mypt1* knockdown. We found that cells in *mypt1* morphants, where there is over activation of non-muscle myosins, were both shorter and wider cells throughout the MHB region (Fig. 16D), which is consistent with the cell shape phenotype found with *mypt1* loss of function in the

hindbrain (Gutzman and Sive, 2010). Together, these data demonstrate that NMIIA is required for regulating the length of cells specifically at the MHBC and not in surrounding regions, while NMIIB is required for regulation of cell width throughout the MHB region. This uncovers a novel differential role for mechanisms by which these two proteins regulate cell shape during brain morphogenesis.

Cell length and cell width during development

Morphogenetic processes require specific changes in cell shape to cause bending of epithelial sheets, tissue invagination, and tube formation. We propose that regulating cell length and cell width may be as important in developmental processes as apical constriction or cell migration; however, investigation and quantification of these more subtle changes in cell shape has been limited. Apical constriction results in decreased surface area on the apical side of the polarized cell changing shape, and is critical in development during gastrulation and vertebrate neural tube formation (Haigo et al., 2003; Lee and Harland, 2007; Martin et al., 2009). Various mechanisms of apical constriction have been described depending on cell type and context, typically involving apical actomyosin networks linked to cell-cell apical junctions (Martin and Goldstein, 2014). Other cell shape changes including changes in cell length, width, or basal constriction have been less well defined and are likely to be regulated via both overlapping and distinct mechanisms. For example, during neural tube formation, cells of the neural plate have been described to lengthen before they apically constrict (Karfunkel, 1974), and although this cell shape change has been defined for decades, the mechanism for this cell lengthening has not been studied. Distinct mechanisms have been

uncovered for regulation of basal constriction. We determined that basal constriction at the MHB, following cell shortening, is laminin dependent, and basal constriction in optic cup morphogenesis requires the novel gene *ojoplano* (Gutzman et al., 2008; Martinez-Morales et al., 2009; Wang et al., 2012). In contrast, follicle cells in drosophila egg chamber elongation are regulated by actomyosin contraction, as in apical constriction; however, the orientation of the filaments is different and the contraction occurs basally, not apically, to shape the tissue (He et al., 2010).

The Kupffer's vesicle also undergoes regional cell shape changes during development. Interestingly, in the Kupffer's vesicle the anterior cells are elongated and the posterior cells shorten and widen over time (Wang et al., 2012), cell shape changes that are similar to those described here for MHB morphogenesis. Furthermore, these cell shape changes are regulated by non-muscle myosin II activity (Wang et al., 2012); however, it was not determined if NMIIA and NMIIB had distinct functions in the shortening or widening of cells. Future experiments to determine the mechanisms that regulate cell shape changes such as length, width, and basal constriction are essential for understanding complex morphogenetic processes.

Function of NMIIA versus NMIIB

The DNA sequence and protein structural similarities between NMIIA and NMIIB might suggest that these proteins are redundant; however, it is becoming more apparent that each isoform has distinct functions. The function of these proteins

has been determined using knockdown studies in many systems. NMIIA and NMIIB knockout mice display different phenotypes, where NMIIA knockouts are embryonic lethal due to cell adhesion defects (Conti et al., 2004), and NMIIB knockouts present with heart, brain, and neuronal migration defects (Ma et al., 2007; Ma et al., 2004). The ablation of NMIIB in mice resulted in structural abnormalities in the brain of mice, consistent with the role for NMIIB neuroepithelial morphogenesis (Tullio et al., 2001). Experiments to test for functional redundancy between NMIIA and NMIIB have suggested only a limited ability for the proteins to compensate for each other. For example, replacement of NMIIB with NMIIA in the mouse rescues brain abnormalities, but does not rescue cardiac defects (Bao et al., 2007). Here we have uncovered new isoform-distinct functions in regulating cell shape at the MHB during brain morphogenesis.

NMIIA and NMIIB have different enzymatic properties during ATP-hydrolysis, which determine their distinct roles in regulating cell shape. Only a small fraction of the head domain of NMIIA is strongly bound to actin at any one time (Kovacs et al., 2003). In contrast, NMIIB is one of the slowest myosins with regard to the rate in which it translocates actin filaments by having a slow ATPase cycle; therefore it spends a significantly longer time strongly bound to actin (Wang et al., 2003). This longer binding may make NMIIB better suited for maintaining cellular tension. These differences in enzymatic activity may account for the role of NMIIB in regulating cell width and area throughout the MHB region, while NMIIA is working more quickly to shorten cells in a specific brain region.

Differential regulation of NMIIA and NMIIB

We determined that NMIIA and NMIIB proteins are not differentially distributed within the cells at the MHB; however, we did discover that knockdown of one can influence the localization of the other (Fig. 15). NMIIA and NMIIB are both activated via phosphorylation of the myosin regulatory light chain (MRLC) (Bresnick, 1999; Ito et al., 2004). Yet, NMIIA and NMIIB are differentially regulating cell shape in the same cell resulting in distinct changes. From our previous work, we know that the level of phosphorylated MRLC in the brain increases from 18 hpf to 21 hpf and then goes back down by 24 hpf (Gutzman and Sive, 2010), indicating the NMII activity is high in the brain during the time of morphogenesis investigated here. MRLC activation can occur via multiple signaling pathways; including via myosin light chain kinase (MLCK) and/or Rho-kinase (ROCK). In cell culture, MLCK and ROCK specifically localize to regulate MRLC phosphorylation in a spatially dependent manner. In 3T3 cells, ROCK is more active in phosphorylating MRLC at the center of the cell, while MLCK is more active in phosphorylating MRLC at the cell periphery (Totsukawa et al., 2004; Totsukawa et al., 2000). It was demonstrated in migratory cells that a given cellular microenvironment may play a role in determining the localization and function of specific NMII isoforms (Raab et al., 2012). Although we do not see a difference in NMIIA and NMIIB localization in normal tissue here, potentially the differential function of the two proteins is determined by differential localization of their upstream activators which have yet to be identified. Another possibility is that, although the proteins are localized in the same parts of the cell, the orientation of the non-muscle myosin heavy chains

may be oriented in opposing directions. For example, NMIIA fibers may run in an apical to basal direction to regulate cell length, while NMIIB fibers may orient perpendicularly to NMIIA to regulate cell width.

Non-muscle myosin heavy chains IIA and IIB can both be phosphorylated on various sites to affect filament assembly and protein function (Vicente-Manzanares et al., 2009). This raises the question as to whether or not there is a difference in the phosphorylation state of the non-muscle myosin heavy chains themselves at the MHB. Phosphorylation of the NMII heavy chains facilitates filament disassembly and NMIIA and NMIIB have different sites in their tail domains making this a possible level of differential activation and regulation. It was also recently demonstrated that NMII isoforms can co-assemble in living cells, forming heterotypic filaments that can perform both isoform specific and redundant functions (Beach et al., 2014). It remains to be seen if these heterotypic filaments are present in the neuroepithelium during development.

Differential distribution of actin with non-muscle myosin knockdown

It is established that NMII protein activity, in response to extra or intra-cellular signals, contributes to the spatial organization of the actin network, resulting in contractility and physiological functions (Kohler et al., 2011). Both NMIIA and NMIIB knockdown resulted in abnormal actin distribution in the MHB region during morphogenesis. Knockdown of NMIIA caused changes in actin localization within the neuroepithelium and at the apical surface of the neural tube, while knockdown of NMIIB caused abnormal actin distribution within the neuroepithelium, and at

both the apical and basal surfaces of the neural tube. The location of actin affected by NMII knockdown may provide some additional clues as to the regulation of the NMII protein. Since *mypt1* appears to regulate NMII activity apically, it is likely to be regulating both NMIIA and NMIIB (Gutzman and Sive, 2010), which is consistent with the *mypt1* knockdown cell shape phenotypes as well. Actomyosin activity is regulated on the basal surface of follicle cells by Rho, ROCK, and cell-cell adhesion during *Drosophila* egg chamber development to cause contraction (He et al., 2010). However, *Drosophila* have only one non-muscle myosin heavy chain (*zipper*), indicating the importance for *in vivo* vertebrate studies to determine how NMIIA and NMIIB are differentially regulating cell shape. These studies will be essential to elucidate additional mechanisms of morphogenetic processes.

Acknowledgments

We thank all members of the Gutzman lab for helpful discussion and comments on the manuscript. Thank you to Dr. Ava Udvadia (University of Wisconsin-Milwaukee) for constructive discussion and comments. We would like to acknowledge Dr. Filipe Alberto (University of Wisconsin-Milwaukee) for his assistance with statistical analyses. A special thank you to Dr. Hazel Sive (Whitehead Institute and MIT, Cambridge, MA) where this work originated. This research was supported by the UWM Research Growth Initiative.

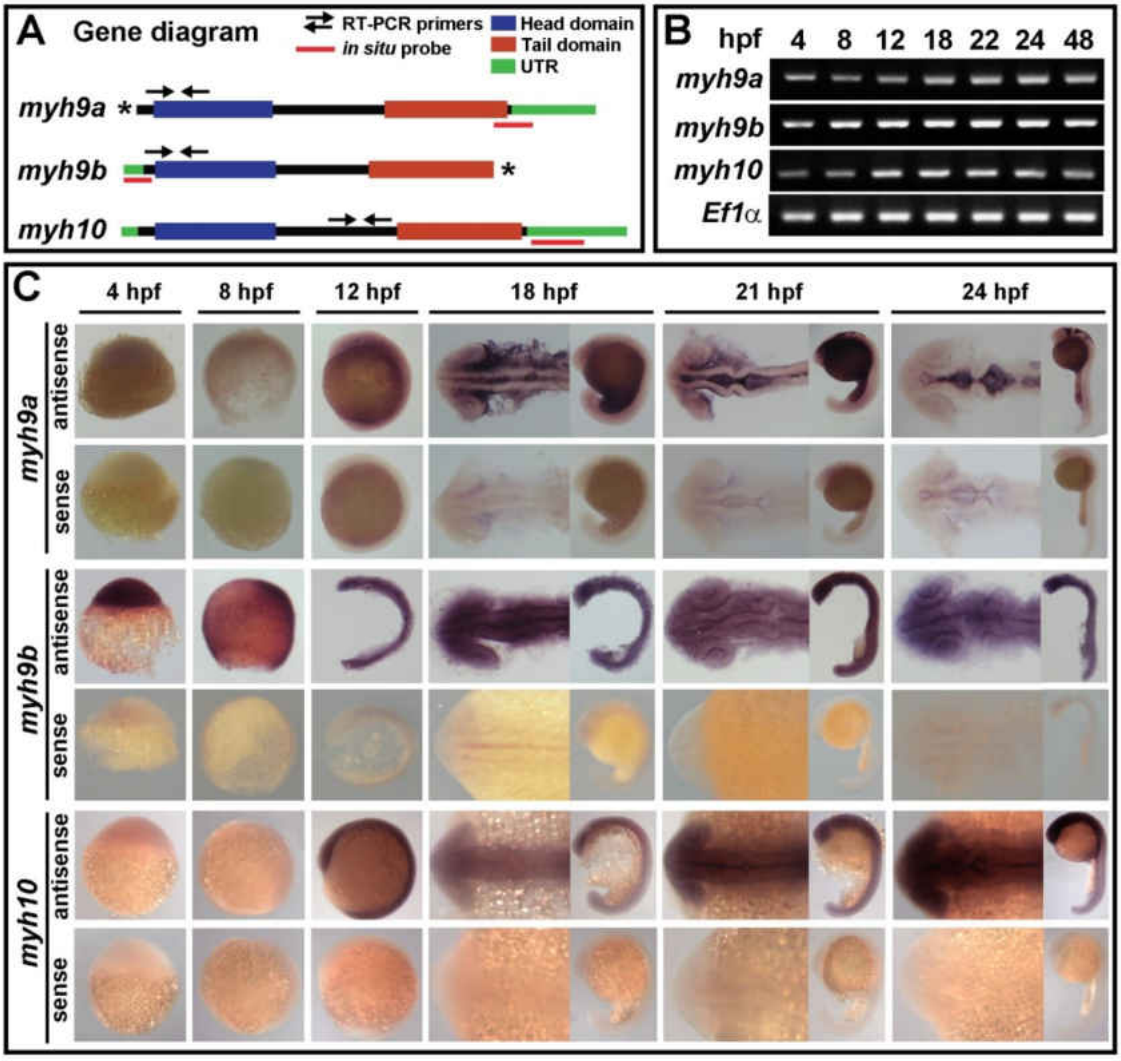

Figure 9. *myh9a*, *myh9b*, and *myh10* are expressed during the time of MHB morphogenesis. (A) Diagram of the zebrafish *myh9a*, *myh9b*, and *myh10* genes. Domain regions are highlighted. Regions amplified for RT-PCR time course expression are shown with arrows (primer details can be found in "Materials and Methods"). Asterisks indicate the regions of the full length *myh9a* and *myh9b* in the current Ensembl zebrafish genome that have not been completely annotated. (B) RT-PCR analysis of *myh9a*, *myh9b*, and *myh10* over a time course of embryonic development spanning MHB morphogenesis. EF1α was used as a control. Primer locations are indicated in panel A. (C) Time course of gene expression by *in situ* hybridization for *myh9a*, *myh9b,* and *myh10* in the developing embryo from 4 hpf- 24 hpf. Each gene is shown with the antisense probe expression pattern and sense control.

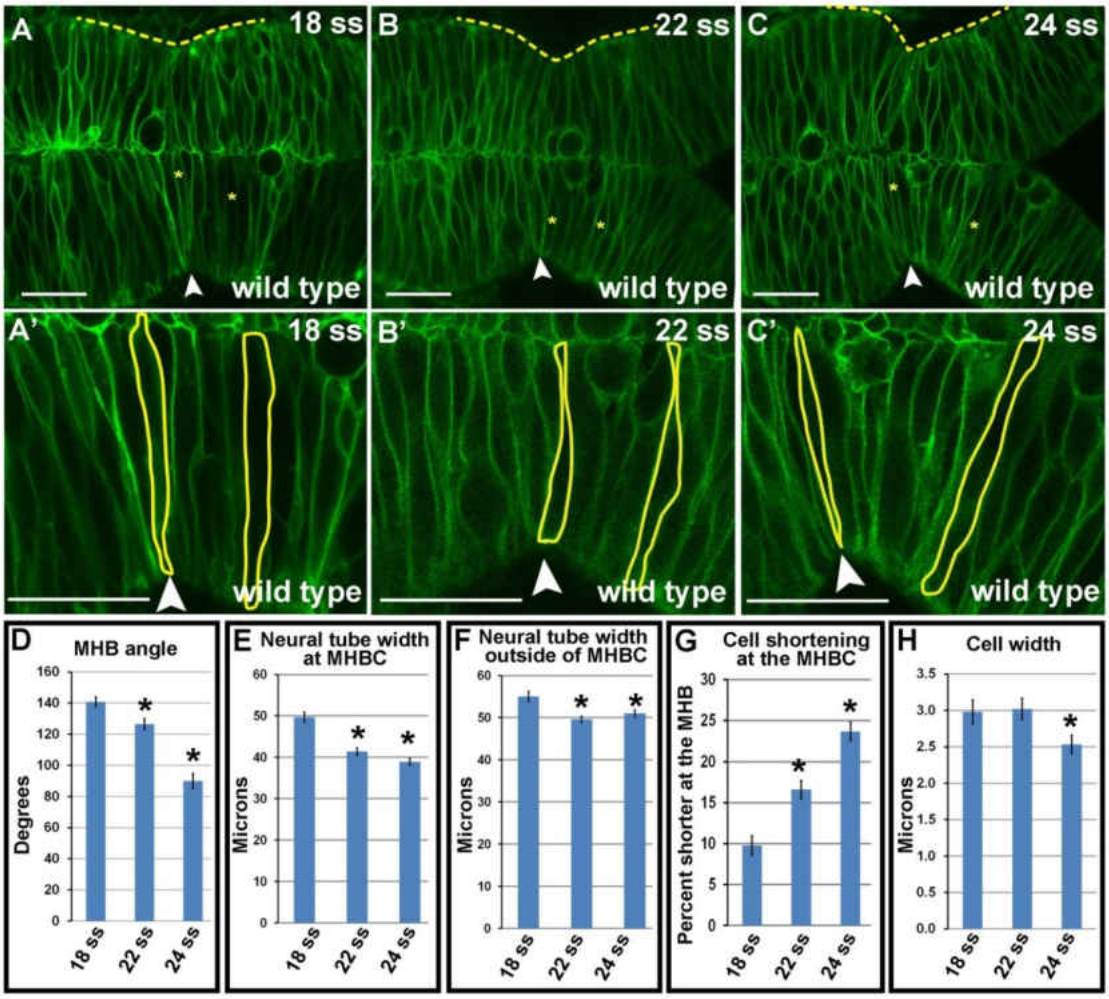

Figure 10. Quantification of wild type tissue and cell shape changes during MHB morphogenesis between 18 and 24 ss. (A-C) Live confocal imaging of wild type embryos injected with mGFP and imaged at the stages indicated. (A'-C') Magnifications of images in A-C with individual cells outlined at the MHBC and posterior to the MHBC towards the hindbrain. (D) Quantification of the MHB angle on the basal side of the neuroepithelium (see dotted lines in A-C). (E) Measurement of neural tube width as a representation of cell length in cells at the MHBC over time. (F) Measurement of neural tube width as a representation of cell length in cells 40 microns posterior to the MHBC over time. (G) Changes in the percentage of cell shortening for cells at the MHBC compared to cells 40 microns outside the MHBC over time. (H) Quantification of cell width measurements over time. Arrowheads indicate MHBC. Asterisks in A-C indicate cells outlined in the images below (A'-C'). One-way ANOVA with multiple t-test comparisons was performed to determine significance, asterisks indicate $p<0.001$. Results are shown as ± s.e.m. 18 ss; $n = 9$; 22 ss, $n = 11$, 24 ss, $n = 11$. Scale bars: 25 μm.

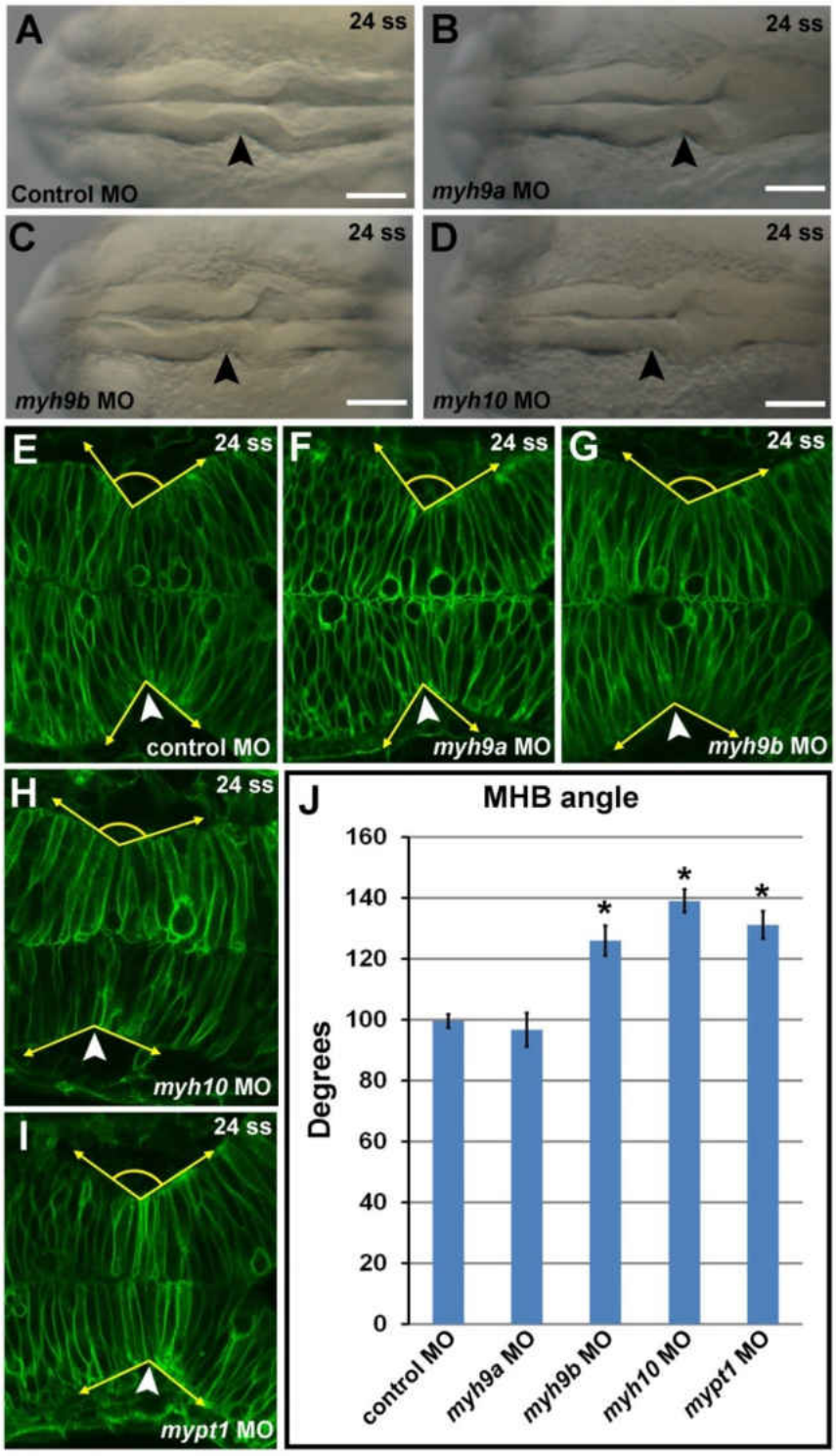

Figure 11. *myh9b*, *myh10* and *mypt1* are required for MHB tissue morphogenesis. (A-D) Brightfield dorsal view images of 24 ss embryos following injection with (A) control MO, (B) *myh9a* MO, (C) *myh9b* MO, (D) *myh10* MO. Anterior is to the left in all images. Arrowheads indicate MHBC. Scale bars: 100 μm. (E-I) Live confocal images showing the MHB region of 24 ss zebrafish

embryos injected with mGFP mRNA and coinjected with control MO (E), *myh9a* MO (F), *myh9b* MO (G), *myh10* MO (H), or *mypt1* MO (I). (J) Quantification of the MHB angle on the basal side of the neuroepithelium (see angle lines in E-I). One-way ANOVA with multiple t-test comparisons was performed to determine significance between control and test groups. Asterisks indicate $p<0.001$. Results are shown as ± s.e.m. For E-I; control MO, $n = 48$; *myh9a* MO, $n = 10$; *myh9b* MO, $n = 16$; *myh10* MO, $n = 18$; *mypt1* MO, $n = 20$.

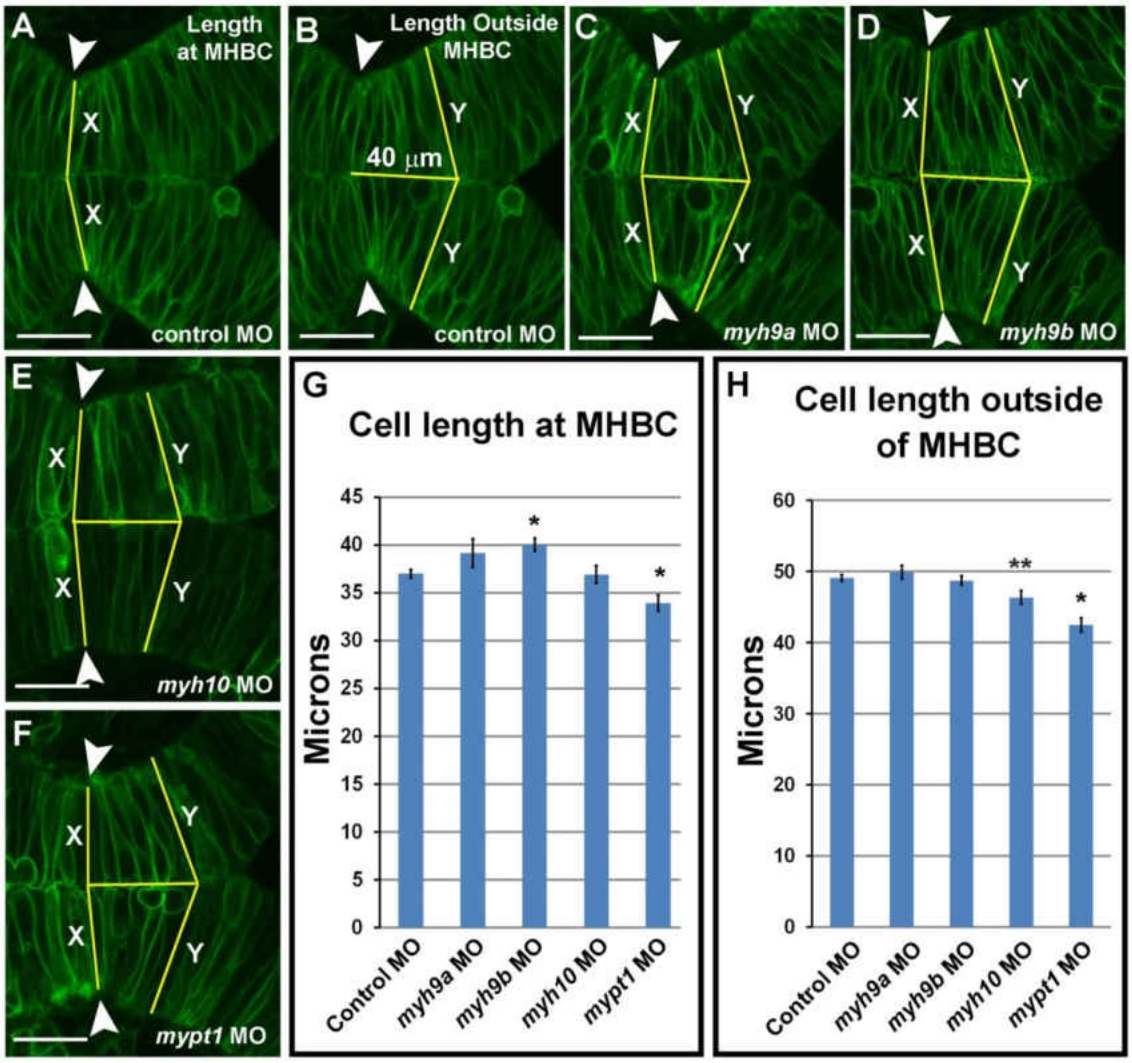

Figure 12. *myh9b* is required for cell shortening at the MHBC during morphogenesis. (A-F) Live confocal images showing the MHB region of 24 ss zebrafish embryos injected with mGFP and coinjected with control MO (A-B), *myh9a* MO (C), *myh9b* MO (D), *myh10* MO (E), or *mypt1* MO (F). (G) Quantification of the cell length (X) at the MHBC (see lines in A, C-F). (H) Quantification of cell length 40 microns outside of the MHBC (Y) (see lines in B-F). One-way ANOVA with multiple t-test comparisons was performed to determine significance between control and test groups. Asterisks indicate $p<0.001$. Double asterisks indicate $p<0.05$. Results are shown as ± s.e.m. Control MO, n = 48; *myh9a* MO, n = 10; *myh9b* MO, n = 16; *myh10* MO, n=18; *mypt1* MO, n=20. Scale bars: 25 μm.

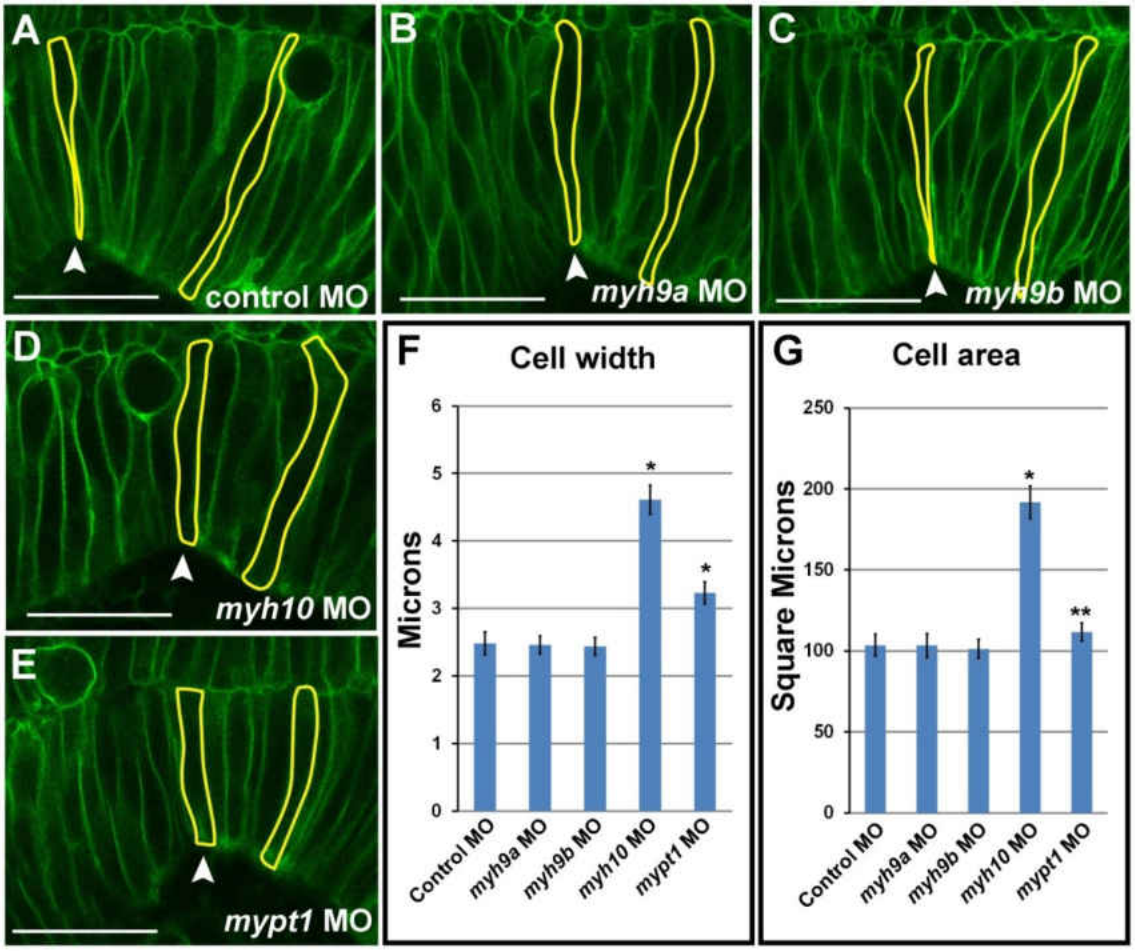

Figure 13. *myh10* is required for regulation of cell width in the MHB during morphogenesis. (A-E) Live confocal images showing one side of the MHB region of 24 ss zebrafish embryos injected with mGFP and coinjected with control MO (A), *myh9a* MO (B), *myh9b* MO (C), *myh10* MO (D), or *mypt1* MO (E). Single representative cells are outlined in each panel. (F) Quantification of the cell width. (G) Quantification of cell area. One-way ANOVA with multiple t-test comparisons was performed to determine significance between control and test groups. Asterisks indicate $p<0.001$. Double asterisks indicate $p<0.05$. Results are shown as ± s.e.m. For each embryo (*n*) a total of 6 cells were outlined: 2 cells at the MHBC were outlined, 2 cells 40 microns posterior to the MHBC were outlined, and 2 cells within the 40 micron region between the MHBC and posterior were outlined. Cells were chosen based on the ability to see an entire cell from apical to basal in a single z-section. Control MO, *n* = 9; *myh9a* MO, *n* = 9; *myh9b* MO, *n* = 14; *myh10* MO, *n*=9; *mypt1* MO, *n*=9. Scale bars: 25 μm.

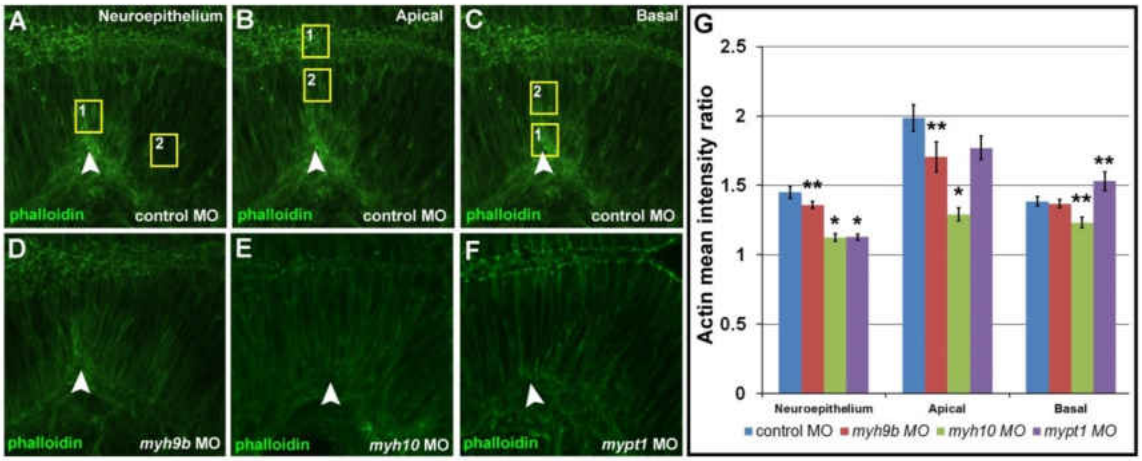

Figure 14. Actin distribution is dependent upon non-muscle myosin II function. (A-F) Embryos were injected as indicated and stained with phalloidin (green) to determine actin localization and regional enrichment. (A-C) Control morphant embryos with normal actin distribution at the MHB. Boxes indicate areas of comparison for determining the mean actin intensity ratio. (A) Comparison of actin intensity with the neuroepithelium at the MHBC region (box 1) compared to the posterior MHB (box 2). (B) Comparison of actin intensity apically at the midline (box 1) compared to the apical region within the neuroepithelial tissue (box 2). (C) Comparison of actin intensity on the basal side of the neuroepithelium (box 1) compared to the basal region within the neuroepithelial tissue (box 2). (G) Quantification of actin distribution comparison ratios for control MO, *myh9b* MO, *myh10* MO, and *mypt1* MO injected embryos in the regions indicated. One-way ANOVA with multiple t-test comparisons was performed to determine significance between control and test groups. Results are shown as ± s.e.m. Asterisks indicate significance compared to control, $p<0.001$. Double asterisks indicate, $p<0.01$. Arrowheads indicate MHBC. Control MO, $n = 8$; *myh9b* MO, $n = 12$; *myh10* MO, $n=13$; *mypt1* MO, $n=8$.

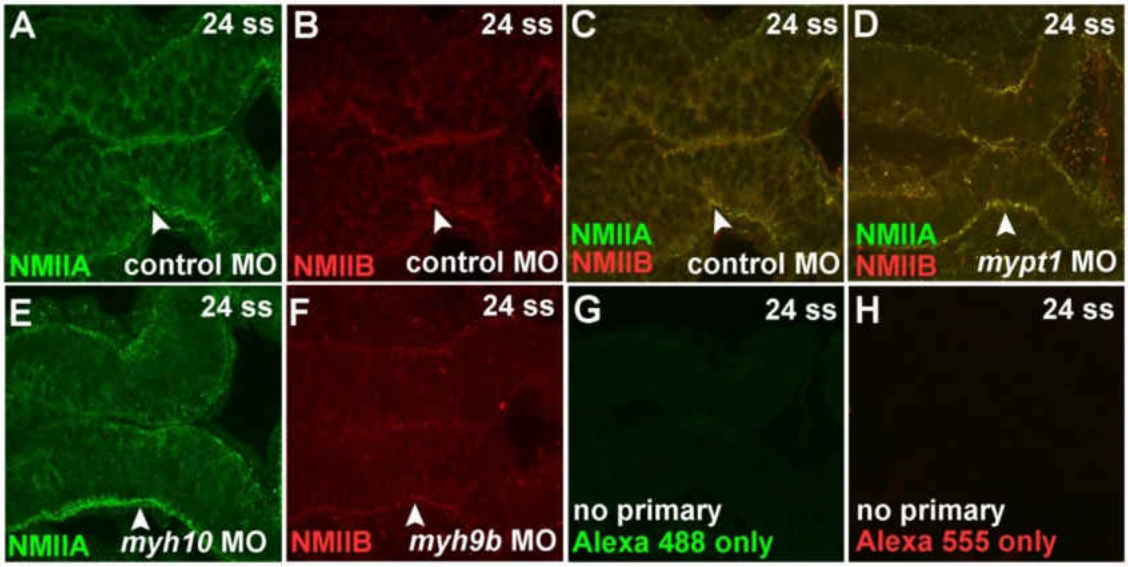

Figure 15. Non-muscle myosin IIA and IIB protein localization. (A-C) NMIIA and NMIIB antibody staining in 24 ss embryos injected with control MO. (A) NMIIA antibody (green), (B) NMIIB antibody (red), (C) overlay of A and B. (D) Overlay of NMIIA and NMIIB immunostaining in a 24 ss *mypt1* MO injected embryo. (E) NMIIA staining with *myh10* MO knockdown. (F) NMIIB staining with *myh9b* MO knockdown. (G-H) No primary control from Alexa 488 and Alexa 555 secondary antibodies. Results are representative of at least three independent experiments. Control MO, n = 8; *mypt1* MO, n = 7; *myh10* MO, n = 14; *myh9b* MO, n = 19; Alexa 488 no primary control, n = 5; Alexa 555 no primary control, n = 5.

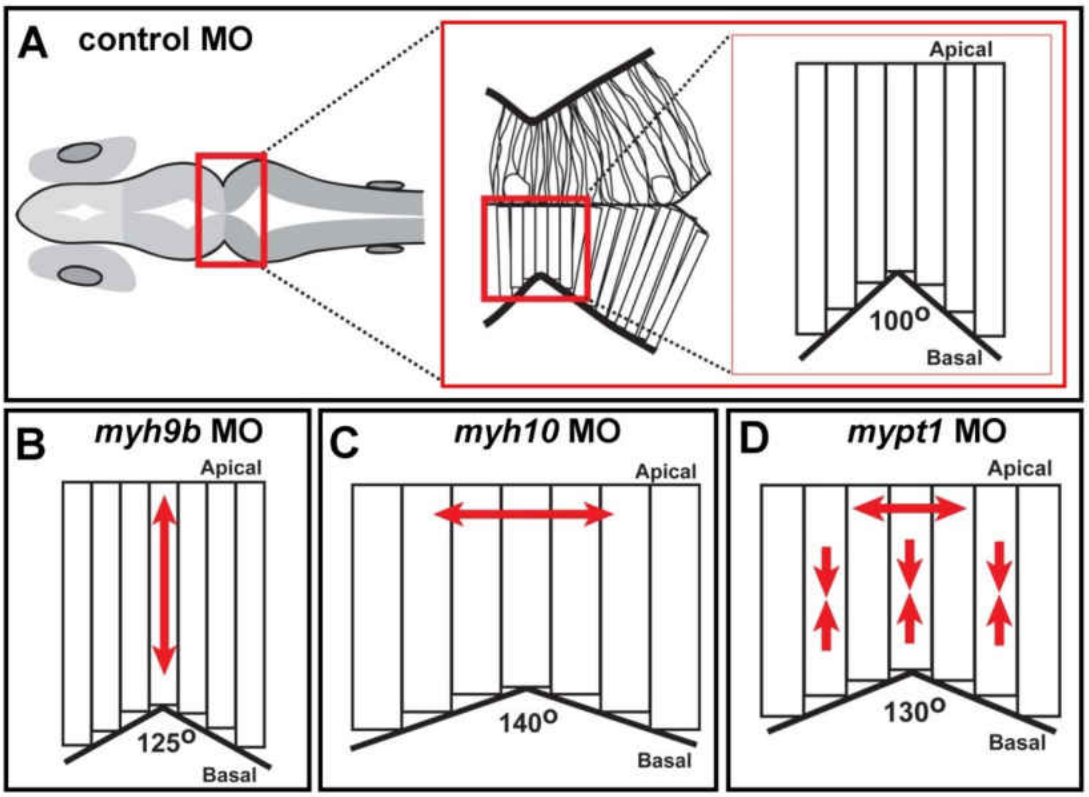

Figure 16. Model for non-muscle myosin IIA and IIB differential regulation of cell shape changes at the MHB during brain morphogenesis. (A) Representation of a wild-type or control morphant embryo at 24 ss with magnification of the MHB region and simplified model of cell shape at the MHB. Wild-type and control morphants have an MHB angle of approximately 100 degrees and cells at the MHBC are almost 25% shorter than surrounding cells, while all cells have equal cell width. (B) *myh9b* knockdown results in an increase in the MHB angle to 125 degrees and this angle difference is due to cells specifically at the MHBC not shortening normally. (C) *myh10* loss-of-function results in an increase in the MHB angle to 140 degrees as a result of increase in cell width with normal cell length at the MHBC. (D) *mypt1* knockdown, and increased activation of both NMIIA and NMIIB, results in both shorter and wider cells throughout the region leading to an increase in the MHB angle to 130 degrees.

Supplemental Materials

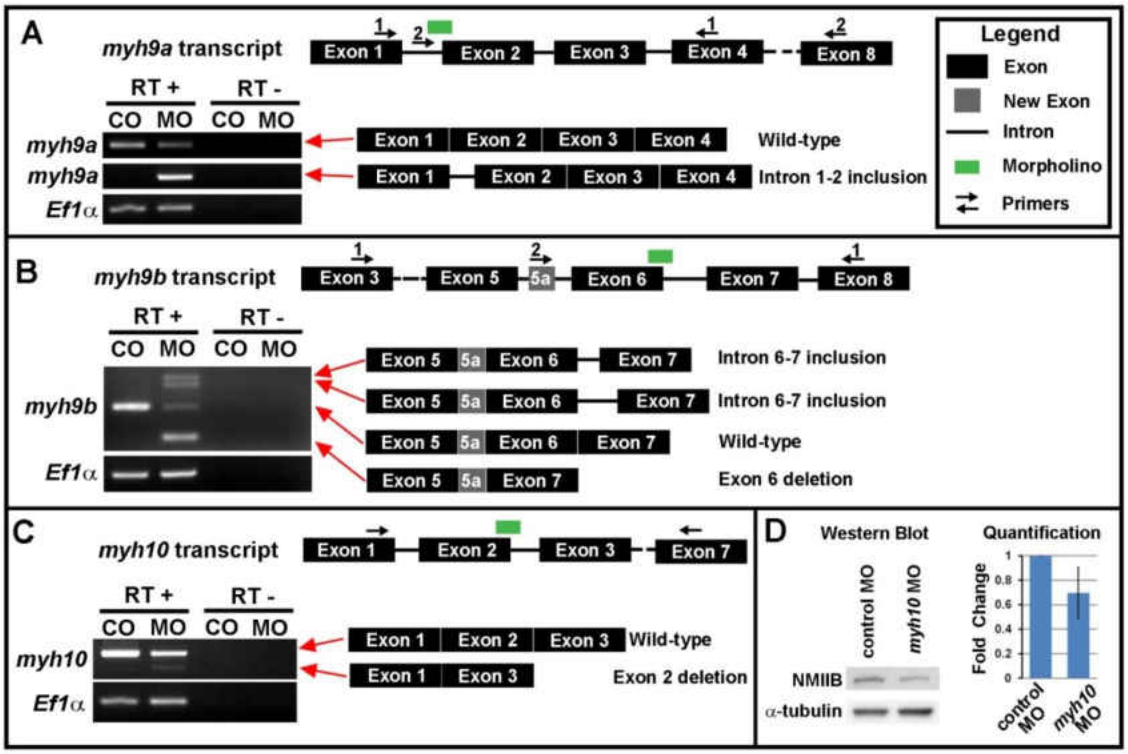

Figure S 1. Details for morpholino induced splice variation and sequence analysis. Single cell embryos were injected with 4ng control MO + 4ng p53 MO, 4ng *myh9a* MO, 3ng *myh9b* MO + 3ng *p53* MO, or 3ng *myh10* MO. All MO confirmation experiments were conducted using the same concentration of MO as was used for all imaging and analysis experiments described in the "Materials and Methods". RNA was collected from control and experimental morphant injected embryos at 24 hpf for RT-PCR analysis. For each MO used, aberrant splicing was detected, as well as a decrease in wild-type transcript. EF1α was used as a control for each RT-PCR experiment. (A) Analysis from RT-PCR experiments confirmed that injection of 4ng of *myh9a* MO resulted in an inclusion of intron 1-2. Wild-type transcript was detected in both control and *myh9a* morphants using the following primers, *myh9a* forward primer 1 (within Exon1) (5'-AAATTCAGCAAGGTG GAGGA-3'); *myh9a* reverse primer 1 (within Exon4) (5'-TTGGTGTTTTCGGTTT TTCC-3'). Aberrant splicing and the inclusion of intron 1 was detected only in the *myh9a* morpholino injected embryos using the following primers; *myh9a* forward primer 2 (within intron 1-2) (5'-tgcaaacttgagctttgtgtt-3') and *myh9a* reverse primer 2 (within Exon 8) (5'-GCACGGGACTTCTCCAATAG-3'). Diagram depicts location of primers, morpholino target, and abnormal splicing product with MO injection. (B) RT-PCR analysis confirmed that injection of 3ng of *myh9b* MO disrupts normal RNA processing. The *myh9b* MO caused three abnormal splice changes; a deletion of Exon 6, and two different length inclusions of intron 6-7. In addition, while investigating the effect of the *myh9b* morpholino on mRNA splicing, upon sequencing RT-PCR products following MO injection, we discovered an

unannotated putative exon between the current Ensembl annotation of Exon 5 and Exon 6 which we have termed Exon 5a. Initial experiments to test for aberrant splicing were conducted using the following primers: *myh9b* forward primer 1 (within Exon 3) (5'-GGTGAATCTGGAGCTGGAAA-3'), and *myh9b* reverse primer 1 (within Exon 8) (5'-TGTGGAAGGTTCGCTCTTCT-3'). Using these primers we discovered that our control samples consistently amplified two bands that were very close in size. Upon sequencing of both control bands, and *myh9b* MO RNA samples, we determined that we had discovered an additional unannotated exon that we have termed Exon 5a. For further testing of the morpholino activity we designed a primer to the Exon5a sequence which allowed us to clearly define the splice changes induced by the *myh9b* MO without multiple bands for each aberrant splicing product. The short Exon 5a sequence (previously annotated as intron) is as follows: "AGCAGCTCCGTCCTGTCA CATGGT". Primers used for the analysis presented in panel B include: *myh9b* forward primer 2 (within Exon5a) (5'-GCAGCTCCGTCCTGTCAC-3'); *myh9b* reverse primer 1 (within Exon 8) (5'-TGTGGAAGGTTCGCTCTTCT-3'). Diagram depicts location of primers, morpholino target, Exon 5a, and abnormal splicing products found with MO injection. (C) RT-PCR analysis confirmed that injection of 3ng of the *myh10* MO causes a deletion of exon2. *myh10* forward primer: (within Exon 1) (5'-CTTC TGAACGGCATGGATTT-3'), *myh10* reverse primer: (within Exon7) (5'-TTGGCAT TTCCAAAGGATTC- 3'). Diagram depicts location of primers, morpholino target, and abnormal splicing product with MO injection. Each abnormal splice variant from these morpholino injections resulted in a frame shift and the introduction of an early stop codon. (D) Representative Western blot for analysis of *myh10* MO knockdown. Wild-type embryos were injected with control or *myh10* MO as described above. At 24 ss the yolk was manually removed from the whole embryo and the whole tissue protein was isolated with a protease inhibitor cocktail (Roche, 04693124001) as previously described (Gutzman and Sive, 2010). Antibodies include, anti-myosin IIB antibody (Santa Cruz Biotechnology, sc-376942, 1:500), anti-α-tubulin (Sigma-Aldrich, T6199, 1:2000), anti-mouse IgG HRP-linked antibody (Cell Signaling Technology Inc., #7076, 1:2000). Blots were imaged using Foto/Analyst Luminary FX imager with Foto/Analyst PC Image software (Fotodyne Inc.). Protein levels were quantified and compared with the α-tubulin controls using Photoshop from four independent experiments.

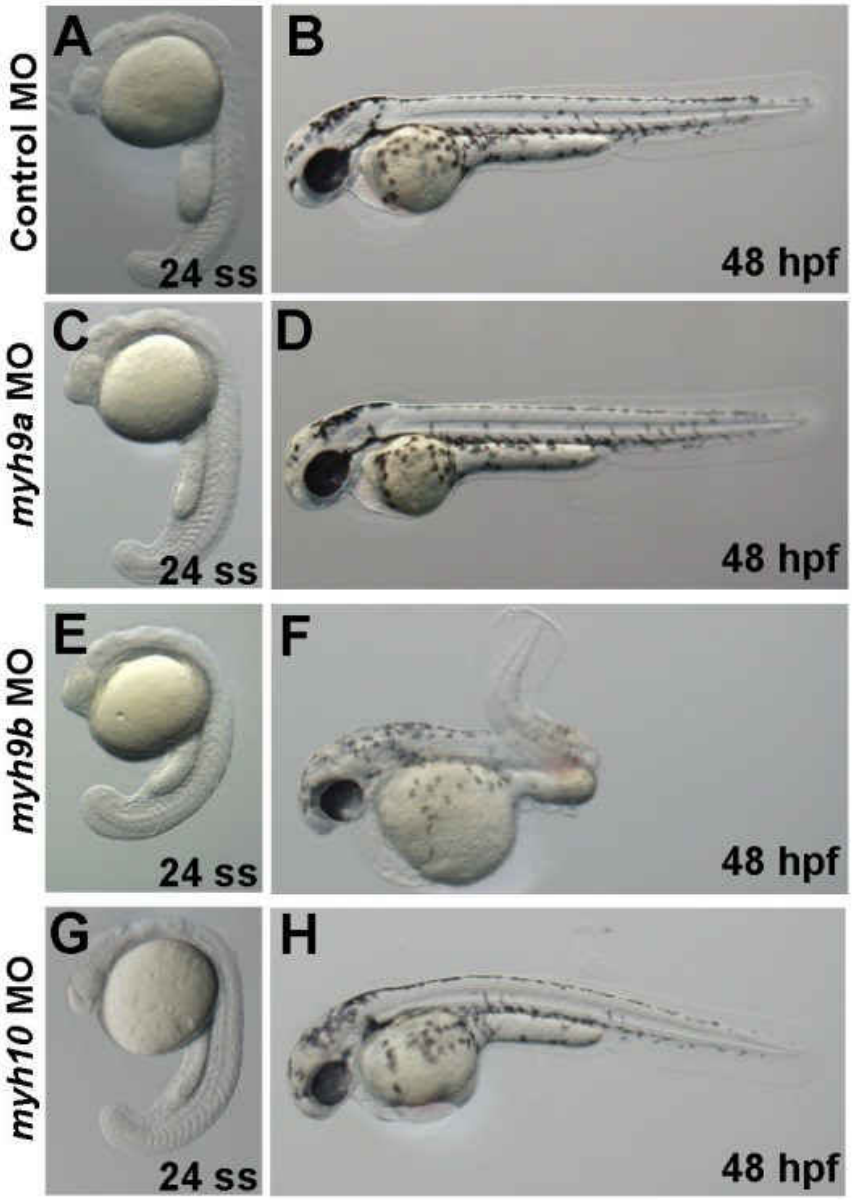

Figure S 2. Whole embryo phenotypes for morpholino injected embryos. Single cell embryos were injected with (A,B) 4ng control MO + 4ng p53 MO, (C,D) 4ng *myh9a* MO, (E,F) 3ng *myh9b* MO + 3ng *p53* MO, or (G,H) 3ng *myh10* MO. Live embryos were imaged using brightfield microscopy at 24 ss and at 48 hpf as indicated. *myh9a* morphants did not demonstrate any obvious phenotypes at the times imaged. For *myh9b* and *myh10* morphants, representative mild phenotypes are shown. *myh9b* morphants demonstrated somite defects, abnormal tail curvature, pigmentation defects, heart abnormalities, slight edema, and abnormal eye and ear formation. *myh10* morphants had abnormal body axis curvature, heart abnormalities, slight edema, and abnormal eye development.

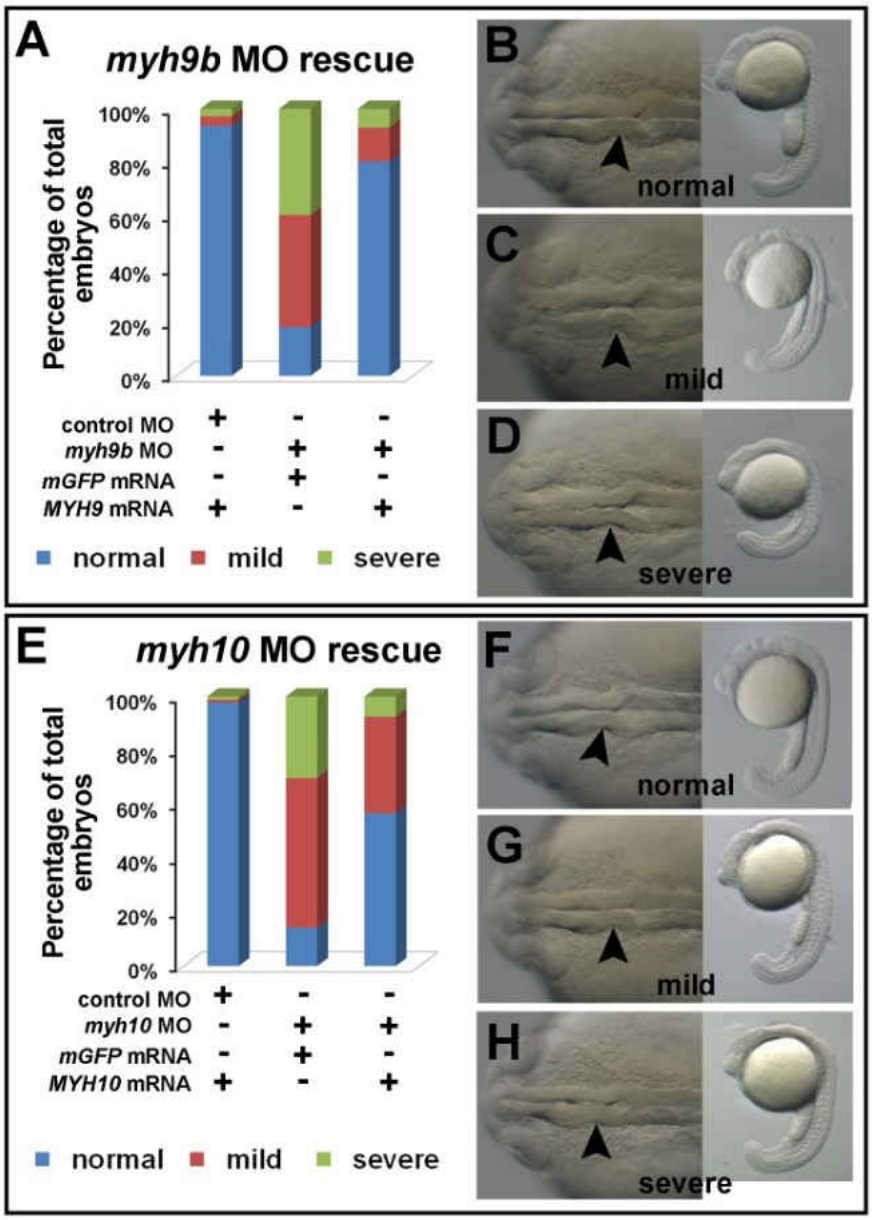

Figure S 3. Rescue of the *myh9b* and *myh10* knockdown MHB phenotype with human mRNA injection. Embryos were injected at the one cell stage with human *MYH9* or *MYH10* mRNA in conjunction with morpholino injections. The human full length DNA for *MYH9* was obtained from Addgene clone 10844 and subcloned into the pCS2+ vector for mRNA expression. Human full length DNA for *MYH10* was obtained from Addgene clone 10845 and subcloned into the pCS2+ vector for mRNA expression. mRNA was transcribed using the mMessage mMachine kit (Ambion). Graphs depict the distribution of “normal”, “mild”, and “severe” MHB phenotypes at 24 ss for each treatment group shown. (A) Embryos injected with *myh9b* MO combined with human *MYH9* mRNA showed partial

rescue of the MHB phenotype. Control MO + mGFP, *n*=140; *myh9b* MO + mGFP, *n*= 148; *myh9b* MO + *MYH9* mRNA, *n*=157. (B-D) Representative images demonstrating the “normal”, “mild”, and “severe” *myh9b* MO phenotypes scored. (E) Rescue of *myh10* MO injected embryos with human *MYH10* mRNA. Embryos injected with *myh10* MO combined with human *MYH10* mRNA showed partial rescue of the MHB phenotype. Control MO + mGFP, *n*= 90; *myh10* MO + mGFP, *n*= 106; *myh10* MO + *MYH10* mRNA, *n*=120. (F-H) Representative images demonstrating the “normal”, “mild”, and “severe” *myh10* MO phenotypes scored. For *myh9b* MO rescue 100 pg of *MYH9* mRNA was co-injected, and for *myh10* MO rescue 200 pg of *MYH10* mRNA was co-injected. Chi-squared test with a 3X3 contingency table (df=4) was performed to test for statistical significance between the three treatment groups and the number of embryos with normal, mild, or severe phenotypes. For panel A (*myh9b* rescue data) Chi-squared = 206.79, $p<0.00001$. For panel E (*myh10* rescue data) Chi-squared = 144.04, $p<0.00001$.

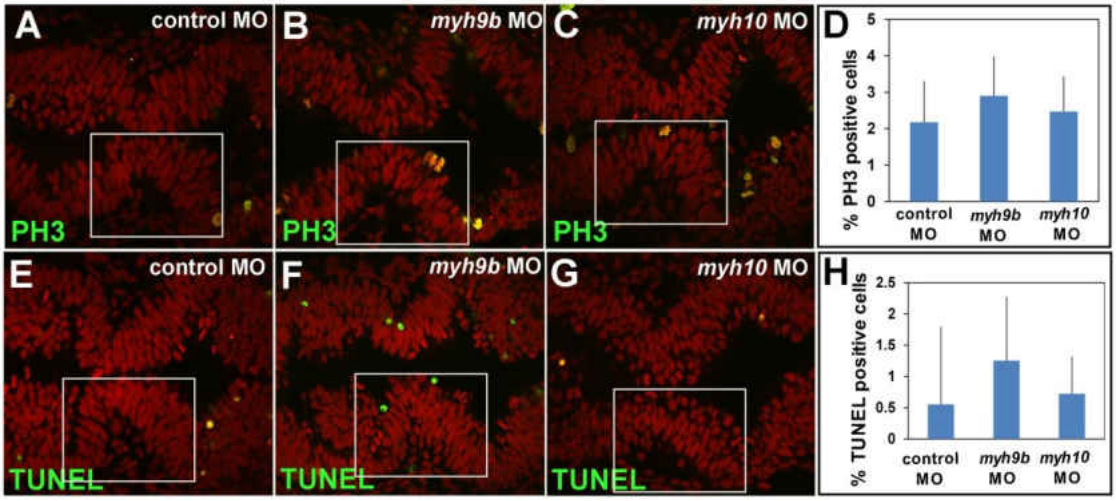

Figure S 4. *myh9b* and *myh10* knockdown does not affect cell proliferation or cell death at the MHB. (A-C) Representative confocal images of control (A), *myh9b* MO (B), and *myh10* MO (C) injected embryos that were fixed at 24 ss and stained with PH3 (green) to label proliferating cells. Embryos were fixed in 4% PFA, deyolked, rinsed in PBT and blocked overnight in (2% NGS, 2% BSA, 1% DMSO, 0.5% TritonX in PBS). Embryos were incubated in primary anti-PH3 antibody, (Millipore, 1:800) overnight, washed, and incubated in secondary antibody Alexa Fluor 488 (goat anti rabbit, 1:500). Propidium iodide was used to stain for nuclei (Invitrogen, P3566, 1:1000 in PBT) for 1 hour. Embryos were washed, mounted in glycerol and imaged using Nikon CS2 laser scanning confocal microscope. Boxes indicate the region of the brain where total cell number and PH3 positive cells were counted within the neural tissue. (D) Quantification of the percentage of PH3 positive cells within the region. Control MO, *n*=22; *myh9b* MO, *n*=14; *myh10* MO, *n*=10. Results are shown as mean ± s.d. No significant differences were detected. (E-G) Representative confocal images of control (E), *myh9b* MO (F), and *myh10* MO (G), injected embryos that were fixed at 24 ss and TUNEL labeled (green) to indicate apoptotic cells. All embryos were counter stained with propidium iodide (red) to label all cells. Apoptosis was detected by the TUNEL method using the Apoptag Kit (Millipore) according to the provided protocol using fluorescent detection of apoptotic cells. Embryos were counterstained with propidium iodide to label nuclei and imaged by laser-scanning confocal microscopy (Nikon CS2). Boxes indicate the region of the brain where total cell number and TUNEL positive cells were counted within the neural tissue. (H) Quantification of the percentage of TUNEL positive cells within the region. Control MO, *n*=10; *myh9b* MO, *n*=14; *myh10* MO, *n*=10. Results are shown as mean ± s.d. No significant differences were detected.

REFERENCES

Bao, J., X. Ma, C. Liu, and R.S. Adelstein. 2007. Replacement of nonmuscle myosin II-B with II-A rescues brain but not cardiac defects in mice. *The Journal of biological chemistry*. 282:22102-22111.

Beach, J.R., L. Shao, K. Remmert, D. Li, E. Betzig, and J.A. Hammer, 3rd. 2014. Nonmuscle Myosin II Isoforms Coassemble in Living Cells. *Curr Biol*. 24:1160-1166.

Brand, M., C.P. Heisenberg, Y.J. Jiang, D. Beuchle, K. Lun, M. Furutani-Seiki, M. Granato, P. Haffter, M. Hammerschmidt, D.A. Kane, R.N. Kelsh, M.C. Mullins, J. Odenthal, F.J. van Eeden, and C. Nusslein-Volhard. 1996. Mutations in zebrafish genes affecting the formation of the boundary between midbrain and hindbrain. *Development*. 123:179-190.

Bresnick, A.R. 1999. Molecular mechanisms of nonmuscle myosin-II regulation. *Curr Opin Cell Biol*. 11:26-33.

Conti, M.A., S. Even-Ram, C. Liu, K.M. Yamada, and R.S. Adelstein. 2004. Defects in cell adhesion and the visceral endoderm following ablation of nonmuscle myosin heavy chain II-A in mice. *The Journal of biological chemistry*. 279:41263-41266.

Flicek, P., I. Ahmed, M.R. Amode, D. Barrell, K. Beal, S. Brent, D. Carvalho-Silva, P. Clapham, G. Coates, S. Fairley, S. Fitzgerald, L. Gil, C. Garcia-Giron, L. Gordon, T. Hourlier, S. Hunt, T. Juettemann, A.K. Kahari, S. Keenan, M. Komorowska, E. Kulesha, I. Longden, T. Maurel, W.M. McLaren, M. Muffato, R. Nag, B. Overduin, M. Pignatelli, B. Pritchard, E. Pritchard, H.S. Riat, G.R. Ritchie, M. Ruffier, M. Schuster, D. Sheppard, D. Sobral, K. Taylor, A. Thormann, S. Trevanion, S. White, S.P. Wilder, B.L. Aken, E. Birney, F. Cunningham, I. Dunham, J. Harrow, J. Herrero, T.J. Hubbard, N. Johnson, R. Kinsella, A. Parker, G. Spudich, A. Yates, A. Zadissa, and S.M. Searle. 2013. Ensembl 2013. *Nucleic Acids Res*. 41:D48-55.

Golomb, E., X. Ma, S.S. Jana, Y.A. Preston, S. Kawamoto, N.G. Shoham, E. Goldin, M.A. Conti, J.R. Sellers, and R.S. Adelstein. 2004. Identification and characterization of nonmuscle myosin II-C, a new member of the myosin II family. *The Journal of biological chemistry*. 279:2800-2808.

Graeden, E., and H. Sive. 2009. Live imaging of the zebrafish embryonic brain by confocal microscopy. *J Vis Exp*.

Gutzman, J.H., E.G. Graeden, L.A. Lowery, H.S. Holley, and H. Sive. 2008. Formation of the zebrafish midbrain-hindbrain boundary constriction requires laminin-dependent basal constriction. *Mechanisms of development*. 125:974-983.

Gutzman, J.H., and H. Sive. 2010. Epithelial relaxation mediated by the myosin phosphatase regulator Mypt1 is required for brain ventricle lumen expansion and hindbrain morphogenesis. *Development*. 137:795-804.

Haigo, S.L., J.D. Hildebrand, R.M. Harland, and J.B. Wallingford. 2003. Shroom induces apical constriction and is required for hingepoint formation during neural tube closure. *Curr Biol*. 13:2125-2137.

Hartshorne, D.J., M. Ito, and F. Erdodi. 2004. Role of protein phosphatase type 1 in contractile functions: myosin phosphatase. *The Journal of biological chemistry*. 279:37211-37214.

He, L., X. Wang, H.L. Tang, and D.J. Montell. 2010. Tissue elongation requires oscillating contractions of a basal actomyosin network. *Nature cell biology*. 12:1133-1142.

Heisenberg, C.P., and Y. Bellaiche. 2013. Forces in tissue morphogenesis and patterning. *Cell*. 153:948-962.

Ito, M., T. Nakano, F. Erdodi, and D.J. Hartshorne. 2004. Myosin phosphatase: structure, regulation and function. *Molecular and cellular biochemistry*. 259:197-209.

Karfunkel, P. 1974. The mechanisms of neural tube formation. *Int Rev Cytol*. 38:245-271.

Kimmel, C.B., W.W. Ballard, S.R. Kimmel, B. Ullmann, and T.F. Schilling. 1995. Stages of embryonic development of the zebrafish. *Developmental dynamics : an official publication of the American Association of Anatomists*. 203:253-310.

Kohler, S., V. Schaller, and A.R. Bausch. 2011. Collective dynamics of active cytoskeletal networks. *PloS one*. 6:e23798.

Kovacs, M., F. Wang, A. Hu, Y. Zhang, and J.R. Sellers. 2003. Functional divergence of human cytoplasmic myosin II: kinetic characterization of the non-muscle IIA isoform. *The Journal of biological chemistry*. 278:38132-38140.

Lecuit, T., and P.F. Lenne. 2007. Cell surface mechanics and the control of cell shape, tissue patterns and morphogenesis. *Nature reviews*. 8:633-644.

Lee, J.Y., and R.M. Harland. 2007. Actomyosin contractility and microtubules drive apical constriction in Xenopus bottle cells. *Developmental biology*. 311:40-52.

Ma, X., J. Bao, and R.S. Adelstein. 2007. Loss of cell adhesion causes hydrocephalus in nonmuscle myosin II-B-ablated and mutated mice. *Molecular biology of the cell*. 18:2305-2312.

Ma, X., S. Kawamoto, Y. Hara, and R.S. Adelstein. 2004. A point mutation in the motor domain of nonmuscle myosin II-B impairs migration of distinct groups of neurons. *Molecular biology of the cell*. 15:2568-2579.

Maciver, S.K. 1996. Myosin II function in non-muscle cells. *Bioessays*. 18:179-182.

Martin, A.C., and B. Goldstein. 2014. Apical constriction: themes and variations on a cellular mechanism driving morphogenesis. *Development*. 141:1987-1998.

Martin, A.C., M. Kaschube, and E.F. Wieschaus. 2009. Pulsed contractions of an actin-myosin network drive apical constriction. *Nature*. 457:495-499.

Martinez-Morales, J.R., M. Rembold, K. Greger, J.C. Simpson, K.E. Brown, R. Quiring, R. Pepperkok, M.D. Martin-Bermudo, H. Himmelbauer, and J. Wittbrodt. 2009. ojoplano-mediated basal constriction is essential for optic cup morphogenesis. *Development*. 136:2165-2175.

Muller, T., E. Rumpel, S. Hradetzky, F. Bollig, H. Wegner, A. Blumenthal, A. Greinacher, K. Endlich, and N. Endlich. 2011. Non-muscle myosin IIA is

required for the development of the zebrafish glomerulus. *Kidney Int*. 80:1055-1063.

Nyholm, M.K., S. Abdelilah-Seyfried, and Y. Grinblat. 2009. A novel genetic mechanism regulates dorsolateral hinge-point formation during zebrafish cranial neurulation. *Journal of cell science*. 122:2137-2148.

Raab, M., J. Swift, P.C. Dingal, P. Shah, J.W. Shin, and D.E. Discher. 2012. Crawling from soft to stiff matrix polarizes the cytoskeleton and phosphoregulates myosin-II heavy chain. *The Journal of cell biology*. 199:669-683.

Rhinn, M., and M. Brand. 2001. The midbrain--hindbrain boundary organizer. *Current opinion in neurobiology*. 11:34-42.

Robu, M.E., J.D. Larson, A. Nasevicius, S. Beiraghi, C. Brenner, S.A. Farber, and S.C. Ekker. 2007. p53 activation by knockdown technologies. *PLoS Genet*. 3:e78.

Totsukawa, G., Y. Wu, Y. Sasaki, D.J. Hartshorne, Y. Yamakita, S. Yamashiro, and F. Matsumura. 2004. Distinct roles of MLCK and ROCK in the regulation of membrane protrusions and focal adhesion dynamics during cell migration of fibroblasts. *The Journal of cell biology*. 164:427-439.

Totsukawa, G., Y. Yamakita, S. Yamashiro, D.J. Hartshorne, Y. Sasaki, and F. Matsumura. 2000. Distinct roles of ROCK (Rho-kinase) and MLCK in spatial regulation of MLC phosphorylation for assembly of stress fibers and focal adhesions in 3T3 fibroblasts. *The Journal of cell biology*. 150:797-806.

Tullio, A.N., P.C. Bridgman, N.J. Tresser, C.C. Chan, M.A. Conti, R.S. Adelstein, and Y. Hara. 2001. Structural abnormalities develop in the brain after ablation of the gene encoding nonmuscle myosin II-B heavy chain. *The Journal of comparative neurology*. 433:62-74.

Urven, L.E., T. Yabe, and F. Pelegri. 2006. A role for non-muscle myosin II function in furrow maturation in the early zebrafish embryo. *Journal of cell science*. 119:4342-4352.

Vicente-Manzanares, M., X. Ma, R.S. Adelstein, and A.R. Horwitz. 2009. Non-muscle myosin II takes centre stage in cell adhesion and migration. *Nature reviews. Molecular cell biology*. 10:778-790.

Wang, A., X. Ma, M.A. Conti, and R.S. Adelstein. 2011. Distinct and redundant roles of the non-muscle myosin II isoforms and functional domains. *Biochemical Society transactions*. 39:1131-1135.

Wang, F., M. Kovacs, A. Hu, J. Limouze, E.V. Harvey, and J.R. Sellers. 2003. Kinetic mechanism of non-muscle myosin IIB: functional adaptations for tension generation and maintenance. *The Journal of biological chemistry*. 278:27439-27448.

Wang, G., M.L. Manning, and J.D. Amack. 2012. Regional cell shape changes control form and function of Kupffer's vesicle in the zebrafish embryo. *Developmental biology*. 370:52-62.

Westerfield, M. 2000. The Zebrafish Book: A guide for the laboratory use of zebrafish (*Danio rerio*). University of Oregon Press, Eugene.

CHAPTER 3
CALCIUM REGULATES CELL LENGTH DURING ZEBRAFISH MIDBRAIN-HINDBRAIN BOUNDARY DEVELOPMENT

A. INTRODUCTION

Calcium signaling plays a vital role in various developmental processes including gastrulation and establishment of body axis (Gilland et al., 1999; McGrath et al., 2003). It promotes airway branching morphogenesis in the developing lung (Brennan et al., 2013) and is important in neuronal development in axonal and dendritic morphogenesis (Ramakers et al., 2001). Calcium is also involved in cellular morphogenesis. Influx of extracellular calcium is required for epithelial cell contraction in carcinoma cell lines (Lee and Auersperg, 1980) and it plays an important role in cell shape change in platelets and endothelial cells (Moore et al., 1998; Porter et al., 2003). Thus, calcium is involved in many developmental and cellular morphogenetic events.

In order for calcium signaling to promote morphogenesis, it must act on downstream effectors of cell shape such as cytoskeletal elements. Gastrulation, dorsal closure and egg chamber elongation are some developmental events that are separately known to be regulated by calcium and non-muscle myosin II (NMII) (Franke et al., 2005; Hunter et al., 2014; Tada and Concha, 2001). Calcium signaling has been classically studied to regulate NMII activity in skeletal and smooth muscle contraction (Porter et al., 2003; Somlyo and Somlyo, 2003; Szent-

Gyorgyi, 1975). Some studies have indicated this interaction to be mediated by myosin light chain kinase (Martinsen et al., 2013; Watanabe et al., 2001).

Using the zebrafish midbrain-hindbrain boundary (MHB) as a model to study epithelial brain morphogenesis, we previously characterized the cell shape changes that occur during MHB formation. We found that the cell shape changes are regulated by non-muscle myosin II (NMII) proteins (Gutzman et al., 2015 and chapter 2) and NMII activity depends on the phosphorylation state of the myosin light chain (MLC) (Gutzman et al.,2010). The myosin phosphatase holoenzyme dephosphorylates the MLC, and is regulated by the *Mypt1* inhibitory regulatory subunit. We have shown that *mypt1* morphants have an abnormal MHB, due to an overactivation of NMII and a cell shape phenotype of shorter and wider cells in the MHB region (Gutzman et al., 2015 and chapter 2). The molecules directly affecting the phosphorylation state of NMII are in turn regulated by upstream signaling pathways which are yet to be elucidated.

In the current study, we hypothesized that the calcium signaling pathway regulates NMII during zebrafish MHB formation. We found that calcium is required for proper MHB development in zebrafish and depletion of intracellular calcium release from the endoplasmic reticulum (ER) by treatment with the pharmacological inhibitor, 2-aminoethoxy phenyl borate (2-APB) showed that the cells at the MHB constriction (MHBC) do not shorten normally. We further discovered that the cell length phenotype seen in *mypt1* morphants can be rescued by inhibition of intracellular calcium release. Overactivation of NMII by *mypt1* knockdown leads to shorter MHBC cells while inhibition of calcium release results in longer MHBC cells.

Successful rescue of the *mypt1* phenotype by calcium inhibition suggests that both molecules may be part of the same signaling pathway regulating the formation of the zebrafish MHB. Thus, teasing apart this pathway can help in improving our understanding of similar mechanisms involved in other developmental morphogenetic events.

B. MATERIALS AND METHODS

Animals

Wild-type AB zebrafish were raised and staged according to standard protocols as previously described (Kimmel et al., 1995). Embryos were staged according to somite stage (ss) for accuracy. 18 ss is 18 hpf and 24 ss is 22 hpf.

Microinjections

Splice-site blocking morpholino antisense oligonucleotides were injected at one-cell stage with a co-injection of membrane GFP (mGFP) at a concentration of 200 ng/μl. mGFP allows visualization of individual cell outlines during confocal imaging. *Mypt1* MO (5-ATTTTTTGTGACTTACTCAGCGATG-3; Gene Tools) that targets exon 2-intron 2 of the zebrafish *mypt1* was used at a concentration of 5 ng/μl (Gutzman and Sive, 2010). A standard control MO (5-CCTCTTACCTCAG TTACAATTTATA-3) and p53 morpholino (5-GCGCCATTGCTTTGCAAGAATTG-3) were also used at equivalent concentrations of 5 ng/μl (Gene Tools).

Drug treatments

Embryos were treated with 2-aminoethoxy phenyl borate (2-APB, Sigma D9754-1G) at 18 ss for 10 minutes at a concentration of 100 μM from a stock solution of 100 mM, and washed in 1X Danieau's solution.

Calcium imaging

Calcium green-1 dextran (Invitrogen molecular probes C3714) and dextran tetramethyl rhodamine (Invitrogen molecular probes D1818, 70000 MW) were injected into embryos at one-cell stage. At 4 hpf, they were manually dechorionated and placed on a glass slide in 0.1% DMSO prepared in 1X Danieau's solution for 10 minutes. Time lapse confocal images were taken once every 10 seconds for 10 minutes to detect calcium signals. The same embryo was imaged again by replacing the solution with 100 μM 2-APB prepared in 1X Danieau's solution after a 10 minute treatment. Changes in fluorescence intensity in individual cell regions were quantified using the NIS Elements analysis software (Nikon).

Western blotting

Wild-type AB embryos were treated with the pharmacological inhibitor 2-APB at 100 μM for 10 minutes at 18 ss. Following morpholino and drug treatment, while in the drug, embryos were dissected posterior to the ear to collect the head portion in a buffer containing Tris (pH 8.0), 10% glycerol, 1% Triton X-100 and protease inhibitor cocktail (Roche- 04693124001). Using a syringe, protein was extracted in lysis buffer and the concentration was estimated using the Bradford assay. 40 μg protein was analyzed by Western blotting. Primary antibody pMLC (Cell signaling #3671) was used at a concentration of 1:1000 and control primary antibody HDAC1 (Abcam ab41407) was used at 1:500. Secondary antibodies, anti-mouse HRP (Cell signaling technologies #7076S) and anti-rabbit HRP (Cell signaling technologies #7074S), were used at a dilution of 1:2000. PVDF membranes were

developed using the Supersignal West Femto maximum sensitivity substrate (Thermoscientific #34095) or the clarity Western ECL substrate (Bio-rad technologies #170-5060). Blots were imaged using a Foto/Analyst FX Imager with Foto/Analyst PC Image software (Fotodyne Inc.) or a Biospectrum 810 imager system (UVP, LLC), and quantified on Photoshop.

Imaging and analysis

Brightfield images were taken using an Olympus SZX12 stereomicroscope with an Olympus DP72 camera. Live embryo confocal imaging was carried out as previously described using Nikon CS2 laser scanning confocal camera and Nikon Elements software (Gutzman et al., 2015 and Chapter 2). Cell shapes were measured and analyzed using Nikon Elements Software, as previously described (Gutzman et al., 2015 and Chapter 2).

Statistical analysis

Statistical analysis was carried out using the Mann-Whitney U-test. This test was used to determine significance between two groups of data (control and treatment group) having unequal sample sizes (n). p-values denoting significance are reported for each experiment within the figure legend.

C. RESULTS

Calcium regulates cell length at the MHBC

To investigate the potential role of calcium signaling in zebrafish MHB development, we utilized the pharmacological drug, 2-aminoethoxy diphenyl-

borate (2-APB), that inhibits the IP3 receptor (IP3R) present on the endoplasmic reticulum (ER), preventing it from opening the calcium channel and consequently inhibiting the release of calcium into the cytosol (Ma et al., 2001; Taylor and Tovey, 2010). We treated zebrafish embryos at 18 ss, immediately before MHB formation begins, with 2-APB or DMSO (Fig. 17A). The embryos were then allowed to develop to 24 ss and imaged using confocal microscopy in order to obtain single cell resolution images. We found that 2-APB treated embryos had abnormal MHB when compared to DMSO treated embryos (Fig. 17B-C'). We further quantified tissue and cell shape changes during MHB formation in the treatment groups (Fig. 17D-E). Measurement of MHBC tissue angle showed a greater, more obtuse angle in 2-APB treated embryos (Fig. 17D and Fig. 18). This phenotype corresponds to an abnormal MHB phenotype, indicating insufficient tissue folding. Interestingly, the width of the neural tube at the MHBC, which represents the MHBC cell length, was also found to be greater in 2-APB treated embryos when compared to DMSO treated embryos (Fig. 17E and Fig. 18). Additional measurements including the width of the neural tube 40 μm away from the MHBC towards the hindbrain, the cell width, and the cell area, all remained unchanged in the 2-APB treated embryos (Fig. 18). Longer MHBC cells upon calcium inhibition suggest a role for calcium signaling in regulating cell length at the MHBC.

In order to confirm the efficacy of 2-APB in decreasing cytosolic calcium levels, we used live imaging of calcium green, a calcium indicator dye that fluoresces green when bound to calcium molecules, enabling us to visualize calcium 'spikes' during development, as previously published by Fetcho, 2007; Reinhard et al., 1995. We

injected single-cell stage embryos with calcium green-1 dextran and treated embryos with DMSO or 2-APB to visualize calcium spikes using confocal microscopy (Fig. 19). We carried out this experiment at an early time point of 4 hpf since the fluorescent signals were undetectable at 24 ss (data not shown). A time-lapse of confocal images for each embryo was taken to quantify the changes in fluorescence intensity. We found that approximately 2-3 cells in the enveloping layer of DMSO treated embryos distinctly fluoresced within this time frame in the region being imaged (Fig. 19A). Next, we treated the same embryo with 2-APB and again carried out time-lapse confocal imaging. We were unable to observe any obvious change in fluorescence in the embryo (Fig. 19B). To quantify these data, we took a ratio of the highest to lowest fluorescence intensity in a given cell area during the period of visualized calcium spikes. Comparison of this fold change in intensity showed that DMSO treated embryos had an average fold change of 1.364 compared to a significantly reduced fold change of 1.2 in 2-APB treated embryos (Fig. 19C). We concluded that at 4 hpf, 2-APB decreases the amounts of cytosolic calcium in zebrafish embryos and is an important confirmation of the efficacy of 2-APB as previously published (Fetcho, 2007; Reinhard et al., 1995). Together, these data indicate that calcium is required for proper MHB formation in the zebrafish by regulation of MHBC cell length.

Overactivation of NMII is rescued by decreasing cytosolic calcium

It is known from previous studies that calcium signaling is involved in regulation of cell length in various cell culture models (Bramlage et al., 2001; White et al., 1993). It is also involved in regulation of NMII activity (Somlyo and Somlyo, 2003; Szent-

Gyorgyi, 1975). Therefore, we hypothesized that calcium signals to NMII to regulate cell length during zebrafish MHB formation. In order to test this hypothesis, we utilized *mypt1* morphant embryos and ER calcium inhibition. *Mypt1* knockdown results in overactivation of NMII and leads to abnormal cell shapes at the MHB with shorter and wider cells (Fig. 20A and Gutzman et al., 2015). We have also shown that reduction of cytosolic calcium by 2-APB results in abnormal MHB with longer MHBC cells (Fig. 17 and Fig. 20B). Therefore, we hypothesized that if calcium signals to NMII, then the cell shape phenotype of overactivation of NMII could be rescued by decreasing cytosolic calcium (Fig. 20C). We injected *mypt1* morpholino into single cell stage embryos along with mGFP and treated them with 2-APB at 18 ss, followed by confocal imaging and cell shape analysis at 24 ss (Fig. 20D-E). We found no difference in the MHB tissue angle in DMSO and 2-APB treated *mypt1* morphants (Fig. 20F and Fig. 21). In fact, the angle phenotype observed with both treatments was the same as what we found in *mypt1* morphants previously (Chapter 2, Figs. 11-13) However, the length of the cells at the MHBC in 2-APB treated *mypt1* morphants was significantly longer compared to DMSO treated *mypt1* morphants (Fig. 20G and Fig. 21). This was the only parameter that was significantly different in our quantification of morphogenetic changes in tissue and cell shape. We did not find any difference in cell length 40 μm away from the MHB towards the hindbrain, cell width, and cell area (Fig. 20F-G and Fig. 21). These data indicate a rescue of the MHBC cell length phenotype, from shorter MHBC cells seen in the *mypt1* morphants to comparatively longer MHBC cells upon calcium inhibition. Although the cell length

was rescued, the MHB angle was still abnormally large because the cell width was not rescued. We know from our previous work that either cell length or cell width abnormalities can result in abnormal tissue angle, which explains why a rescue of only cell length does not rescue the MHB tissue angle (Chapter 2, Figs. 11-13). Thus, in *mypt1* morphants, MHBC cell length is the sole cell shape parameter measured that is rescued by inhibition of cytosolic calcium.

To further test for calcium as an upstream signal regulating NMII, we hypothesized that inhibition of calcium ER release by 2-APB would result in reduced amounts of phosphorylated MLC (pMLC), which would be an indication of activation of NMII molecules. However, Western blotting determined no significant changes in pMLC levels (Fig. 22A). We have previously seen that knockdown of *mypt1* in zebrafish brain leads to increased quantities of pMLC (Gutzman and Sive, 2010). In order to take a different approach, we hypothesized that *mypt1* morphants with increased pMLC levels would show a visible reduction in the pMLC amount when treated with 2-APB. Surprisingly, we did not find any changes in pMLC levels here as well (Fig. 22B). This could be attributed to the small size of the pMLC protein, making the change undetectable on blots. Therefore, the role for calcium signaling in regulation of pMLC requires further investigation. From these experiments, we conclude that calcium signaling is required for proper shortening of MHBC cells during this morphogenetic process.

D. DISCUSSION

Calcium regulates cell length during MHB formation

Calcium ions can enter the cell from the external environment through calcium channels on the cell membrane, or from intracellular storage organelles, and affect cytosolic calcium concentration (Westfall et al., 2003). One major source of intracellular calcium is the ER, where opening of calcium channels are regulated by IP3R (Berridge et al., 2003; Berridge et al., 2000; Slusarski and Pelegri, 2007). Calcium signaling has been previously studied for its role in regulating cell shape in platelet and endothelial cells (Moore et al., 1998; Porter et al., 2003). Here, our investigation of the role of calcium signaling in zebrafish MHB formation identified an important role for calcium in cellular morphogenesis. We found that calcium is required for proper MHB formation and has a specific role in cell shortening at the MHBC (Fig. 17). Regulation of cell shortening by calcium waves has been previously seen in adult cardiac myocytes *in vitro* (Bramlage et al., 2001). For the first time, we show calcium mediated regulation of cell length during morphogenesis in a live vertebrate model. Additionally, this result draws a potential important correlation to our previous finding of the role of NMIIA in regulating cell length during zebrafish MHB formation (Gutzman et al., 2015). Both inhibition of ER calcium release and NMIIA knockdown show the same MHB cell shape phenotype, possibly suggesting that both molecules may be functioning as part of the same signaling pathway (Fig. 23B).

Calcium regulates cell length during MHB formation through NMII

Although there have been studies involving calcium mediated regulation of NMII activity, these studies have been mostly done in cell culture (Martinsen et al., 2013; Watanabe et al., 2001). Here, we show that the cell length phenotype in *mypt1* morphants, with overactive NMII, is rescued when calcium release from the ER is inhibited, suggesting an important correlation between the two signaling molecules. Interestingly, we observed that the MHB tissue angle is not rescued along with the cell length phenotype. A possible explanation could be that the cell width phenotype of *mypt1* morphants is not rescued and we know that cell width is also a contributor to normal MHB tissue angle (Chapter 2, Gutzman et al., 2015). Myosin phosphatase dephosphorylates the MLC for both NMII homologs, NMIIA and NMIIB. Hence, knockdown of *mypt1* inhibits the action of myosin phosphatase for both class II non-muscle myosins, resulting in overactive NMIIA and NMIIB (Hartshorne et al., 2004). Rescue of only the cell length phenotype of *mypt1* knockdown by calcium inhibition, leads us to hypothesize that calcium specifically regulates NMIIA. Thus, we hypothesize that both calcium and NMIIA function in the same signaling pathway through intermediate signaling molecules (Fig. 23B).

Calcium, being an inorganic molecule, typically interacts with calcium binding proteins to signal to downstream molecules such as ones that make up the cytoskeleton. Calmodulin is a calcium binding protein and has been shown to be required for morphogenesis in yeast (Kraus et al., 2005; Paranjape et al., 1990). Calcium, calmodulin and myosin have also been studied together to regulate cell shape change in *Euglena* (Lonergan, 1984; Lonergan, 1985). Additionally, it has

been shown that various CAM kinase II isoforms are expressed in the zebrafish brain during early development, making calmodulin a possible candidate in zebrafish MHB development (Rothschild et al., 2007). The activation of NMII is carried out by various kinases such as the myosin light chain kinase (MLCK), also a potential molecule in the calcium signaling pathway due to its involvement in various developmental morphogenetic processes (Ewald et al., 2008). A proposed model for the regulation of NMII activity through the calcium signaling pathway is shown in figure 23B. The precise molecular interactions between these molecules are yet to be determined and serve to be the basis of future experiments.

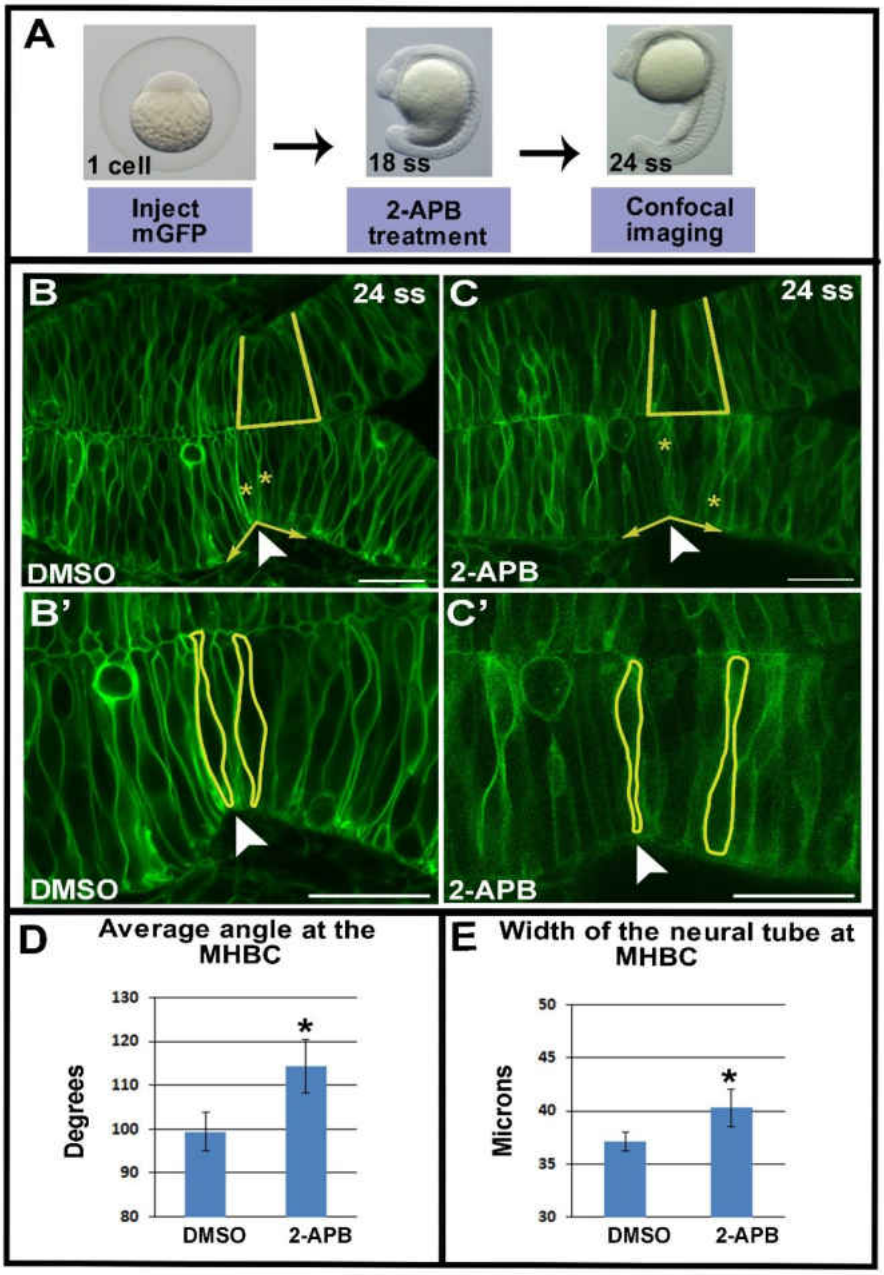

Figure 17. Calcium regulates cell length during MHB formation. (A) Experimental procedure. Single cell stage zebrafish embryos were injected with mGFP, treated with 0.1% DMSO or 100 μM 2-APB at 18 ss, and imaged at 24 ss. (B-C) Confocal images of treated embryos as indicated at 24 ss. (B'-C') Magnifications of images in B-C showing shape outlines of cells marked with yellow asterisks. Arrowheads indicate MHBC. (D) Comparison of average tissue angle at the MHBC and (E) average width of the neural tube at the MHBC (see lines in B,C). Mann-Whitney U-test was performed to determine significance between control and test groups. Asterisk indicates $p < 0.05$. DMSO, n=9; 2-APB, n=8. Error bars are ±s.e.m.

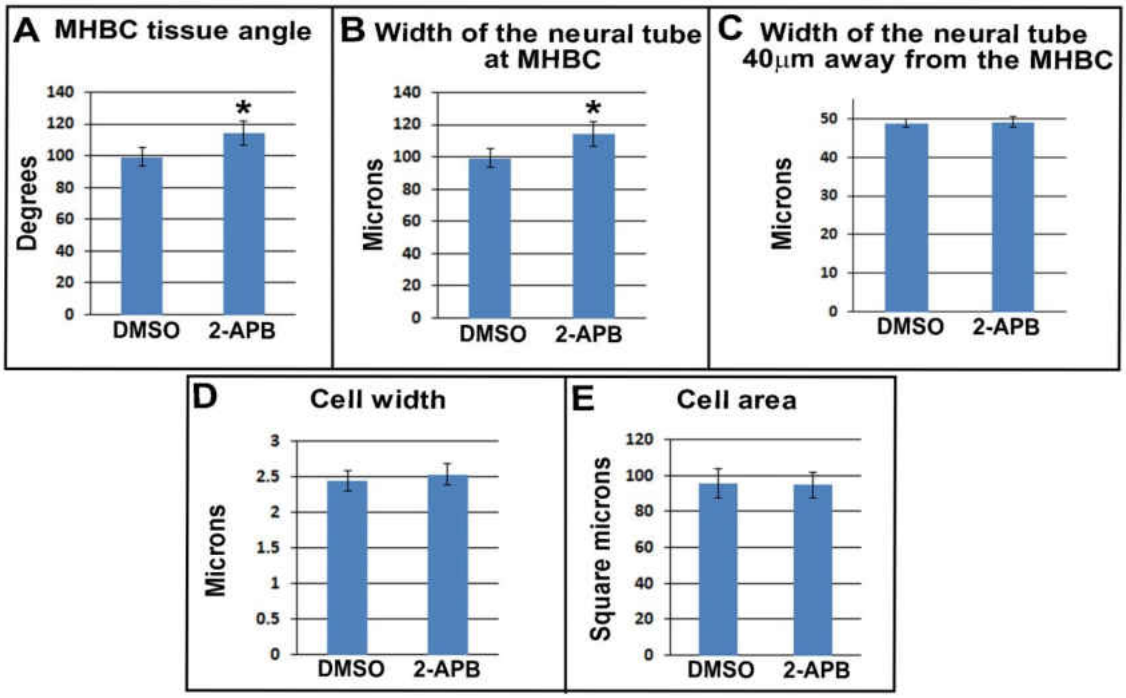

Figure 18. Quantification of cell shape parameters in 2-APB treated embryos. (A) Neuroepithelial MHB tissue angle, (B) Width of the neural tube at the MHBC or cell length at th MHBC, (C) Width of the neural tube 40 μm away from the MHBC or cell length 40 μm away from the MHBC towards the hindbrain region, (D) Cell width and (E) Cell area. Mann-Whitney U-test was performed to determine significance between control and test groups. Asterisk represents $p < 0.05$. For angle and cell length measurements, n=12; for cell width and area measurements, n=7. Error bars are ±s.e.m.

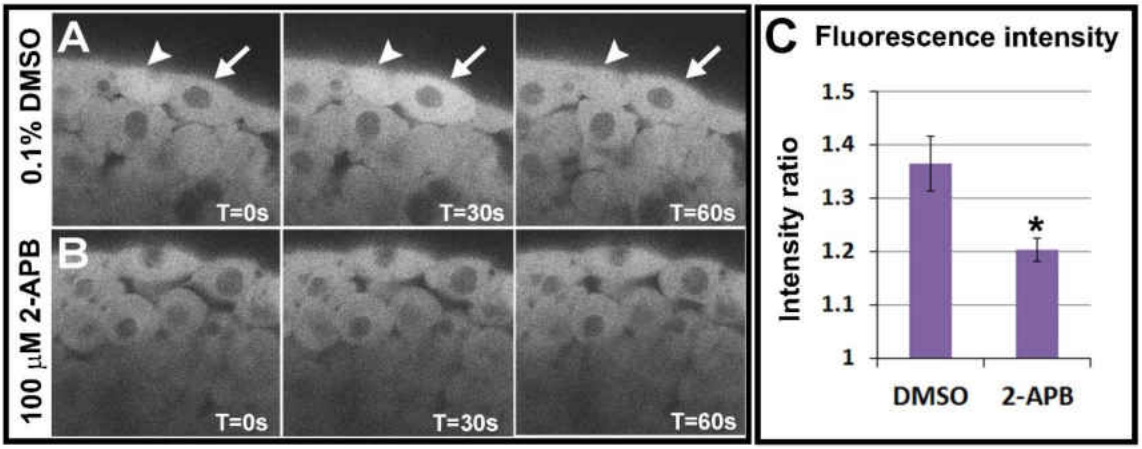

Figure 19. Calcium green-1 dextran imaging confirms inhibition of intracellular calcium levels by 2-APB. (A-B) Timelapse confocal images of zebrafish embryos injected with the calcium indicator and treated and imaged at 4 hpf with (A) 0.1% DMSO and (B) 100 μM 2-APB. Timelapse was done once every 10 seconds for 10 minutes. Arrows and arrowheads indicate rapidly changing calcium dynamics in two different cells. (C) Quantification of change in fluorescence intensity. Mann-Whitney U-test was performed to determine significance between control and test groups. Asterisk indicates $p<0.001$. n=6 each. Error bars are ±s.e.m.

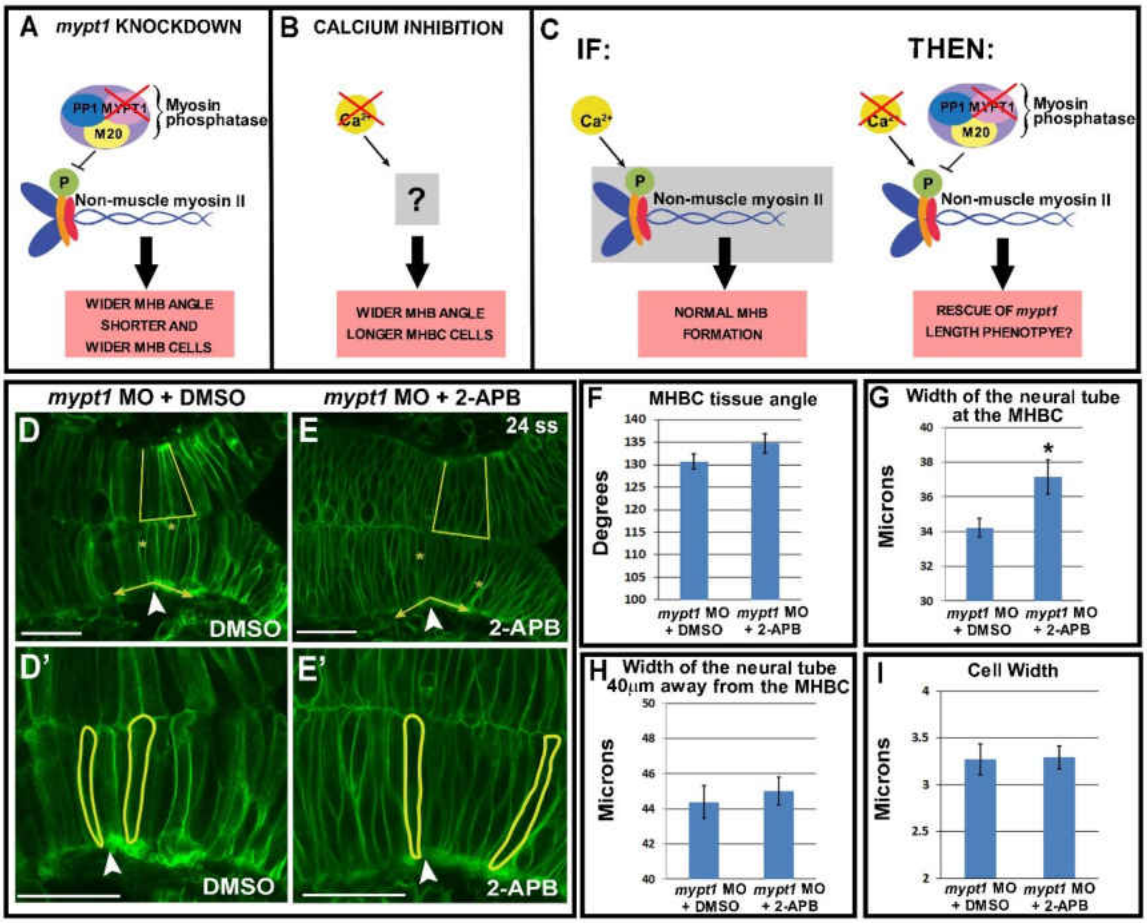

Figure 20. Inhibition of cytosolic calcium rescues cell length phenotype of overactivation of NMII. (A-C) Schematic of experimental hypothesis. (A) *Mypt1* knockdown results in overactivation of myosin light chain and abnormal MHB with shorter and wider MHB cells. (B) Inhibition of calcium release from ER by 2-APB results in abnormal MHB with longer MHBC cells. (C) IF: calcium signals to NMII, THEN: inhibition of calcium release in *mypt1* knockdown embryo would rescue MHB cell shape phenotype. (D-E) Confocal images of 24 ss embryos injected with mGFP and *mypt1* morpholino and treated with (D) 0.1% DMSO and (E) 100 μM 2-APB at 18 ss. (D'-E') Magnified images from D-E. Arrowheads indicate MHBC. (F-I) Quantification of cell shape changes occuring during MHB formation- (F) MHBC tissue angle, (G) width of the neural tube at the MHBC, (H) width of the neural tube 40 μm away from the MHBC and (I) cell width. Only width of the neural tube at the MHBC (G) is different between the two treatment groups. Mann-Whitney U-test was performed to determine significance between control and test groups. Asterisk indicates $p<0.01$. For angle and length measurements, DMSO, n=13; 2-APB, n=17; for cell width measurement, n=13 embryos each. Error bars are ±s.e.m.

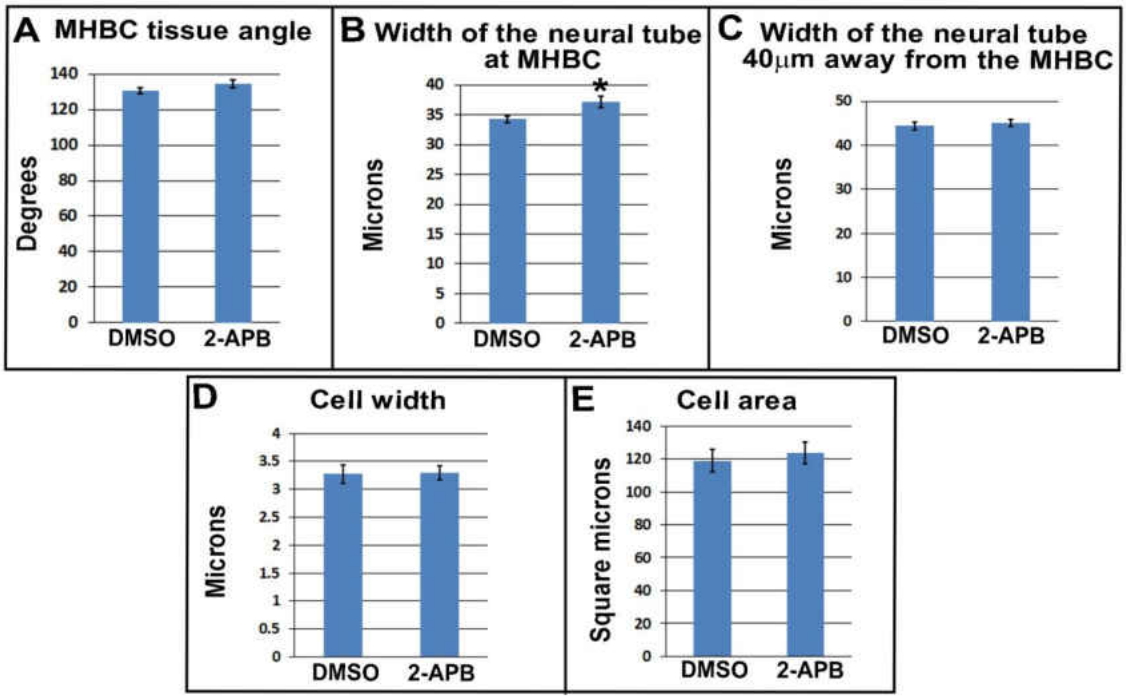

Figure 21. Quantification of cell shape parameters in 2-APB treated mypt1 morphant embryos. Quantification of cell shape parameters in 2-APB treated *mypt1* morphant embryos. (A) Neuroepithelial MHB tissue angle, (B) Width of the neural tube at the MHBC or cell length at the MHBC, (C) Width of the neural tube 40 μm away from the MHBC or cell length 40 μm away from the MHBC towards the hindbrain region, (D) Cell width and (E) Cell area. Mann-Whitney U-test was performed to determine significance between control and test groups. Asterisk indicates $p<0.01$. For angle and length measurements, DMSO, n=13; 2-APB, n=17. For cell width and area measurement, n=13 embryos each. Error bars are ±s.e.m.

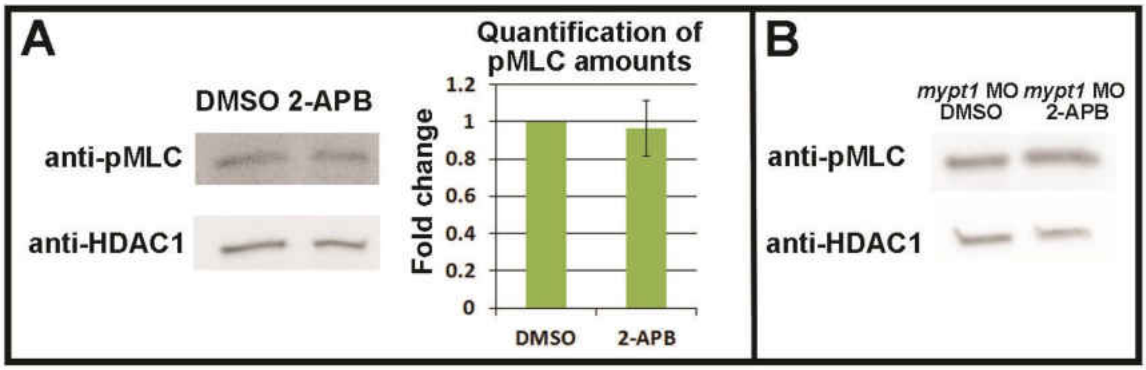

Figure 22. pMLC Western blotting. (A) Western blotting for pMLC using wild-type embryonic brain tissue treated with DMSO or 2-APB showed no difference in phosphorylation of MLC. Graph represents quantification of Western blotting data and is an average of six independent experiments. Mann-Whitney U-test was performed to determine significance between control and test groups. Error bar is ±s.e.m. (B) Western blotting for pMLC using *mypt1* morphants treated with DMSO or 2-APB also showed no difference in phosphorylation levels of NMII. Hdac1 was used as loading control.

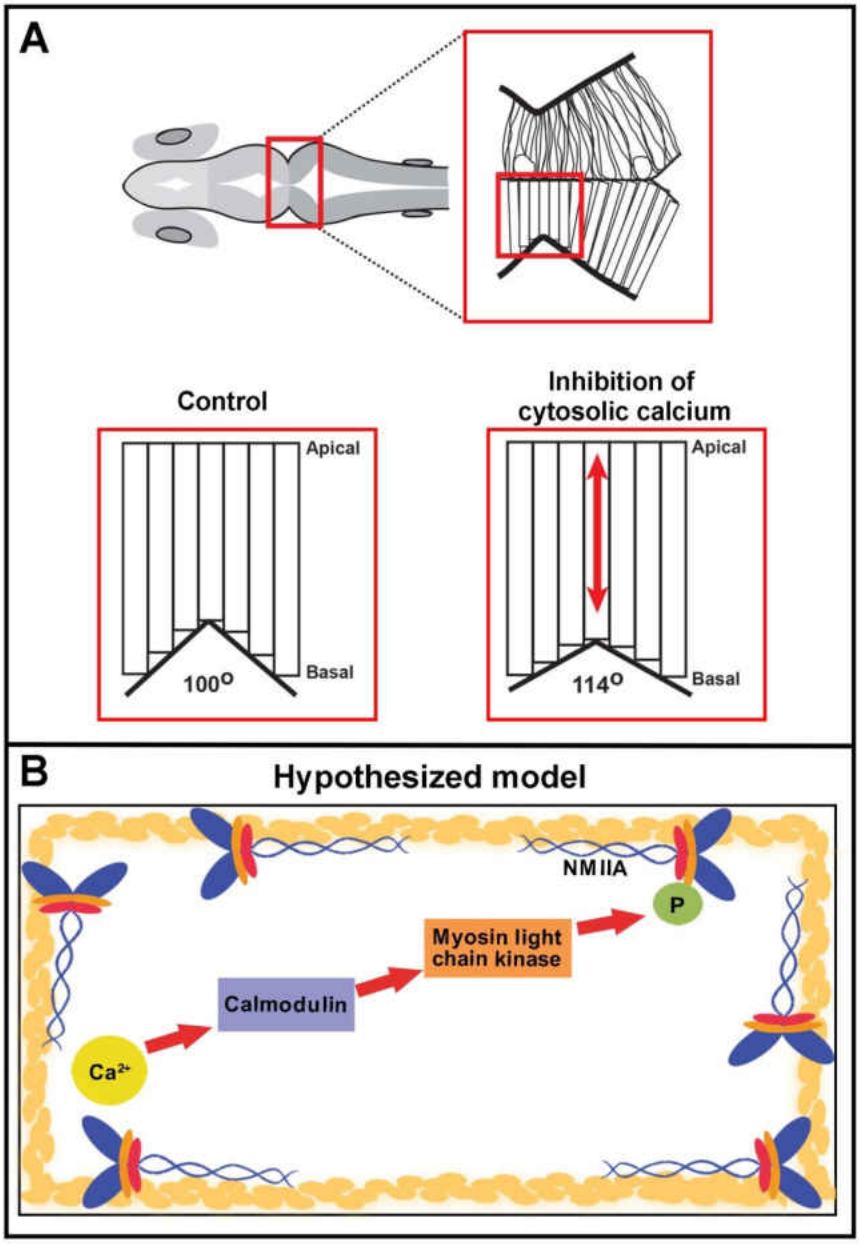

Figure 23. Summary and hypothesized model of the calcium signaling pathway regulating NMII. (A) Diagram representing a zebrafish embryonic brain viewed dorsally with magnified view of the MHB and a simplified model depicting normal MHB cell shapes at 24 ss. Control or wild-type embryos have a normal MHB tissue angle of 100 degrees while decrease in cytosolic calcium leads to abnormal MHB formation due to MHBC cells not shortening properly. Figure adapted from Gutzman et al., 2015. (B) Diagram representing the hypothesis that the calcium signaling pathway via calmodulin and myosin light chain kinase, signals to activate NMIIA, regulating cell length during zebrafish MHB morphogenesis. Red arrows indicate hypothesized interaction.

REFERENCES

Berridge, M.J., M.D. Bootman, and H.L. Roderick. 2003. Calcium signalling: dynamics, homeostasis and remodelling. *Nature reviews. Molecular cell biology*. 4:517-529.

Berridge, M.J., P. Lipp, and M.D. Bootman. 2000. The versatility and universality of calcium signalling. *Nature reviews. Molecular cell biology*. 1:11-21.

Bramlage, P., G. Joss, A. Staudt, A. Jarrin, S. Podlowski, G. Baumann, K. Stangl, S.B. Felix, and V. Stangl. 2001. Computer-aided measurement of cell shortening and calcium transients in adult cardiac myocytes. *Biotechnology progress*. 17:929-934.

Brennan, S.C., B.A. Finney, M. Lazarou, A.E. Rosser, C. Scherf, D. Adriaensen, P.J. Kemp, and D. Riccardi. 2013. Fetal calcium regulates branching morphogenesis in the developing human and mouse lung: involvement of voltage-gated calcium channels. *PloS one*. 8:e80294.

Ewald, A.J., A. Brenot, M. Duong, B.S. Chan, and Z. Werb. 2008. Collective epithelial migration and cell rearrangements drive mammary branching morphogenesis. *Developmental cell*. 14:570-581.

Fetcho, J.R. 2007. Imaging neuronal activity with calcium indicators in larval zebrafish. *CSH protocols*. 2007:pdb prot4781.

Franke, J.D., R.A. Montague, and D.P. Kiehart. 2005. Nonmuscle myosin II generates forces that transmit tension and drive contraction in multiple tissues during dorsal closure. *Current biology : CB*. 15:2208-2221.

Gilland, E., A.L. Miller, E. Karplus, R. Baker, and S.E. Webb. 1999. Imaging of multicellular large-scale rhythmic calcium waves during zebrafish gastrulation. *Proceedings of the National Academy of Sciences of the United States of America*. 96:157-161.

Gutzman, J.H., E.G. Graeden, L.A. Lowery, H.S. Holley, and H. Sive. 2008. Formation of the zebrafish midbrain-hindbrain boundary constriction requires laminin-dependent basal constriction. *Mechanisms of development*. 125:974-983.

Gutzman, J.H., S.U. Sahu, and C. Kwas. 2015. Non-muscle myosin IIA and IIB differentially regulate cell shape changes during zebrafish brain morphogenesis. *Developmental biology*. 397:103-115.

Gutzman, J.H., and H. Sive. 2010. Epithelial relaxation mediated by the myosin phosphatase regulator Mypt1 is required for brain ventricle lumen expansion and hindbrain morphogenesis. *Development*. 137:795-804.

Hartshorne, D.J., M. Ito, and F. Erdodi. 2004. Role of protein phosphatase type 1 in contractile functions: myosin phosphatase. *The Journal of biological chemistry*. 279:37211-37214.

Hunter, G.L., J.M. Crawford, J.Z. Genkins, and D.P. Kiehart. 2014. Ion channels contribute to the regulation of cell sheet forces during Drosophila dorsal closure. *Development*. 141:325-334.

Kimmel, C.B., W.W. Ballard, S.R. Kimmel, B. Ullmann, and T.F. Schilling. 1995. Stages of embryonic development of the zebrafish. *Developmental dynamics : an official publication of the American Association of Anatomists*. 203:253-310.

Kraus, P.R., C.B. Nichols, and J. Heitman. 2005. Calcium- and calcineurin-independent roles for calmodulin in Cryptococcus neoformans morphogenesis and high-temperature growth. *Eukaryotic cell*. 4:1079-1087.

Lee, H.C., and N. Auersperg. 1980. Calcium in epithelial cell contraction. *The Journal of cell biology*. 85:325-336.

Lonergan, T.A. 1984. Regulation of cell shape in Euglena gracilis. II. The effects of altered extra- and intracellular Ca2+ concentrations and the effect of calmodulin antagonists. *Journal of cell science*. 71:37-50.

Lonergan, T.A. 1985. Regulation of cell shape in Euglena gracilis. IV. Localization of actin, myosin and calmodulin. *Journal of cell science*. 77:197-208.

Lowery, L.A., and H. Sive. 2009. Totally tubular: the mystery behind function and origin of the brain ventricular system. *BioEssays : news and reviews in molecular, cellular and developmental biology*. 31:446-458.

Ma, H.T., K. Venkatachalam, H.S. Li, C. Montell, T. Kurosaki, R.L. Patterson, and D.L. Gill. 2001. Assessment of the role of the inositol 1,4,5-trisphosphate receptor in the activation of transient receptor potential channels and store-operated Ca2+ entry channels. *The Journal of biological chemistry*. 276:18888-18896.

Martinsen, A., O. Schakman, X. Yerna, C. Dessy, and N. Morel. 2013. Myosin light chain kinase controls voltage-dependent calcium channels in vascular smooth muscle. *Pflugers Archiv : European journal of physiology*.

McGrath, J., S. Somlo, S. Makova, X. Tian, and M. Brueckner. 2003. Two populations of node monocilia initiate left-right asymmetry in the mouse. *Cell*. 114:61-73.

Moore, T.M., G.H. Brough, P. Babal, J.J. Kelly, M. Li, and T. Stevens. 1998. Store-operated calcium entry promotes shape change in pulmonary endothelial cells expressing Trp1. *The American journal of physiology*. 275:L574-582.

Paranjape, V., B.G. Roy, and A. Datta. 1990. Involvement of calcium, calmodulin and protein phosphorylation in morphogenesis of Candida albicans. *Journal of general microbiology*. 136:2149-2154.

Porter, G.A., Jr., R.F. Makuck, and S.A. Rivkees. 2003. Intracellular calcium plays an essential role in cardiac development. *Developmental dynamics : an official publication of the American Association of Anatomists*. 227:280-290.

Ramakers, G.J., B. Avci, P. van Hulten, A. van Ooyen, J. van Pelt, C.W. Pool, and M.B. Lequin. 2001. The role of calcium signaling in early axonal and dendritic morphogenesis of rat cerebral cortex neurons under non-stimulated growth conditions. *Brain research. Developmental brain research*. 126:163-172.

Reinhard, E., H. Yokoe, K.R. Niebling, N.L. Allbritton, M.A. Kuhn, and T. Meyer. 1995. Localized calcium signals in early zebrafish development. *Developmental biology*. 170:50-61.

Rothschild, S.C., J.A. Lister, and R.M. Tombes. 2007. Differential expression of CaMK-II genes during early zebrafish embryogenesis. *Developmental dynamics : an official publication of the American Association of Anatomists*. 236:295-305.

Slusarski, D.C., and F. Pelegri. 2007. Calcium signaling in vertebrate embryonic patterning and morphogenesis. *Developmental biology*. 307:1-13.

Somlyo, A.P., and A.V. Somlyo. 2003. Ca2+ sensitivity of smooth muscle and nonmuscle myosin II: modulated by G proteins, kinases, and myosin phosphatase. *Physiological reviews*. 83:1325-1358.

Szent-Gyorgyi, A.G. 1975. Calcium regulation of muscle contraction. *Biophysical journal*. 15:707-723.

Tada, M., and M.L. Concha. 2001. Vertebrate gastrulation: calcium waves orchestrate cell movements. *Current biology : CB*. 11:R470-472.

Taylor, C.W., and S.C. Tovey. 2010. IP(3) receptors: toward understanding their activation. *Cold Spring Harbor perspectives in biology*. 2:a004010.

Watanabe, H., Q.K. Tran, K. Takeuchi, M. Fukao, M.Y. Liu, M. Kanno, T. Hayashi, A. Iguchi, M. Seto, and K. Ohashi. 2001. Myosin light-chain kinase regulates endothelial calcium entry and endothelium-dependent vasodilation. *FASEB journal : official publication of the Federation of American Societies for Experimental Biology*. 15:282-284.

Westfall, T.A., B. Hjertos, and D.C. Slusarski. 2003. Requirement for intracellular calcium modulation in zebrafish dorsal-ventral patterning. *Developmental biology*. 259:380-391.

White, E., J.Y. Le Guennec, J.M. Nigretto, F. Gannier, J.A. Argibay, and D. Garnier. 1993. The effects of increasing cell length on auxotonic contractions; membrane potential and intracellular calcium transients in single guinea-pig ventricular myocytes. *Experimental physiology*. 78:65-78.

CHAPTER 4

CONCLUSIONS AND FUTURE DIRECTIONS

A. CONCLUSIONS

The primary aim of this project was to characterize the morphogenetic events occurring during midbrain-hindbrain boundary (MHB) formation using zebrafish as a model, and further understand and elucidate the mechanisms responsible for this epithelial morphogenetic process. We first characterized the neuroepithelial cell shape changes that occur during this process (Chapter 2, Fig. 10). We concentrated on a shorter time frame when the MHB first folds, between 18 ss and 24 ss. We found that the neuroepithelial MHB tissue angle decreases over time, depicting the formation of the constriction. During this process, the MHB cells shorten and narrow to enable the folding of the tissue, resulting in the formation of a proper MHB with a deep MHB constriction (MHBC).

NMIIA and NMIIB differentially regulate zebrafish MHB morphogenesis

We hypothesized that non-muscle myosin II (NMII) proteins are required for zebrafish MHB formation and we tested this by gene knockdown and consequent confocal microscopic study and analysis. We determined a novel role for NMIIA and NMIIB in regulating cell shape during zebrafish MHB morphogenesis. We found that *myh9b*, a zebrafish ohnolog for the human *MYH9* gene that encodes for NMIIA, is responsible for the shortening of cells at the MHBC and *myh10*, encoding for NMIIB, is required for cells throughout the MHB region to narrow (Chapter 2, Figs. 12-13). The identification of a differential function for NMIIA and NMIIB in the

formation of the zebrafish MHB led to the question of how they carry out these distinct functions. We found that both proteins are not differentially localized within the MHB but we observed differential disruption in actin distribution upon knockdown of NMIIA and NMIIB (Chapter 2, Fig. 14).

Calcium regulates zebrafish MHB formation

We also hypothesized that calcium signaling plays a role in MHB development and is an upstream regulator of NMII. To test the first hypothesis, we employed the use of 2-APB, a drug that inhibits the release of calcium from the endoplasmic reticulum (ER). We found that depletion of cytosolic calcium resulted in an abnormal MHB angle and longer MHBC cells, showing that calcium is required for zebrafish MHB formation (Chapter 3, Fig. 17). Interestingly, this phenotype is similar to the phenotype seen with the knockdown of *myh9b* (Chapter 2, Figs. 11-12), suggesting the possible involvement of calcium and NMII within the same signaling pathway in MHB formation.

We further hypothesized that calcium signals to activate NMII. We had previously determined that both NMIIA knockdown and cytosolic calcium inhibition result in abnormal MHB with longer MHBC cells. We had also shown that knockdown of *mypt1*, which corresponds to overactivation of NMII, also results in abnormal MHB with shorter and wider MHB cells. Thus, if calcium signals to NMII, then overactivation of NMII would be rescued by inhibition of cytosolic calcium. We found that only the MHBC cell length phenotype seen in *mypt1* morphants was rescued upon 2-APB treatment (Chapter 3, Fig. 19). Since we have also

determined that cell length is regulated by NMIIA (Chapter 2, Fig. 11), we further hypothesize that calcium differentially signals to NMIIA, and not NMIIB.

B. FUTURE DIRECTIONS

How do NMIIA and NMIIB function differentially?

Although we have discovered distinct functions for NMIIA and NMIIB in zebrafish MHB morphogenesis, the mechanisms by which they carry out their differential function remains unknown. The following questions address different hypotheses regarding how NMIIA and NMIIB may function differently to regulate cell shape and outline future experiments to test each of these hypotheses.

- **Are NMIIA and NMIIB filaments oriented differentially?**

Since we did not observe any difference in localization of NMII isoforms in the MHB region, it is possible that the NMIIA and NMIIB fibers are oriented differentially. We hypothesize that NMIIA fibers are oriented longitudinally, along the apical-basal axis to regulate cell length, while NMIIB is oriented perpendicular to the apical-basal axis of the cells, regulating cell width. Total internal reflection fluorescence microscopy (TIRF) is a recent advancement in the field of microscopy, which allows visualization at the level of single molecules and is dynamic, allowing us to see the active processes going on inside living systems (Sako et al., 2000). While the movement of NMII isoforms has been studied in a similar way using TIRF in cell culture, visualization of single molecules in live organisms such as *C. elegans*, medaka and zebrafish has also been made possible recently (Beach et al., 2014;

Wang et al., 2010). To test our hypothesis, we could fluorescently tag NMIIA and NMIIB to visualize the movement of the molecules along actin fibers using TIRF. With respect to the cell shape changes occurring during zebrafish MHB morphogenesis, we would expect to see NMIIA fibers move longitudinally along the apical-basal axis and NMIIB molecules to move in the perpendicular direction. This would provide an answer to the question of how NMIIA and NMIIB function differentially during MHB formation in the zebrafish.

- **Can NMII function be regulated by molecules that differentially phosphorylate the MLC of NMIIA and NMIIB?**

The MLC of NMII is known to be phosphorylated by various kinases, two of the most studied are Rho kinase and myosin light chain kinase (MLCK) (Betapudi, 2014). Since we have already determined that calcium regulates only MHBC cell length, and not cell width, which corresponds to findings from NMIIA knockdown phenotype (Chapter 3, Fig. 17), we hypothesize that the calcium-calmodulin dependent MLCK phosphorylates NMIIA, while Rho kinase phosphorylates NMIIB. To test this hypothesis, activation of MLCK can be inhibited using a pharmacological drug, ML-7 (Saitoh et al., 1987), followed by a co-immunoprecipitation (co-IP) assay for pMLC with NMIIA and NMIIB, through Western blotting analysis. We would expect to see reduced amounts of NMIIA in ML-7 treated embryos, but no difference in NMIIB abundance. This would suggest that MLCK phosphorylates NMIIA, but not NMIIB. Similarly, we would inhibit Rho kinase using its specific inhibitor Y27632 (Ishizaki et al., 2000), and carry out a co-IP and Western blot analysis of pMLC with NMIIA or NMIIB. We would expect to

see reduced amounts of NMIIB in Rho inhibited embryos, but no reduction in NMIIA levels. This will suggest that Rho preferentially signals to phosphorylate NMIIB.

- **Can differential regulation of NMII isoforms occur through phosphorylation of the myosin heavy chain?**

The NMII heavy chain has multiple phosphorylation sites, some of which are specific to individual homologs. The NMIIA heavy chain has a ser-1943 site that can be phosphorylated by casein kinase II. Absence of this phosphorylation prevents its binding to s100A4, a member of the s100 family of calcium binding proteins. This phosphorylation event results in inhibition of filament assembly, disrupting its regular function (Vicente-Manzanares et al., 2009). The NMIIB heavy chain also has a ser-1937 site phosphorylated by protein kinase C (PKC), which is responsible for filament assembly (Vicente-Manzanares et al., 2009). These distinct sites in the two homologs phosphorylated by different enzymes, but carrying out the same function could indicate a differential regulation of the two heavy chains. Using specific antibodies against each of these phosphorylated sites on the heavy chains, we could carry out immunostaining to identify differences in NMIIA and NMIIB protein localization. We would expect to see differential localization of the phosphorylated forms of the two proteins which would help us explain their respective differential functions.

How does the calcium signaling pathway regulate zebrafish MHB morphogenesis?

In this research, we have discovered a novel role for calcium signaling in regulating cell length during zebrafish MHB morphogenesis. It remains to be determined if and how calcium signaling regulates NMII during this process. The following questions address this, and will help us to determine the specific pathway through which NMII is regulated.

- **How can we confirm the efficacy of 2-APB at 24 ss?**

We confirmed the efficacy of 2-APB in depleting cytosolic calcium levels by calcium green-1 dextran, a calcium indicator (Chapter 3). However, this experiment was carried out at 4 hpf, while all our experiments have been done in the time range of 18-24 ss. Since the fluorescence of calcium green-1 dextran does not give a good signal at 24 ss, a different calcium indicator is required for better confirmation. This can be done by using a genetically encoded calcium indicator, GCaMP. GCaMP6, one of the recent sensitive and efficient calcium indicators for live visualization of calcium, has been utilized for imaging in zebrafish (Chen et al., 2013). We have obtained plasmid constructs of the GCaMP6 gene (a kind gift from Phillip Keller, Howard Hughes Medical Institute) which can be utilized to synthesize mRNA and inject it into single cell embryos, followed by imaging at a more relevant time point to test for the efficacy of 2-APB. Time-lapse confocal imaging of 2-APB treated embryos, upon comparison with control DMSO treated embryos would reveal decreased amounts of fluorescent calcium, or loss of visualization of excitatory

cells, and this will confirm the efficacy of 2-APB at 24 ss, the time-point at which our experiments were carried out.

- **Do we need additional confirmation of the role of calcium in zebrafish MHB development?**

Signaling pathways involving calcium are complicated and difficult to study because, unlike other signaling molecules that are products of cellular transcription and translation, calcium is an inorganic diffusible molecule not synthesized by the body. Studies on calcium signaling typically involve manipulation of its concentration through pharmacological drugs that either increase or decrease its cytosolic levels. Use of these drugs can result in variable effects *in vivo* versus *in vitro* and this makes it important to test the functionality of the drug within *in vivo* systems using tools such as the GCaMP6 calcium indicator described above. Further, due to the nature of the drugs and variability in the efficacy of the drugs in live organisms, it is important that more than one drug be used to confirm the findings.

It is established that a major source of cytosolic calcium is by its release from the ER and from previously published studies and our own findings, we know that calcium levels can be regulated by manipulation of the IP3 receptors (Westfall et al., 2003). Apart from 2-APB, other pharmacological drugs such as thapsigargin, xestospongin C, and calcium ionophore A23187, which either increase or decrease intracellular calcium levels, can be used to additionally confirm the identified role of calcium in MHB morphogenesis (Westfall et al., 2003).

Xestospongin C is similar to 2-APB, and inhibits IP3R, preventing the opening of the calcium channels on the ER membrane (Gafni et al., 1997; Westfall et al., 2003). Thapsigargin and ionophore A23187 work to increase the cytosolic calcium levels. Treatment with thapsigargin inhibits the calcium-ATPase pump on ER membranes, depleting calcium from the ER and resulting in increase in cytosolic calcium. It also blocks the calcium pumps on the cell membrane, increasing influx of calcium from outside the cell. However, it is important to note that once the drug is washed out, the effect of the drug is reversible (Kluver et al., 2011; Westfall et al., 2003). Calcium ionophore A23187 allows calcium from extracellular sources to enter the cell, also causing an increase in intracellular calcium concentration (Lee et al., 1999; Shu et al., 2007). Embryos can be treated with each of these drugs at 18 ss and imaged on the confocal microscope at 24 ss to quantify cell shape changes. We would expect to see abnormal MHB tissue angle in each of the treatment groups. Depending on the drug treatment we would predict different effects on MHB cell shape. Xestospongin C treated embryos would show longer MHBC cells while thapsigargin and ionophore treated embryos would show shorter MHBC cells than in control. These experiments would help us determine whether calcium has a role in regulating cell length during zebrafish MHB formation.

- **Is calcium an upstream regulator of NMII during zebrafish MHB formation?**

In order to determine if NMII is regulated by calcium upstream, we depleted cytosolic calcium by 2-APB treatment and carried out a Western blot to determine changes in pMLC levels (Chapter 3, Fig. S7). However, we did not find any

observable reduction in pMLC abundance in wild-type or *mypt1* morphant embryos. MLC is a relatively small protein of 20 KDa size with low protein abundance and it is possible that the decrease in protein level is not detectable by Western blot. However, a small change in the amount of pMLC may still be sufficient to cause significant changes in morphogenesis. As an alternative, thapsigargin and calcium ionophore A23187 are both pharmacological drugs that increase the amount of intracellular calcium, which could potentially improve detection of changes in pMLC levels. Thus, we would expect to see an increase in pMLC abundance in thapsigargin or ionophore treated embryos by Western blotting. This would help us in determining if calcium signals to NMII.

- **Does calcium differentially signal to NMIIA?**

The finding that calcium inhibition results in longer MHBC cells, along with rescue of only the cell length phenotype in *mypt1* morphants upon 2-APB treatment, led us to hypothesize that calcium differentially signals to NMIIA. To test this hypothesis, we would treat 18 ss embryos with 2-APB (or an alternate drug that proves to be more efficient) and carry out a co-immunoprecipitation, by assaying for pMLC and Western blotting for NMIIA and NMIIB. We would expect to detect reduced amounts of NMIIA in the blot and no difference in levels of NMIIB. This reduction in pMLC-NMIIA quantity upon inhibition of cytosolic calcium would suggest that calcium signals differentially to NMIIA.

- **What are the intermediate molecules in the calcium-NMII signaling pathway?**

We hypothesize that calmodulin and myosin light chain kinase (MLCK) mediate the interaction of calcium with NMII (Chapter 3, fig. 20). Calmodulin is a calcium binding protein that plays a role in yeast cell morphogenesis (Kraus et al., 2005; Paranjape et al., 1990). CAM kinase II, a calcium/calmodulin-dependent protein kinase, is important in developmental events such as cardiac and fin morphogenesis (Rothschild et al., 2009). It is also expressed in the brain during early development and is required for zebrafish brain morphogenesis (Hsu and Tseng, 2010; Senga et al., 2013). This makes calmodulin a possible candidate required for zebrafish MHB morphogenesis. Further, it has been shown that calcium/calmodulin-dependent MLCK regulates NMII in renal collecting ducts (Chou et al., 2004). *Calmodulin 1a* (*calm1a*) is specifically expressed at the MHB during time points of interest and hence would be the ideal candidate (Friedberg and Taliaferro, 2005; Thisse, 2001). The role of calmodulin can be studied by morpholino mediated knockdown and mutants generated by targeted gene editing of *calm1a,* followed by analysis of MHB cell shapes in 24 ss embryos. We would expect to see longer MHBC cells in these morphants and knock out mutants, which would result in wider MHB tissue angle, representing an abnormal MHB.

In order to test the role of MLCK in MHB morphogenesis, we could inhibit it with the pharmacological inhibitor, ML-7 (Saitoh et al., 1987). ML-7 inhibits the activation of MLCK, preventing its functioning. Alternately, a dominant-negative construct for MLCK can also be used to prevent the normal functioning of the

kinase (Shimizu et al., 2006). Embryos treated with either ML-7 or injected with the dominant-negative MLCK could be analyzed for cell shapes at 24 ss using confocal microscopy. If MLCK phosphorylates NMIIA, we would expect to see abnormal MHB formation with longer MHBC cells. Additionally, a co-immunoprecipitation can be done, by pulling down pMLC and Western blotting for NMIIA and NMIIB, in conditions where MLCK is inhibited. We would expect to see a decrease in the amount of NMIIA, and not NMIIB in the test group of embryos when compared to control. A decrease in amount of pMLC-NMIIA upon inhibition of MLCK would indicate that MLCK signals to NMIIA. This would allow us to conclude if our hypothesis that MLCK differentially activates NMIIA is correct.

What are the signaling pathways regulating zebrafish MHB morphogenesis?

Any morphogenetic event during development is a complex process involving multiple signaling pathways. Hence, in order to tease out these pathways, a more global approach is required. A proteomic mass spectrometric analysis of embryonic brain tissue before and during MHB formation, and comparison of changes in protein levels would help identify molecules that may regulate MHB formation. It may also lead to discovery of novel molecules involved in this process. After identification of potential molecules and signaling pathways, we could specifically investigate individual downstream pathways to identify their roles in zebrafish MHB formation.

Thus, in this thesis, we characterized the cell shape changes occurring during zebrafish MHB formation and discovered an important role for NMII proteins in this morphogenetic process. We found that NMIIA regulates MHBC cell length and NMIIB regulates MHB cell width. We also determined that calcium is required for MHB morphogenesis, by its regulation of MHBC cell length. We further discovered that only the MHBC cell length phenotype of NMII overactivation is rescued by inhibition of calcium, which suggests possible differential regulation of NMIIA by calcium signaling. However, further investigation is required to elucidate how NMII proteins function differentially. These findings are likely to be similar in other morphogenetic events and will help expand our knowledge of the molecular mechanisms behind other developmental processes as well.

REFERENCES

Beach, J.R., L. Shao, K. Remmert, D. Li, E. Betzig, and J.A. Hammer, 3rd. 2014. Nonmuscle myosin II isoforms coassemble in living cells. *Current biology : CB*. 24:1160-1166.

Betapudi, V. 2014. Life without double-headed non-muscle myosin II motor proteins. *Frontiers in chemistry*. 2:45.

Chen, T.W., T.J. Wardill, Y. Sun, S.R. Pulver, S.L. Renninger, A. Baohan, E.R. Schreiter, R.A. Kerr, M.B. Orger, V. Jayaraman, L.L. Looger, K. Svoboda, and D.S. Kim. 2013. Ultrasensitive fluorescent proteins for imaging neuronal activity. *Nature*. 499:295-300.

Chou, C.L., B.M. Christensen, S. Frische, H. Vorum, R.A. Desai, J.D. Hoffert, P. de Lanerolle, S. Nielsen, and M.A. Knepper. 2004. Non-muscle myosin II and myosin light chain kinase are downstream targets for vasopressin signaling in the renal collecting duct. *The Journal of biological chemistry*. 279:49026-49035.

Friedberg, F., and L. Taliaferro. 2005. Calmodulin genes in zebrafish (revisited). *Molecular biology reports*. 32:55-60.

Gafni, J., J.A. Munsch, T.H. Lam, M.C. Catlin, L.G. Costa, T.F. Molinski, and I.N. Pessah. 1997. Xestospongins: potent membrane permeable blockers of the inositol 1,4,5-trisphosphate receptor. *Neuron*. 19:723-733.

Hsu, L.S., and C.Y. Tseng. 2010. Zebrafish calcium/calmodulin-dependent protein kinase II (cam-kii) inhibitors: expression patterns and their roles in zebrafish brain development. *Developmental dynamics : an official publication of the American Association of Anatomists*. 239:3098-3105.

Ishizaki, T., M. Uehata, I. Tamechika, J. Keel, K. Nonomura, M. Maekawa, and S. Narumiya. 2000. Pharmacological properties of Y-27632, a specific inhibitor of rho-associated kinases. *Molecular pharmacology*. 57:976-983.

Kluver, N., L. Yang, W. Busch, K. Scheffler, P. Renner, U. Strahle, and S. Scholz. 2011. Transcriptional response of zebrafish embryos exposed to neurotoxic compounds reveals a muscle activity dependent hspb11 expression. *PloS one*. 6:e29063.

Kraus, P.R., C.B. Nichols, and J. Heitman. 2005. Calcium- and calcineurin-independent roles for calmodulin in Cryptococcus neoformans morphogenesis and high-temperature growth. *Eukaryotic cell*. 4:1079-1087.

Lee, K.W., S.E. Webb, and A.L. Miller. 1999. A wave of free cytosolic calcium traverses zebrafish eggs on activation. *Developmental biology*. 214:168-180.

Paranjape, V., B.G. Roy, and A. Datta. 1990. Involvement of calcium, calmodulin and protein phosphorylation in morphogenesis of Candida albicans. *Journal of general microbiology*. 136:2149-2154.

Rothschild, S.C., C.A.t. Easley, L. Francescatto, J.A. Lister, D.M. Garrity, and R.M. Tombes. 2009. Tbx5-mediated expression of Ca(2+)/calmodulin-dependent protein kinase II is necessary for zebrafish cardiac and pectoral fin morphogenesis. *Developmental biology*. 330:175-184.

Saitoh, M., T. Ishikawa, S. Matsushima, M. Naka, and H. Hidaka. 1987. Selective inhibition of catalytic activity of smooth muscle myosin light chain kinase. *The Journal of biological chemistry*. 262:7796-7801.

Sako, Y., S. Minoghchi, and T. Yanagida. 2000. Single-molecule imaging of EGFR signalling on the surface of living cells. *Nature cell biology*. 2:168-172.

Senga, Y., K. Yoshioka, I. Kameshita, and N. Sueyoshi. 2013. Expression and gene knockdown of zebrafish Ca(2+)/calmodulin-dependent protein kinase Idelta-LL. *Archives of biochemistry and biophysics*. 540:41-52.

Shimizu, S., T. Yoshida, M. Wakamori, M. Ishii, T. Okada, M. Takahashi, M. Seto, K. Sakurada, Y. Kiuchi, and Y. Mori. 2006. Ca2+-calmodulin-dependent myosin light chain kinase is essential for activation of TRPC5 channels expressed in HEK293 cells. *The Journal of physiology*. 570:219-235.

Shu, X., J. Huang, Y. Dong, J. Choi, A. Langenbacher, and J.N. Chen. 2007. Na,K-ATPase alpha2 and Ncx4a regulate zebrafish left-right patterning. *Development*. 134:1921-1930.

Thisse, B., Pflumio, S., Fürthauer, M., Loppin, B., Heyer, V., Degrave, A., Woehl, R., Lux, A., Steffan, T., Charbonnier, X.Q. and Thisse, C. . 2001. Expression of the zebrafish genome during embryogenesis (NIH R01 RR15402). *ZFIN Direct Data Submission*.

Vicente-Manzanares, M., X. Ma, R.S. Adelstein, and A.R. Horwitz. 2009. Non-muscle myosin II takes centre stage in cell adhesion and migration. *Nature reviews. Molecular cell biology*. 10:778-790.

Wang, X., T. Wohland, and V. Korzh. 2010. Developing in vivo biophysics by fishing for single molecules. *Developmental biology*. 347:1-8.

Westfall, T.A., B. Hjertos, and D.C. Slusarski. 2003. Requirement for intracellular calcium modulation in zebrafish dorsal-ventral patterning. *Developmental biology*. 259:380-391.